NASA

TECHNICAL MEMORANDUM

X-303

STABILITY AND CONTROL CHARACTERISTICS AT LOW SUBSONIC

SPEEDS OF AN AIRPLANE CONFIGURATION HAVING

TWO TYPES OF VARIABLE-SWEEP WINGS

By Bernard Spencer, Jr.

Langley Research Center
Langley Field, Va.

GPO PRICE $ _____

CFSTI PRICE(S) $ _____

Hard copy (HC) _3.00_

Microfiche (MF) _75_

M 653 July 65

NATIONAL AERONAUTICS AND SPACE ADMINISTRATION

WASHINGTON

August 1960

:: :::: :: :.. :: :::: ::
: : : : : :█████████ : : : :
:: ::: :: :.. :: :::: ::

NATIONAL AERONAUTICS AND SPACE ADMINISTRATION

TECHNICAL MEMORANDUM X-303

STABILITY AND CONTROL CHARACTERISTICS AT LOW SUBSONIC

SPEEDS OF AN AIRPLANE CONFIGURATION HAVING

TWO TYPES OF VARIABLE-SWEEP WINGS*

By Bernard Spencer, Jr.

DECLASSIFIED- AUTHORITY
US 1166
DROBKA TO LEBOW MEMO DATED
APRIL 19, 1966

SUMMARY

An investigation to determine the static stability and control char-
acteristics associated with two types of variable-sweep wings mounted on
a fuselage representative of current supersonic fighter airplanes has
been made in the Langley 300-MPH 7- by 10-foot tunnel. One of the wings
having an outboard pivot was an advanced design of a previously tested
wing which indicated small static-stability changes with changes in wing
sweep. The second wing involved had a pivot-point location inside the
fuselage, which may be a more desirable location from a structural
standpoint.

These low-speed tests indicated that by careful design of the wing
and location of the outboard pivot the longitudinal stability could be
maintained at essentially the same level for wing sweepback angles
of 25° and 75°; thereby the conclusions previously reached with the
simplified research model were substantiated. An analysis of the pres-
ent wind-tunnel results for three supersonic designs having combinations
of a wing and horizontal tail, a wing, horizontal tail and canard sur-
face, and a wing and canard surface has been made for the configuration
having an outboard pivot location. The wing and canard-surface arrange-
ment indicated reduced static margin with increasing sweep. This fact
may have important implications regarding reductions in the transonic
stability shift and reductions in trim drag at the design Mach number
realized from use of a canard surface.

INTRODUCTION

In recent years there has been a renewed interest in variable-wing-
sweep aircraft generated both by the desire for multimission aircraft and

*█████████████████████
█████████
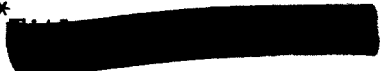
by the fact that the design supersonic Mach numbers now being considered
are such that considerably greater penalties, associated with the super-
sonic wing planform requirements, are now being encountered at subsonic
speeds. In addition to the obvious implications at subsonic speeds
these penalties, through excess fuel consumption, can seriously limit
the supersonic phase of a given mission. The National Aeronautics and
Space Administration, therefore, has undertaken a research program for
the purpose of developing variable-wing-sweep configurations which would
fulfill the current requirements better than would those developed in
the past. For example, a considerably higher sweep range is needed
because of the high supersonic Mach numbers required. Also, a method
of avoiding the wing translation, utilized in previous variable-sweep
aircraft as a means of minimizing the stability changes associated with
the wing rotation, would be desirable.

The development of a variable-wing-sweep configuration which appears
to satisfy reasonably the current requirements is described in refer-
ence 1, and detailed subsonic, transonic, and supersonic aerodynamic
data for the configuration are presented in references 2 to 6. This con-
figuration possessed essentially the same longitudinal stability charac-
teristics at both 25° wing sweep and 75° wing sweep without wing transla-
tion. However, the wind-tunnel model used in this study was simplified
in order to be more adaptable to configuration development; therefore,
it appeared desirable to test the variable-sweep wing developed on a
model more representative of current fighter airplanes. A research pro-
gram which will provide such information for a Mach number range from
low subsonic to a Mach number of 2.0 has, therefore, been initiated.

In the present investigation, two sets of variable-sweep wings were
studied. One, which is referred to as configuration I, is an advanced
version of the outboard pivot design described in references 1 and 2.
Although the aerodynamic superiority of this type of variable-sweep wing
over one having an inboard pivot has been fairly well established, the
possible structural penalties must, of course, be considered in applying
the principle to an aircraft. It therefore appeared desirable to pro-
vide aerodynamic data for both types of wings on a given configuration
in order to facilitate the weighing of aerodynamic and structural con-
siderations. In view of this a second wing, referred to as configura-
tion II, having a more conventional planform and a pivot located within
the fuselage was also tested.

The purpose of this paper is to present the results of the low-
speed tests made in the Langley 300-MPH 7- by 10-foot tunnel.

L
1
0
2
4

SYMBOLS

The forces and moments are referred to the body axis system except the lift and drag which, of course, are referred to the wind axis. (See fig. 1.) It is important to note that all coefficients are based on the highest sweptback-wing geometry of the configuration in question, and the moment reference point for both configurations is located 0.609 inch above the fuselage center line at a body station 67.03 percent of the body length. The effects of changes in center of gravity due to weight associated with changes in the sweep of the wing panels have been neglected. The coefficients and symbols are defined as follows:

C_L lift coefficient, $\dfrac{\text{Lift}}{qS}$

C_D drag coefficient, $\dfrac{\text{Drag}}{qS}$

C_m pitching-moment coefficient, $\dfrac{\text{Pitching moment}}{qS\bar{c}}$

C_l rolling-moment coefficient, $\dfrac{\text{Rolling moment}}{qSb}$

C_n yawing-moment coefficient, $\dfrac{\text{Yawing moment}}{qSb}$

C_Y lateral-force coefficient, $\dfrac{\text{Lateral force}}{qS}$

q dynamic pressure, lb/sq ft

α angle of attack, deg

β angle of sideslip, deg

C_{l_β} effective-dihedral parameter, $\dfrac{\partial C_l}{\partial \beta}$, per deg

C_{n_β} directional-stability parameter, $\dfrac{\partial C_n}{\partial \beta}$, per deg

C_{Y_β} side-force parameter, $\dfrac{\partial C_Y}{\partial \beta}$, per deg
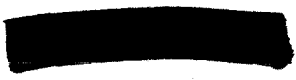
c_l section lift coefficient

$\dfrac{\partial C_m}{\partial C_L}$ longitudinal-stability parameter

C_{L_α} lift-curve slope, $\dfrac{\partial C_L}{\partial \alpha}$, per deg unless otherwise noted

$C_{n_{\delta_h}}$ yawing-moment effectiveness parameter due to roll control, $\dfrac{\partial C_n}{\partial \delta_h}$, per deg

$C_{l_{\delta_h}}$ roll-control effectiveness parameter, $\dfrac{\partial C_l}{\partial \delta_h}$, per deg

$(L/D)_{max}$ maximum lift-drag ratio, $\dfrac{C_L}{C_D}$

$\bar{c}$ mean aerodynamic chord, $\dfrac{\displaystyle\int_0^{b/2} c^2 \, dy}{\displaystyle\int_0^{b/2} c \, dy}$, in.

c local chord, in.

c_{av} average chord, in.

$x_{c/4}$ longitudinal distance from wing apex to $0.25c$, in.

$\bar{x}_{c/4}$ longitudinal distance from wing apex to $0.25\bar{c}$, $\dfrac{\displaystyle\int_0^{b/2} c\left(x_{c/4}\right) dy}{\displaystyle\int_0^{b/2} c \, dy}$, in.

y spanwise distance measured from root chord, in.

$\bar{y}$ lateral distance from fuselage center line to $\bar{c}$,

$$\frac{\int_0^{b/2} cy \, dy}{\int_0^{b/2} c \, dy}, \text{ in.}$$

S wing area including enclosed area, $2\int_0^{b/2} c \, dy$, sq ft

b wing span, in.

λ taper ratio

A aspect ratio

Λ_{LE} wing leading-edge sweep angle, deg

δ_h horizontal-tail deflection, positive with trailing edge down, deg

δ_c canard-surface deflection, positive with trailing edge down, deg

δ_v vertical-tail deflection, positive with trailing edge left, deg

δ_n wing nose-flap deflection, positive with trailing edge down, deg

Γ_t horizontal-tail dihedral angle, negative with tip chord down, deg

Γ_c canard dihedral angle, negative with tip chord down, deg

Configuration component part designations:

W   wing

B   body

C   canard surface

T   horizontal tail

MODELS

Configuration I

Geometric characteristics of configuration I are presented in figure 2, and photographs of this configuration in the tunnel showing the wing-sweep angles of 25° and 75° are presented as figure 3.

The fixed portion of this configuration had a leading-edge sweep of 60°, and the leading edge intercepted the fuselage center line at a station 17.9 inches from the nose. The outer panel with the wing leading edge swept back 25° had an NACA 65A006 airfoil section in the streamwise direction, and the inboard or fixed portion of the wing had an NACA 65A004.4 airfoil section in the streamwise direction. The pivot-point location for the configuration corresponded to 51.08 percent of the semispan of the wing swept back 75° and was located 0.735 inch behind the moment reference point. This pivot location was selected primarily from stability considerations. (See ref. 1.) The wing was displaced vertically 1.775 inches above the fuselage reference line.

A 15-percent-chord leading-edge flap was tested with the wing swept back 25° in an effort to increase the maximum lift-drag ratio of this configuration.

The horizontal tail employed in this investigation had an aspect ratio of 2.425, based on the exposed area and span with a leading-edge sweepback of 51.7°. These panels could be deflected 5, 0, -5, -10, and -15 to provide pitch or roll control and could be set at dihedral angles of 0° and -20°.

The canard surfaces were of wedge airfoil section with a fixed dihedral position of -20°. Incidence angles of ±10° could be obtained with these controls.

The fuselage used in this investigation was representative of current high-speed, twin-engine fighter airplane having a high-fineness-ratio forebody ahead of the engine inlets and with the engines housed in the fuselage. The entrance or capture area of the inlets was 6.020 sq in. and the exit area was 7.192 sq in.

Configuration II

Geometric characteristics of configuration II are presented in figure 4, and photographs of this configuration in the tunnel with the wings swept back 43.03° and 70.50° are presented as figure 5. The small fixed glove at the wing-fuselage juncture had a leading-edge sweep

L
1
0
2
4
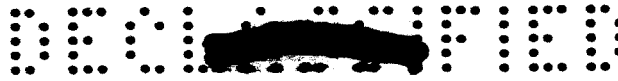
of 60°, with the wing-apex intercept at the same position as for configuration I. The wing with the leading edge swept back 43.03° had an NACA 65A005 airfoil section in the streamwise direction. The wing pivot point was located within the fuselage and corresponded to 28.05 percent of the wing semispan for the 70.50° sweepback condition and was located 3.85 inches ahead of the moment reference point. This pivot location was selected primarily from structural considerations.

The wing was displaced vertically 1.775 inches above the fuselage reference line and was tested at leading-edge sweepback angles of 30.00°, 43.03°, 60.50°, and 70.50° with aspect-ratio variation of 4.494, 4.000, 2.582, and 1.754, at zero incidence and dihedral.

Control surfaces for this configuration were the same as those for configuration I, and the relative positions and pertinent geometry of these controls are presented in figure 2.

TESTS AND CORRECTIONS

The tests were made in the Langley 300-MPH 7- by 10-foot tunnel at a tunnel dynamic pressure of 80 lb/sq ft for configuration I and 63 lb/sq ft for configuration II.

The Reynolds number for configuration I, based on the mean aerodynamic chord of the wing swept back 75°, was 2.382×10^6, and the Reynolds number for configuration II, based on the wing swept back 70.50°, was 2.219×10^6. The models were sting-mounted (figs. 3 and 5) and all forces and moments were measured with a six-component strain-gage balance.

Jet-boundary corrections as determined from reference 7 have been applied to pitching moment, drag, and angle of attack. Blockage corrections as determined by the methods of reference 8 have been applied to the dynamic pressures and drag. The base pressure was measured and the drag was adjusted to a condition of free-stream static pressure at the base. The internal duct drag was also measured and subtracted from the total drag. The angle of attack and angle of sideslip have been corrected for sting bending and balance deflections under load.

Transition was fixed on all surfaces including the fuselage. Number 100 carborundum grains were used at the 10-percent streamwise chord lines for the wings of configurations I and II swept back 25° and 30.00°, respectively, and on the horizontal and vertical tails at similar positions. The fuselage transition strip was placed at a position 10 percent of the fuselage length aft of the nose.
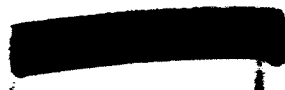
PRESENTATION OF RESULTS

A fairly extensive investigation of the stability and control characteristics of configurations I and II has been made at low subsonic speeds, and in order to aid in locating a particular set of data, tables showing the locations by figure number of the basic data for both configurations are given in this section.

Configuration I.-

L
1
0
2
4

Configuration II.-

Summary plots are presented in figures 42 to 44 and for the most part the discussion will be limited to these figures in order to expedite publication.

DISCUSSION

Longitudinal Stability and Control

Figure 42(a) presents the variation of pitching moment with lift coefficient for configurations I and II with the horizontal tail off for the range of wing leading-edge sweep angles tested. Both configurations indicate increasing instability with increasing lift coefficient. In addition, the results for configuration II indicate a rather large variation in stability level with sweep variations.

The results with the horizontal tail on are presented in figure 42(b), and it will be noted that for both configurations the addition of the tail tended to linearize the variation of pitching moment with lift coefficient. This favorable effect is associated with the location of the horizontal tail below the chord plane. However, a wide variation of stability with sweep angle is still encountered for configuration II with appreciable nonlinearities in pitching moment indicated for all sweepback angles except 70.50°. For configuration I, the change in stability level realized from increasing sweep is very small compared with the large change in stability encountered for configuration II.

A comparison of the variation of longitudinal low-lift stability, untrimmed maximum lift-drag ratios, and lift-curve slope with changes in wing leading-edge sweep angle is presented in figure 43 for the two configurations tested. A change in static margin of approximately 11.5 percent $\bar{c}$ is noted for the wing-body combination and a change of approximately 14 percent $\bar{c}$ in static margin for the wing-body-tail combination of configuration II is encountered when sweeping the wing through a range of 40.50°. For the wing-body-tail combination of configuration I, however, an increase in stability of only 2 percent $\bar{c}$ is noted for an increase of 50° in sweep. It must be kept in mind that at some intermediate sweep a somewhat larger rearward shift will be encountered (see ref. 2). However, since this higher static margin will be encountered only during transition between the design sweep angles, it appears to pose no problem. An interesting point shown in figure 43 for configuration I is that for the tail-off configuration the aerodynamic-center location for the 75° sweep condition is ahead of the aerodynamic center location for the wing leading-edge sweep of 25°. This is a rather graphic illustration of the effectiveness of this type of variable-sweep wing in controlling the stability. The

increase in stability of the low-sweep condition over that of the high-sweep condition is due to the fact that the instability associated with the fixed portion of the wing is reduced because of the increase in overall lift-curve slope which accompanies the reduction in wing sweep. For the case presented herein this more than compensates for the forward movement of the outer panel aerodynamic center.

With regard to the variation of the lift-curve slope with sweep angle, the results (fig. 43) for both configurations indicate a decrease of approximately 50 percent at low angles of attack as the sweep is increased from the minimum to the maximum angle. This decrease, of course, would provide appreciable reduction in the gust loads encountered in a low-level mission with the wing in the high-sweep position. For landing, take-off, and low-speed loiter, advantage could be taken of the higher lift and corresponding lower drag due to lift (as indicated by the lift-drag ratios of fig. 43) associated with the low-sweep high-aspect-ratio wing setting. Large decreases in $(L/D)_{max}$ with increases in sweep are noted for both configurations as would be expected. A comparison of values of untrimmed $(L/D)_{max}$ with and without the horizontal tail is also presented in figure 43 for both configurations. Addition of the horizontal tail reduces the values of $(L/D)_{max}$ for both configurations with the wing in the least sweptback position $\left(\Lambda_{LE} = 25^{\circ}\right.$ for configuration I and $\Lambda_{LE} = 30.00^{\circ}$ for configuration II$\left.\right)$. This effect is seen to diminish with increasing sweep, apparently due to changes in wing-induced-flow characteristics on the horizontal tails. With regard to the lift-drag ratios, it must be realized that considerably higher values would be expected at flight Reynolds numbers.

Regarding longitudinal control, the basic-data plots indicate sufficient horizontal-tail effectiveness throughout the entire lift range for all configurations at subsonic speeds.

Since configuration I appears more desirable from a longitudinal-stability standpoint (through a minimum of aerodynamic-center shift with wing sweep) while maintaining essentially the same variation in lift-curve slope and lift-drag ratio, an analysis was made of three arrangements of configuration I considered as possible supersonic airplanes, and the results are presented in figure 44. The arrangements presented include combinations of a wing and horizontal tail, a wing, horizontal tail, and canard surface, and a wing and canard surface. For comparison purposes, the moment reference location for the three configurations has been adjusted so that for the 25° wing-sweep condition each configuration has the same static margin of about $5\frac{1}{2}$ percent $\bar{c}$.
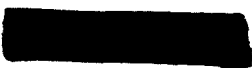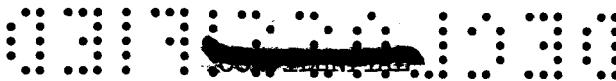
Sweeping the wing from 25° to 75° for the combination of the wing and horizontal tail results in an increase in stability of about 2 percent $\bar{c}$; whereas the combination of wing, horizontal tail, and canard surface indicates no increase in stability, and the combination of the wing and canard surface provides a decrease in stability for increasing sweep. For the moment reference chosen, the combination of the wing and canard surface shows essentially neutral stability for the 75° sweep condition. An arrangement of this type may prove useful as viewed from the effects of minimizing transonic aerodynamic-center shift. If the configuration were considered to have a static margin of $5\frac{1}{2}$ percent $\bar{c}$ with a wing sweep of 25° at subsonic speeds, and were designed for supersonic speeds with the wing swept back 75°, then, the total increase in static margin realized from sweeping to 75° and increasing Mach number to supersonic would only amount to approximately 10 percent $\bar{c}$, assuming a typical transonic aerodynamic-center shift of approximately 16 percent $\bar{c}$. This fact, plus the reduction in trim drag realized from comparison of canard arrangements with conventional tail-rearward configurations, appear to make this type arrangement promising from performance and stability viewpoints. It must be kept in mind, however, that some type of stability "fix" would probably be required to reduce the nonlinearities encountered at the high lift coefficients.

Figure 45 presents the span-load distribution for configuration I with the wing swept back 25° and 75° as calculated by the methods of reference 9. Wing alone aerodynamic-center locations and lift-curve slope are also presented in the table included in figure 45. The calculated loadings are based on the areas and spans of the respective wing in question, as indicated by the figure.

Lateral-Directional Stability and Control

None of the configurations tested indicated any unusual lateral or directional stability characteristics. (See figs. 17 to 20, 40, and 41.) Adequate directional stability was maintained to angles of attack of 20° or better which should cover the range of acceptable landing attitudes. Positive effective dihedral was obtained over approximately the same range of angles of attack.

Figure 41 presents the effectiveness of the roll-control tail (differential deflecting of the horizontal tail) for configuration II with the wing in the 70.50° sweepback condition. Wing-off results are also presented and illustrate the effect of the wing in delaying the reduction in roll effectiveness to higher angles of attack. This is apparently due to wing downwash allowing the tail to operate in the linear portion of its lift curve.
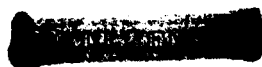
The yawing moments induced by the roll control tail are also presented in figure 41. Over a good portion of the angle-of-attack range, the yaw-to-roll ratio is about 0.3, a value considerably lower than that obtained with the configuration of reference 2. This favorable condition is probably associated with the shorter wing-tail coupling of the present configuration. At the higher angles the ratio is reduced even further due, in part at least, to the horizontal-tail differential drag.

CONCLUDING REMARKS

These low-speed tests of two types of variable-sweep wings on a representative fighter airplane indicated that by careful wing design the subsonic longitudinal stability can be maintained at essentially the same level for wing sweep angles of 25° and 75° for configuration I; thereby the conclusions previously reached with a simplified research model were substantiated. An analysis of the present wind-tunnel results for three supersonic designs having combinations of a wing and horizontal tail, a wing, horizontal tail and canard surface, and a wing and canard surface has been made for the configuration having an outboard pivot location. The combination of wing and canard surface indicated reduced static margin with increasing sweep. This fact may have important implications regarding reductions in the transonic stability shift and reductions in trim drag at the design Mach number which were realized from use of a canard surface.

Langley Research Center,
    National Aeronautics and Space Administration,
        Langley Field, Va., May 13, 1960.
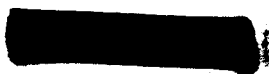
REFERENCES

1. Alford, William J., Jr., and Henderson, William P.: An Exploratory Investigation of the Low-Speed Aerodynamic Characteristics of Variable-Wing-Sweep Airplane Configurations. NASA TM X-142, 1959.

2. Alford, William J., Jr., Luoma, Arvo A., and Henderson, William P.: Wind-Tunnel Studies at Subsonic and Transonic Speeds of a Multiple-Mission Variable-Wing-Sweep Airplane Configuration. NASA TM X-206, 1959.

3. Spearman, M. Leroy, and Foster, Gerald V.: Stability and Control Characteristics at a Mach Number of 2.01 of a Variable-Wing-Sweep Configuration With Outboard Wing Panels Swept Back 75°. NASA TM X-32, 1959.

4. Spearman, M. Leroy, and Foster, Gerald V.: Effects of Various Modifications on the Supersonic Stability Characteristics of a Variable-Wing-Sweep Configuration at a Mach Number of 2.01. NASA TM X-260, 1960.

5. Foster, Gerald V.: Stability and Control Characteristics at Mach Numbers of 2.50, 3.00, and 3.71 of a Variable-Wing-Sweep Configuration With Outboard Wing Panels Swept Back 75°. NASA TM X-267, 1960.

6. Foster, Gerald V.: Effects of Spoiler-Slot-Deflector Control on the Aerodynamic Characteristics at a Mach Number of 2.01 of a Variable-Wing-Sweep Configuration With the Outer Wing Panels Swept Back 75°. NASA TM X-273, 1960.

7. Herriot, John G.: Blockage Corrections for Three-Dimensional-Flow Closed-Throat Wind Tunnels, With Consideration of the Effect of Compressibility. NACA Rep. 995, 1950. (Supersedes NACA RM A7B28.)

8. Sanders, J., and Pounder, J. R.: Wall Interference in Wind Tunnels of Closed Rectangular Section. Aero. Rep. AR-7, Nat. Res. Council of Canada (Ottawa), 1949.

9. Campbell, George S.: A Finite-Step Method of Calculations of Span Loadings of Unusual Plan Forms. NACA RM L50L13, 1951.
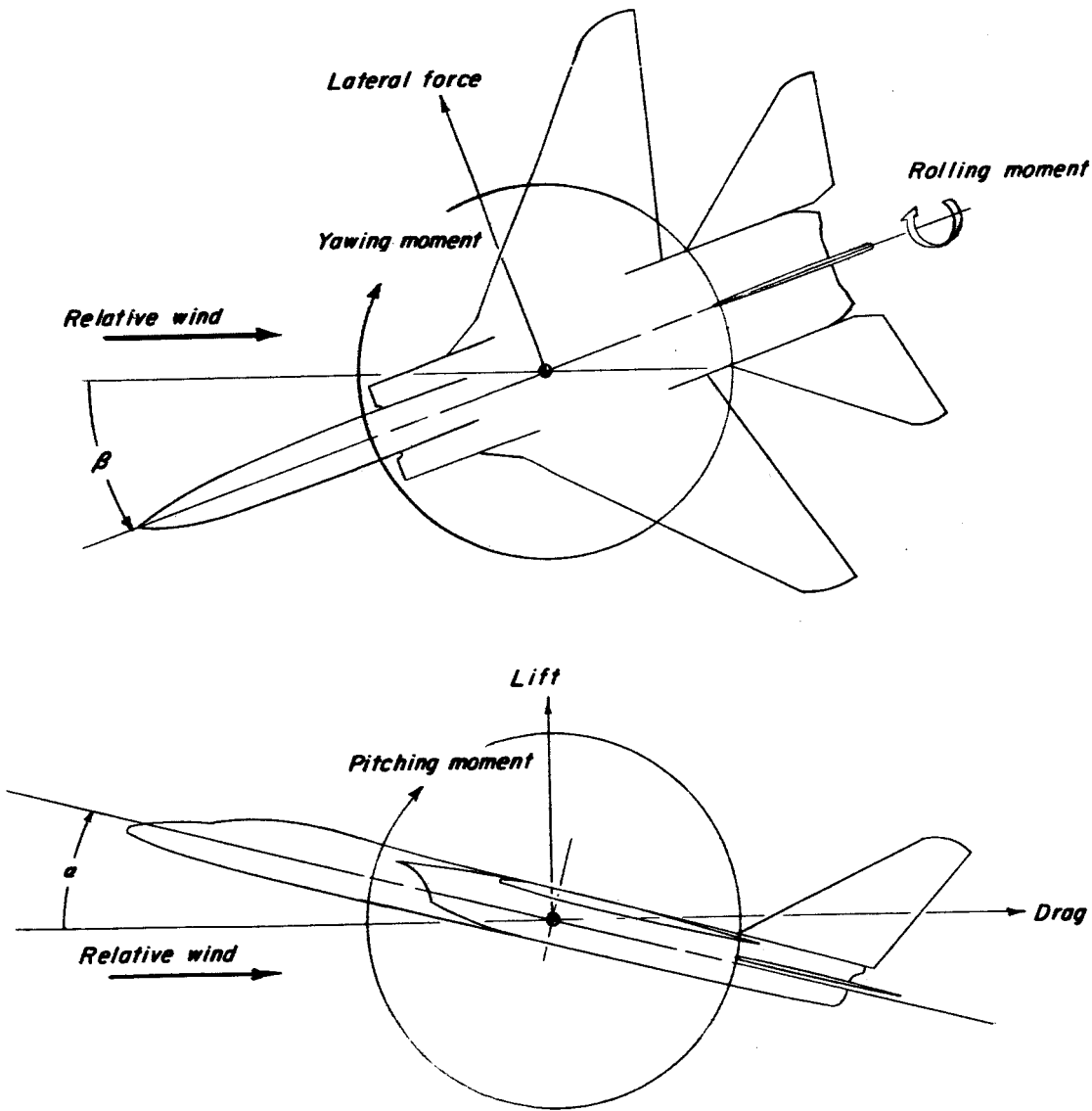
Figure 1.- System of axes used showing the positive direction of forces, moments, and angles.

$A_{LE} = 75°$
$S = 3.3451 ft^2$
$\bar{c} = 18.2115$
$\bar{y} = 6.0831$
$\bar{x}_{1/4} = 15.9791$
$b = 30.204$
$A = 1.894$
$\lambda = 0$

$A_{LE} = 25°$
$S = 3.6531 ft^2$
$\bar{c} = 14.3333$
$\bar{y} = 8.2548$
$\bar{x}_{1/4} = 15.3870$
$b = 52.044$
$A = 5.148$
$\lambda = .089$

Leading edge flap
of 15c

Hinge line

Pivot point

Moment reference

Hinge line
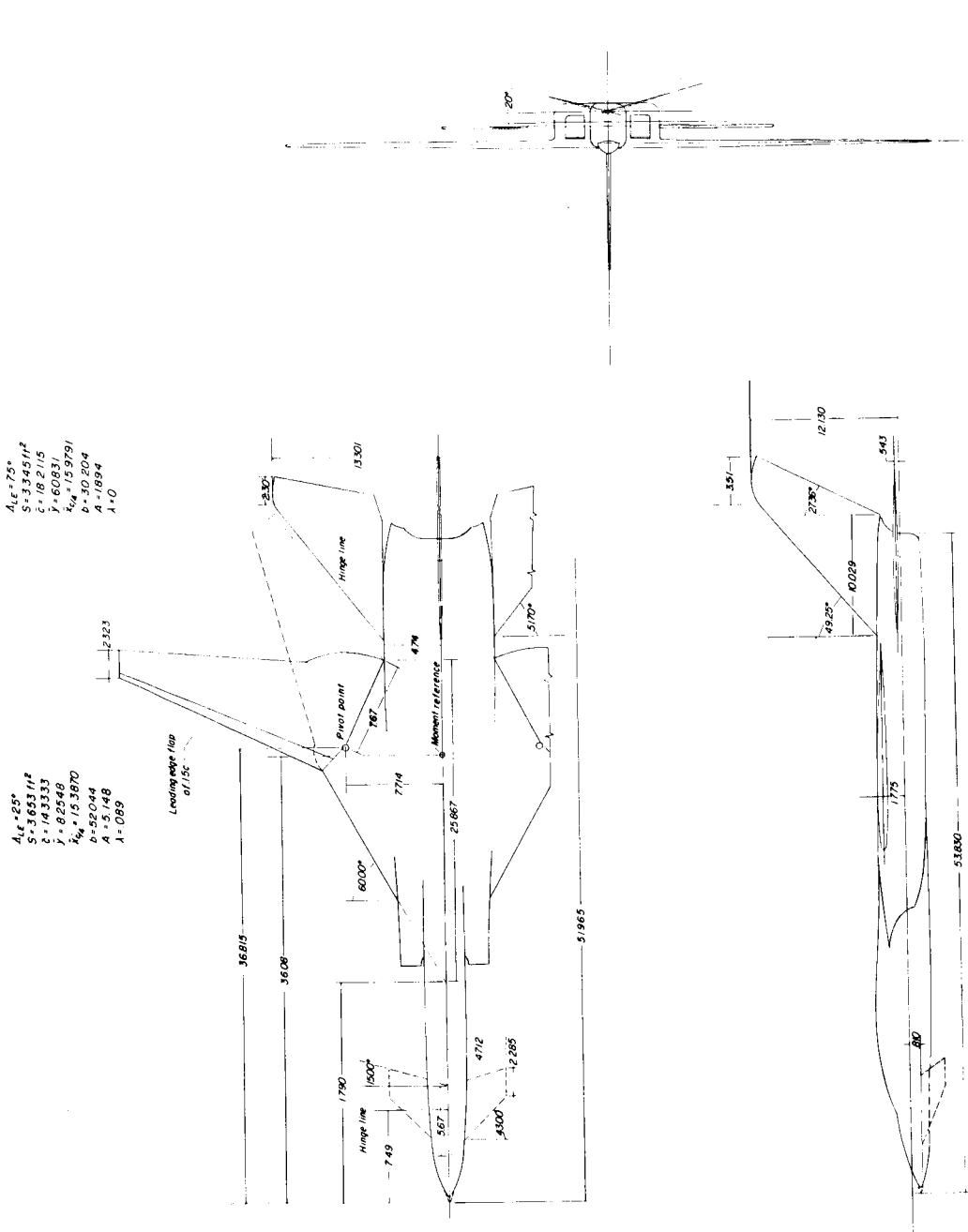
Figure 2.— Details of configuration I with pertinent dimensions presented. All dimensions in inches, except as otherwise noted.

DECLASSIFIED

L-1024
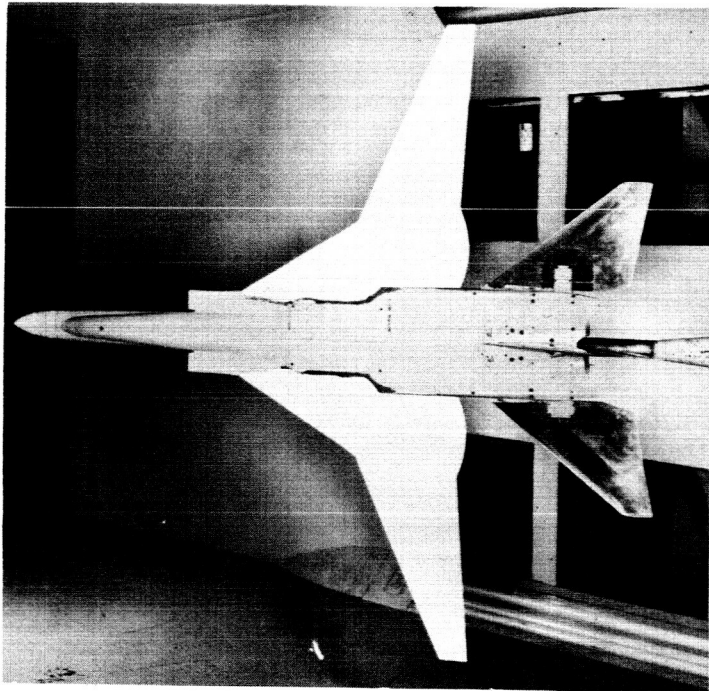
(a) Wing swept back, $\Lambda_{LE} = 25^{\circ}$.

L-59-8261
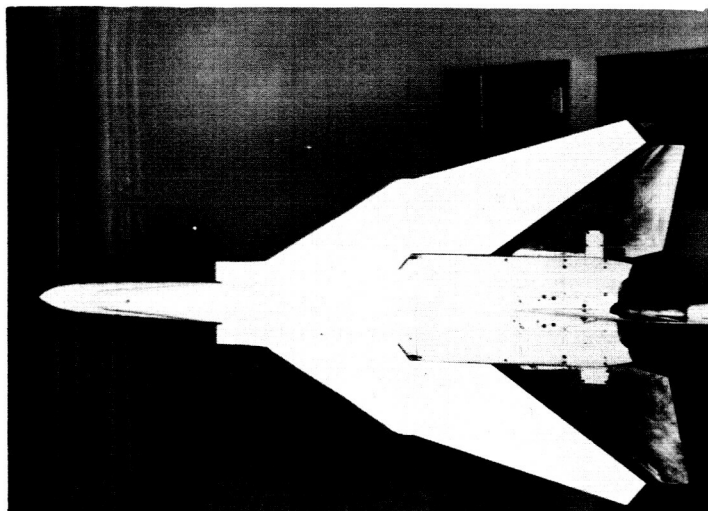
(b) Wing swept back, $\Lambda_{LE} = 75^{\circ}$.

L-59-8263

Figure 3.- Photographs of configuration I showing wing in 75° and 25° sweepback conditions.
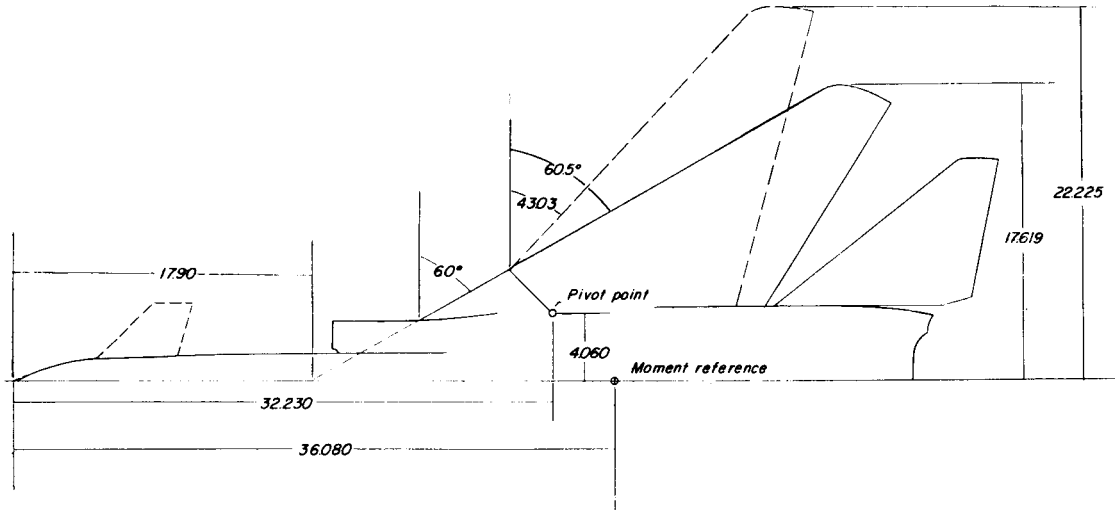
Wing in intermediate sweep conditions

1790

22.225

17.619

60.5°
43.03
60°

Pivot point

4.060

Moment reference

32.230

36.080

$S = 3.851 ft^2$
$\bar{c} = 14.270$
$\bar{y} = 8.896$
$x_{\bar{c}/4} = 10.882$
$A = 4.494$

$S = 3.329 ft^2$
$\bar{c} = 19.129$
$\bar{y} = 6.082$
$x_{\bar{c}/4} = 10.937$
$A = 1.754$

24.960

14.497

70.5°
30.00
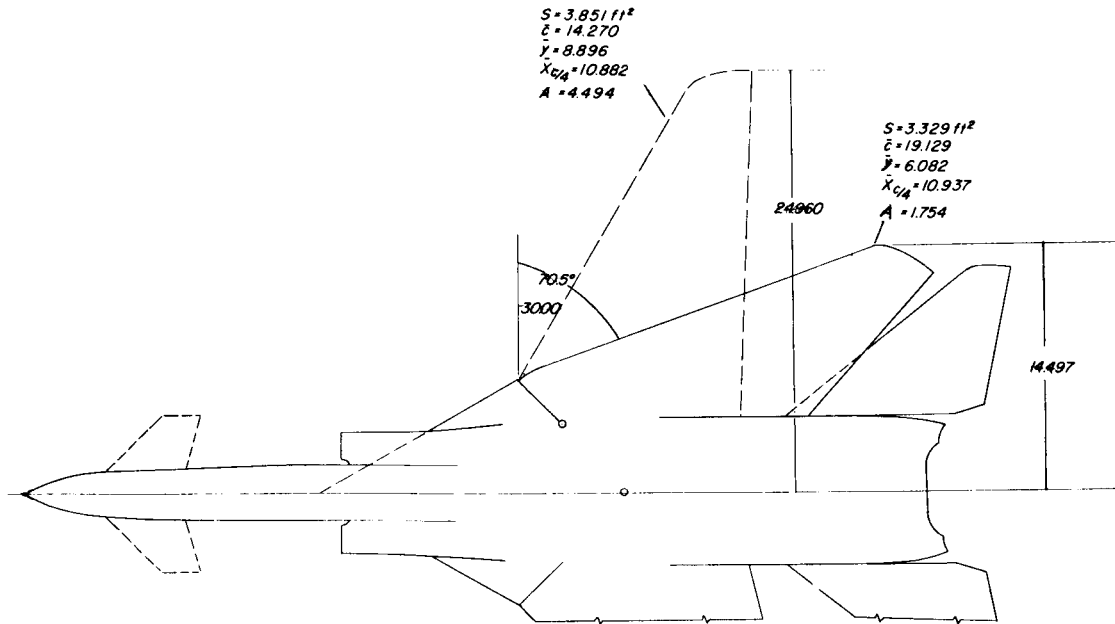
Wing swept 30.00° and 70.50°

Figure 4.- Two-view drawing of configuration II showing pertinent dimensions. All dimensions in inches, except as otherwise noted.
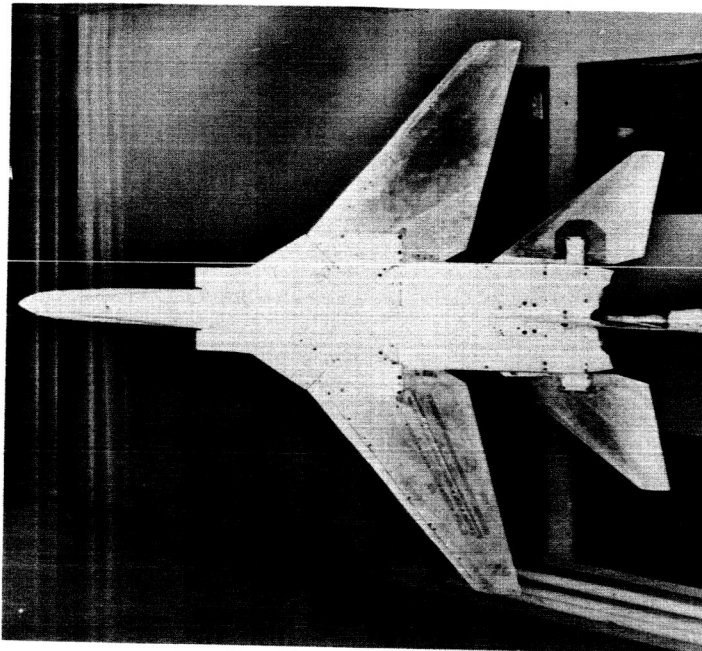
(a) Wing swept back, $\Lambda_{LE} = 43.03^\circ$.   L-59-8260
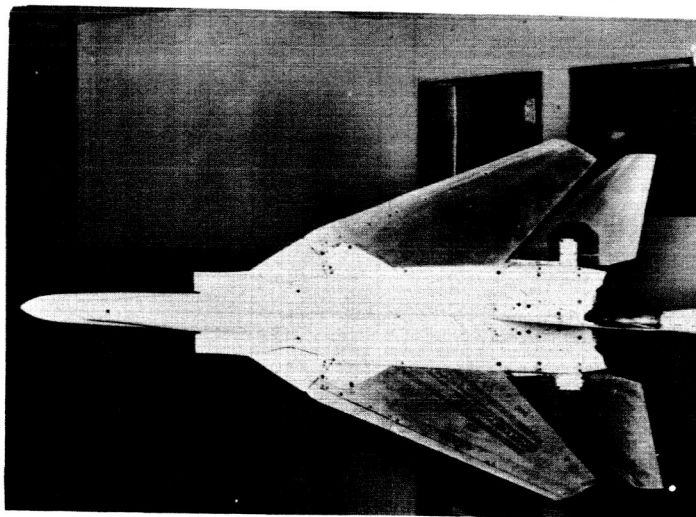
(b) Wing swept back, $\Lambda_{LE} = 70.50^\circ$.

L-59-8262

Figure 5.- Photographs of configuration II, showing wing in 70.50° and 43.03° sweepback conditions.

L-1024
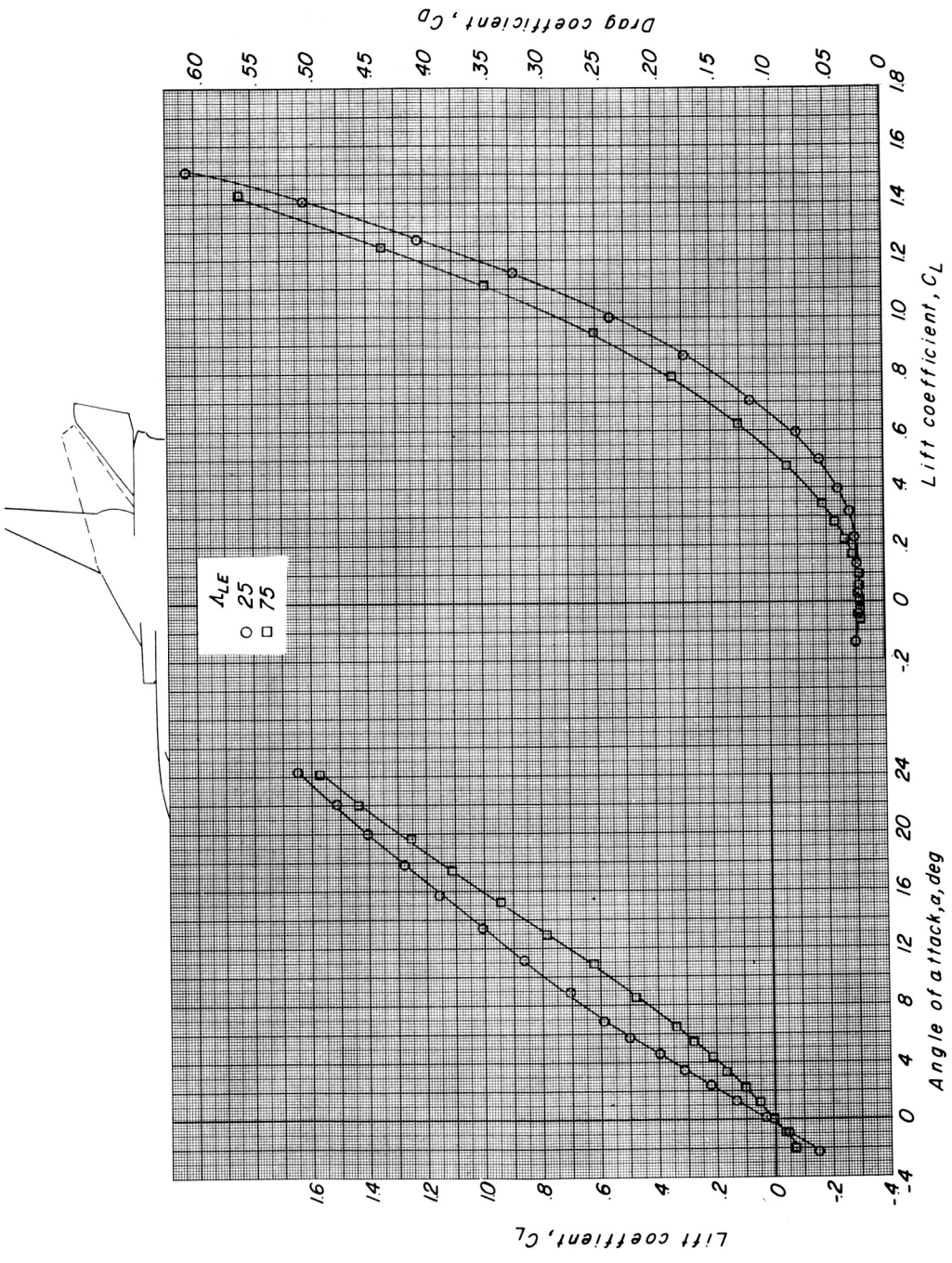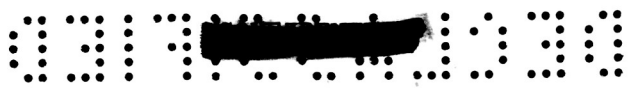
Figure 6.- The effects of wing sweep in the longitudinal aerodynamic characteristics of configuration I with canard surface off and horizontal tail on. $\Gamma_t = 0^\circ$; $\delta_h = 0^\circ$.
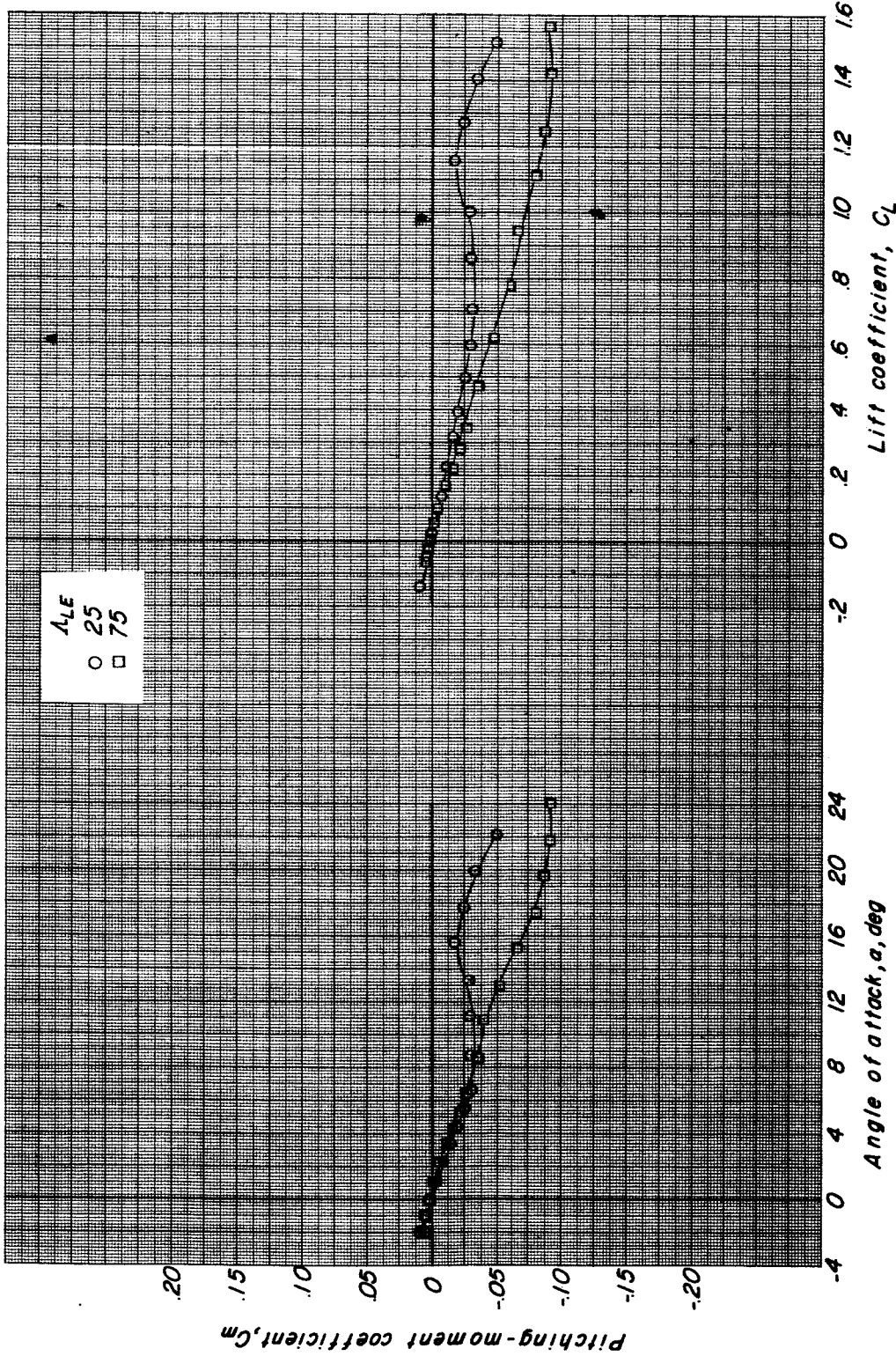
Figure 6.- Concluded.

L-1024
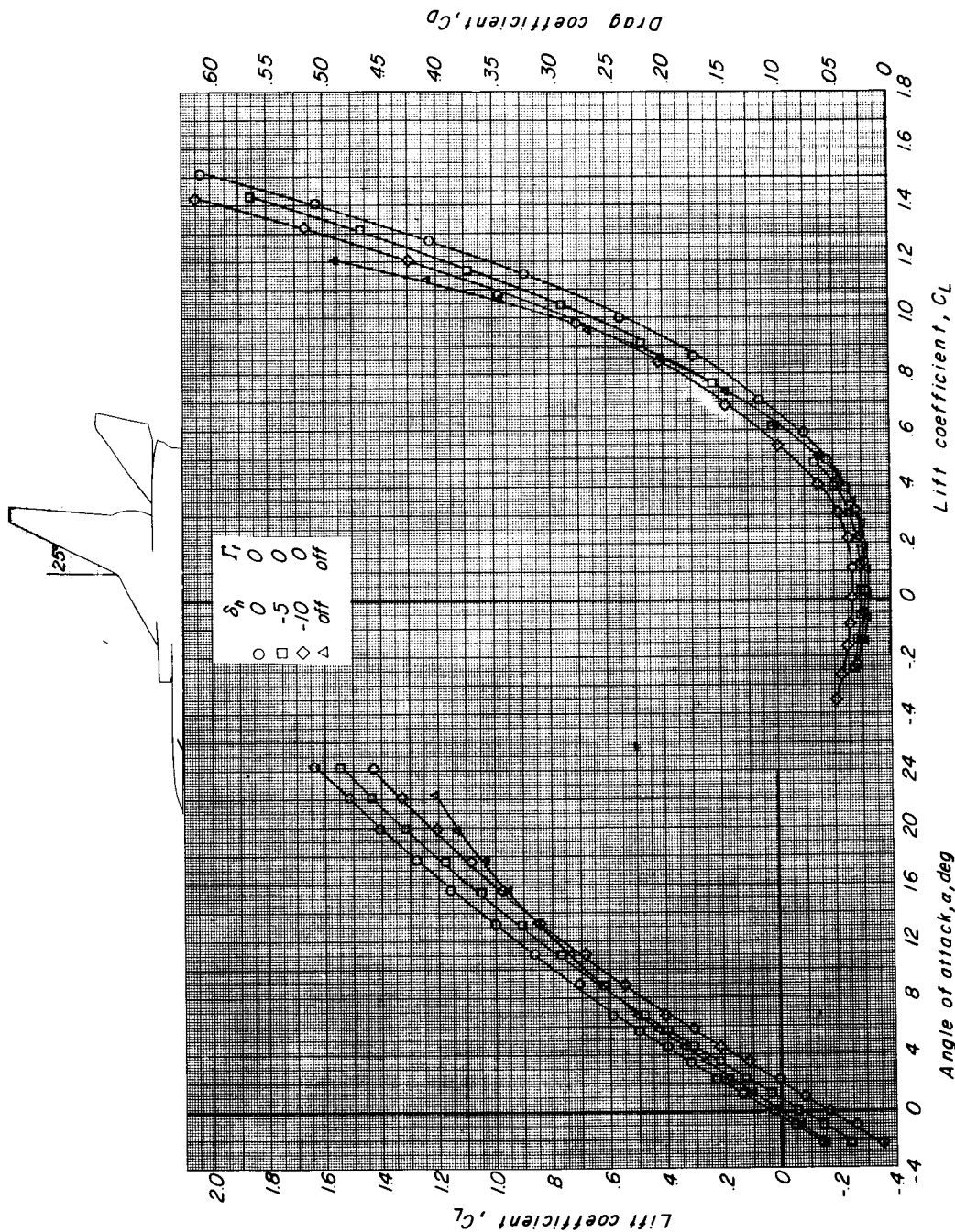
Figure 7.- The effects of horizontal-tail deflection on the longitudinal aerodynamic character-
istics of configuration I with canard surface off. $\Lambda_{LE} = 25^{\circ}$.
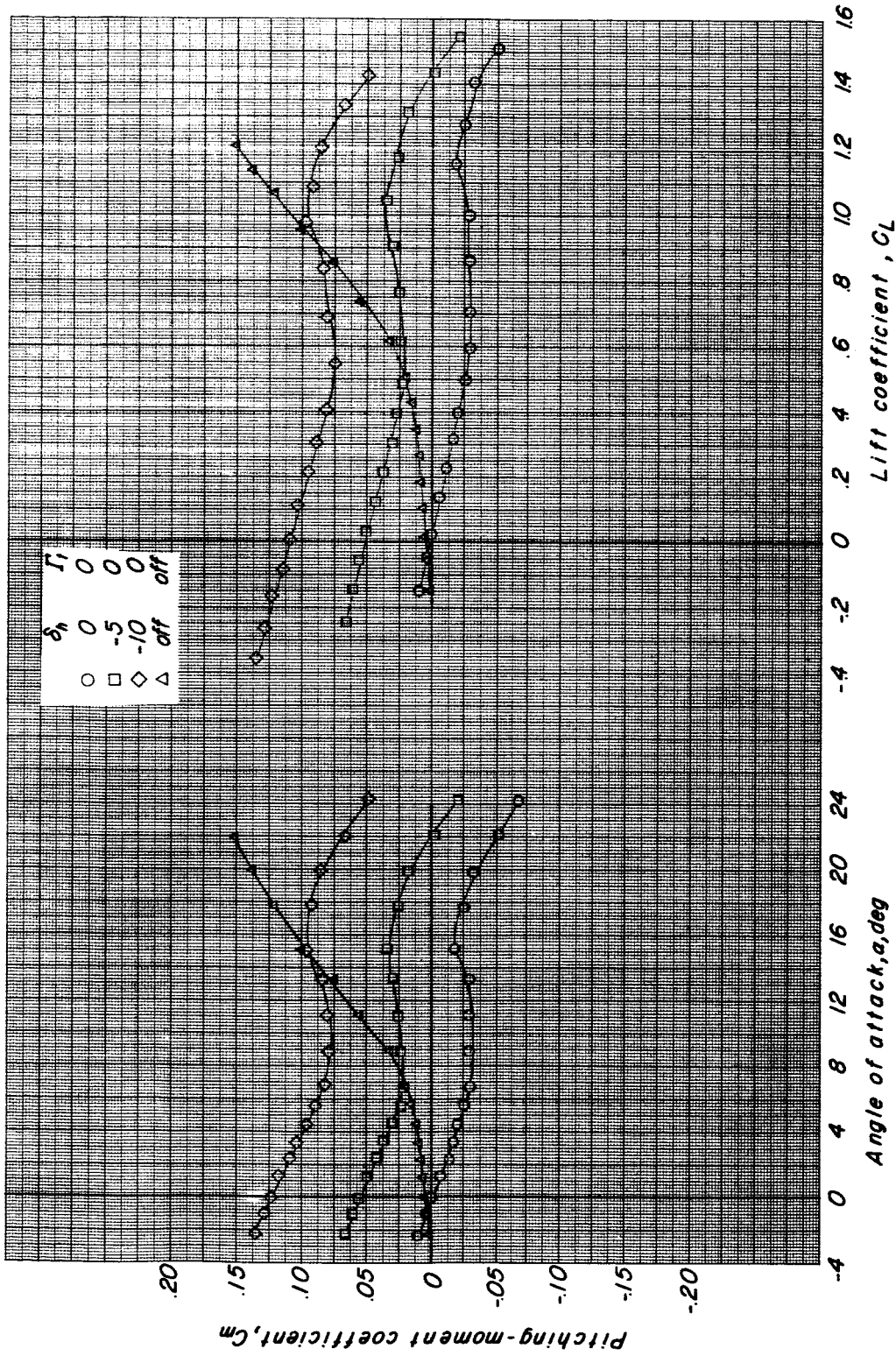
Figure 7.- Concluded.
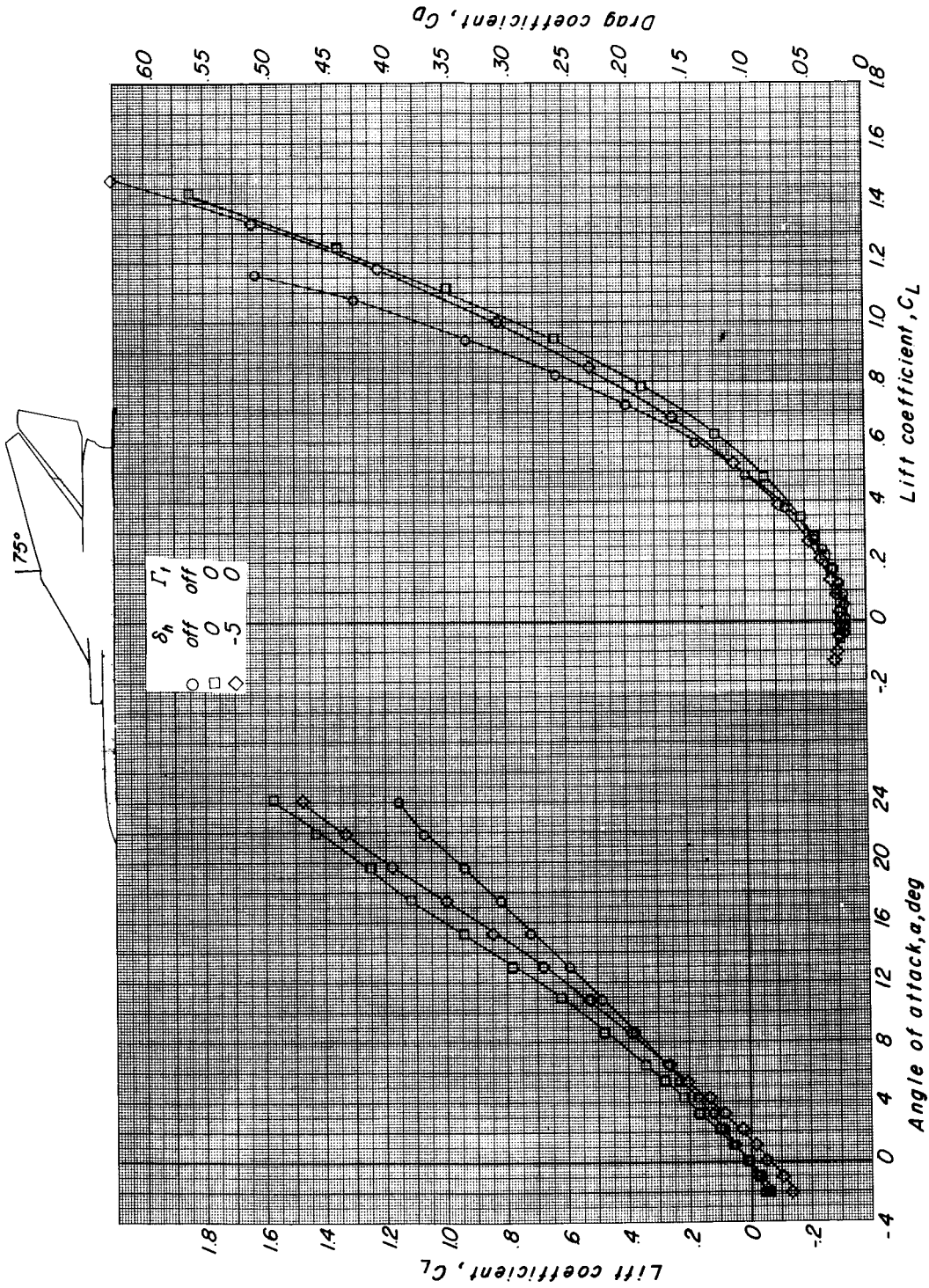
Figure 8.- The effects of horizontal-tail deflection on the longitudinal aerodynamic character-
istics of configuration I with canard surface off. $\Lambda_{LE} = 75^{o}$.
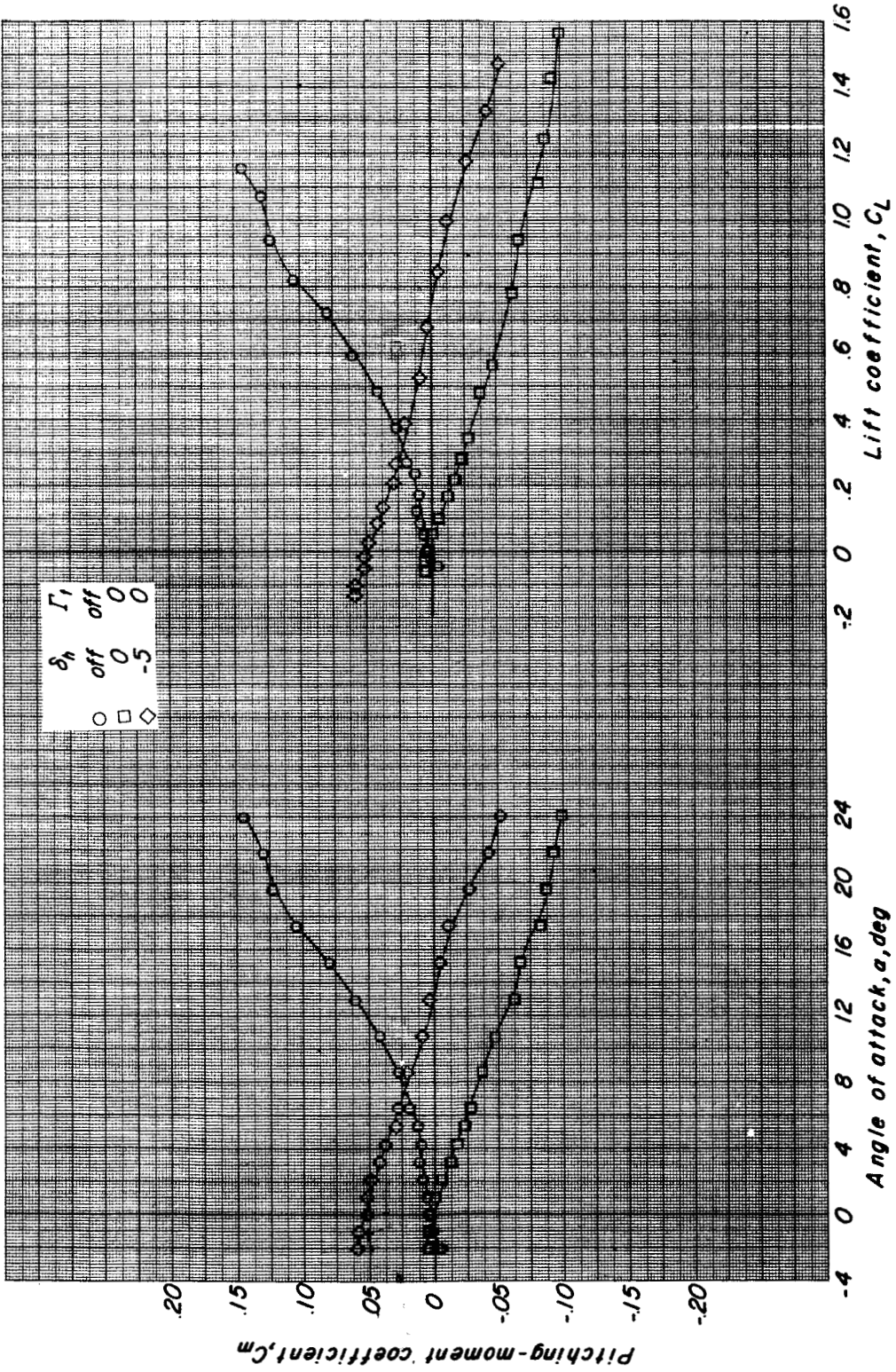
L-1024

Figure 8.- Concluded.
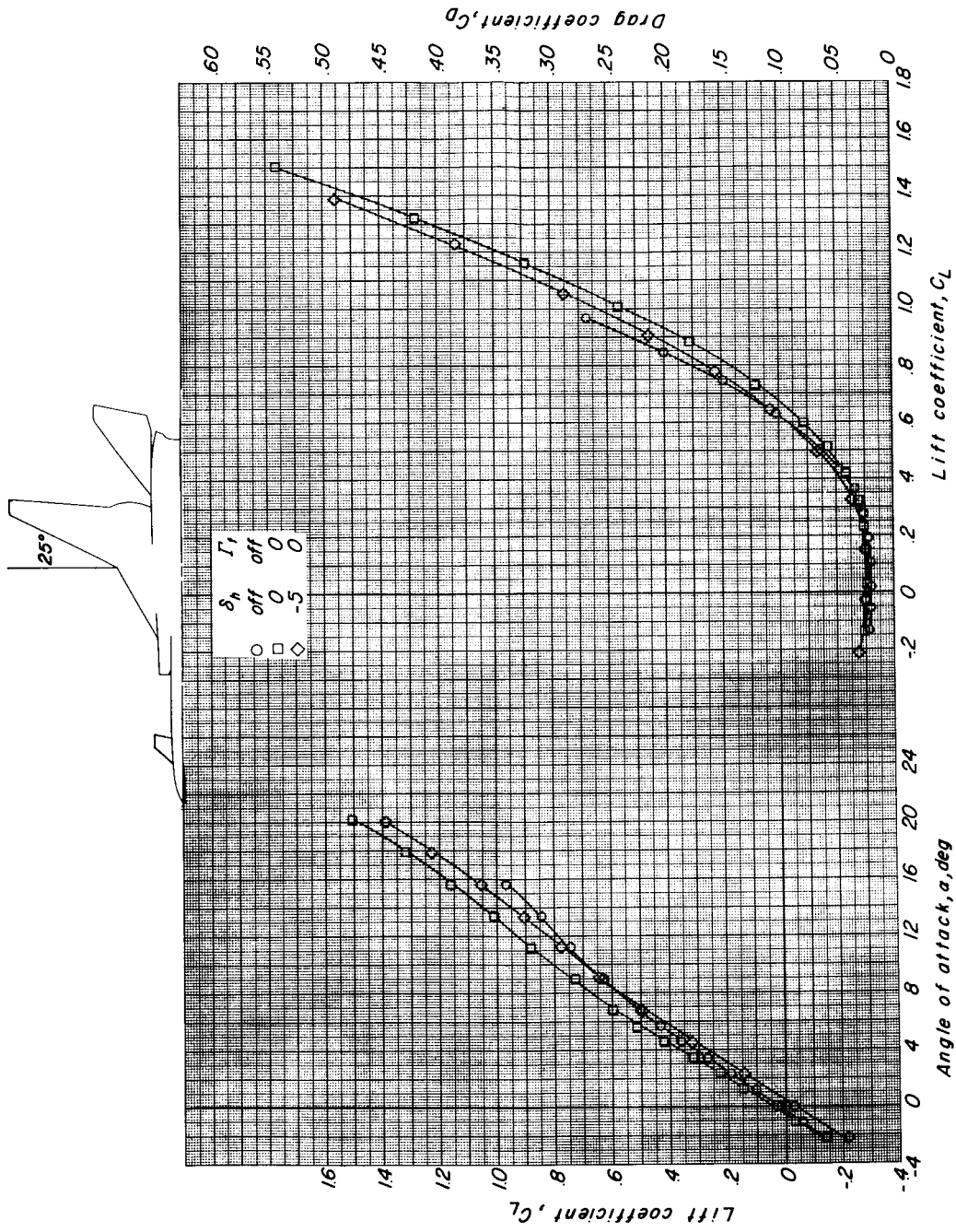
Figure 9.- The effects of horizontal-tail deflection on the longitudinal aerodynamic character-
istics of configuration I with canard surface on. $\Lambda_{LE} = 25°$; $\delta_c = 0°$.
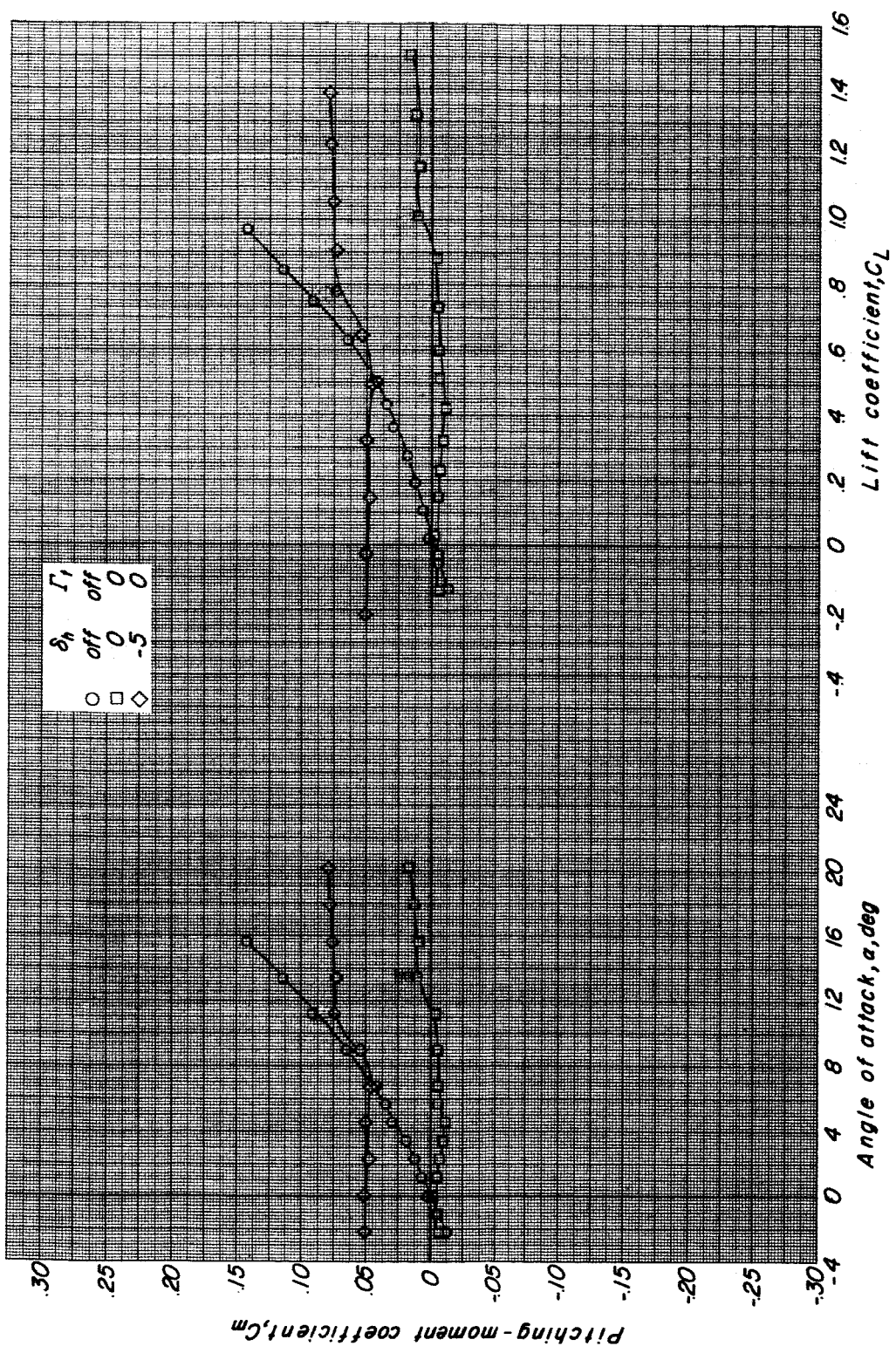
L-1024

Figure 9.- Concluded.
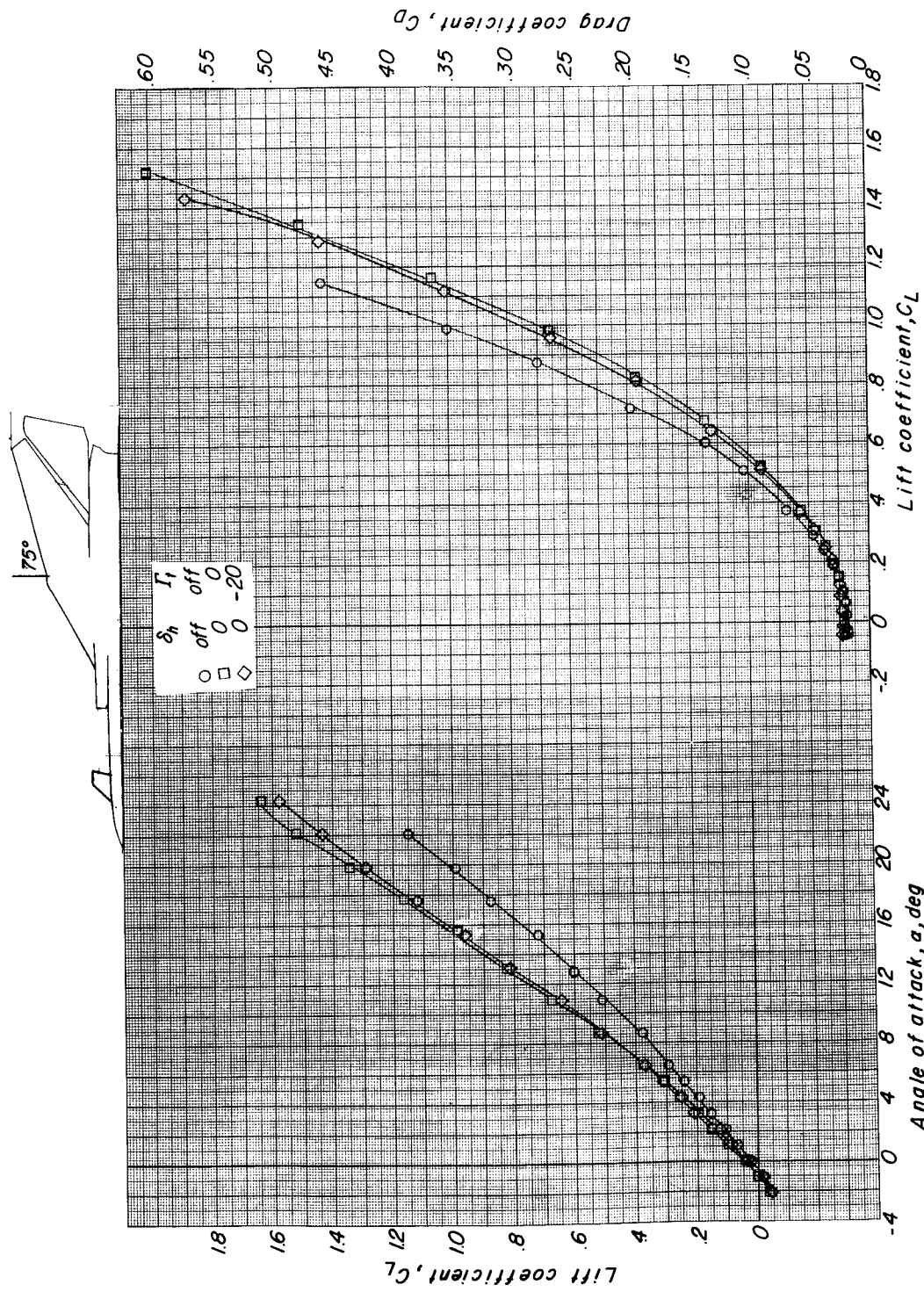
Figure 10.- The effects of horizontal-tail dihedral on the longitudinal aerodynamic character-
istics of configuration I with canard surface on. $\Lambda_{LE} = 75^\circ$; $\delta_c = 0^\circ$.

L-1024

L-1024
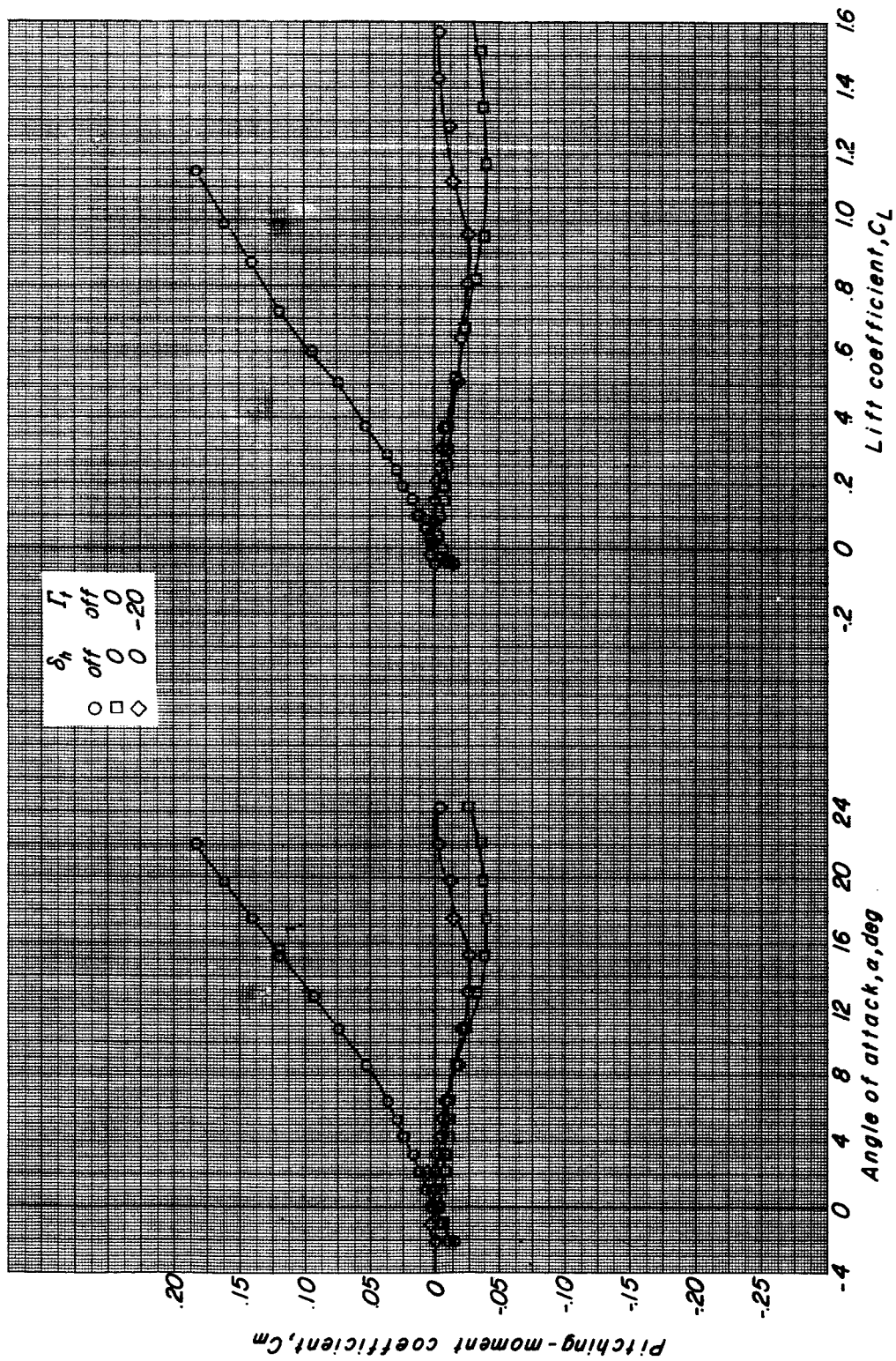
Figure 10.- Concluded.
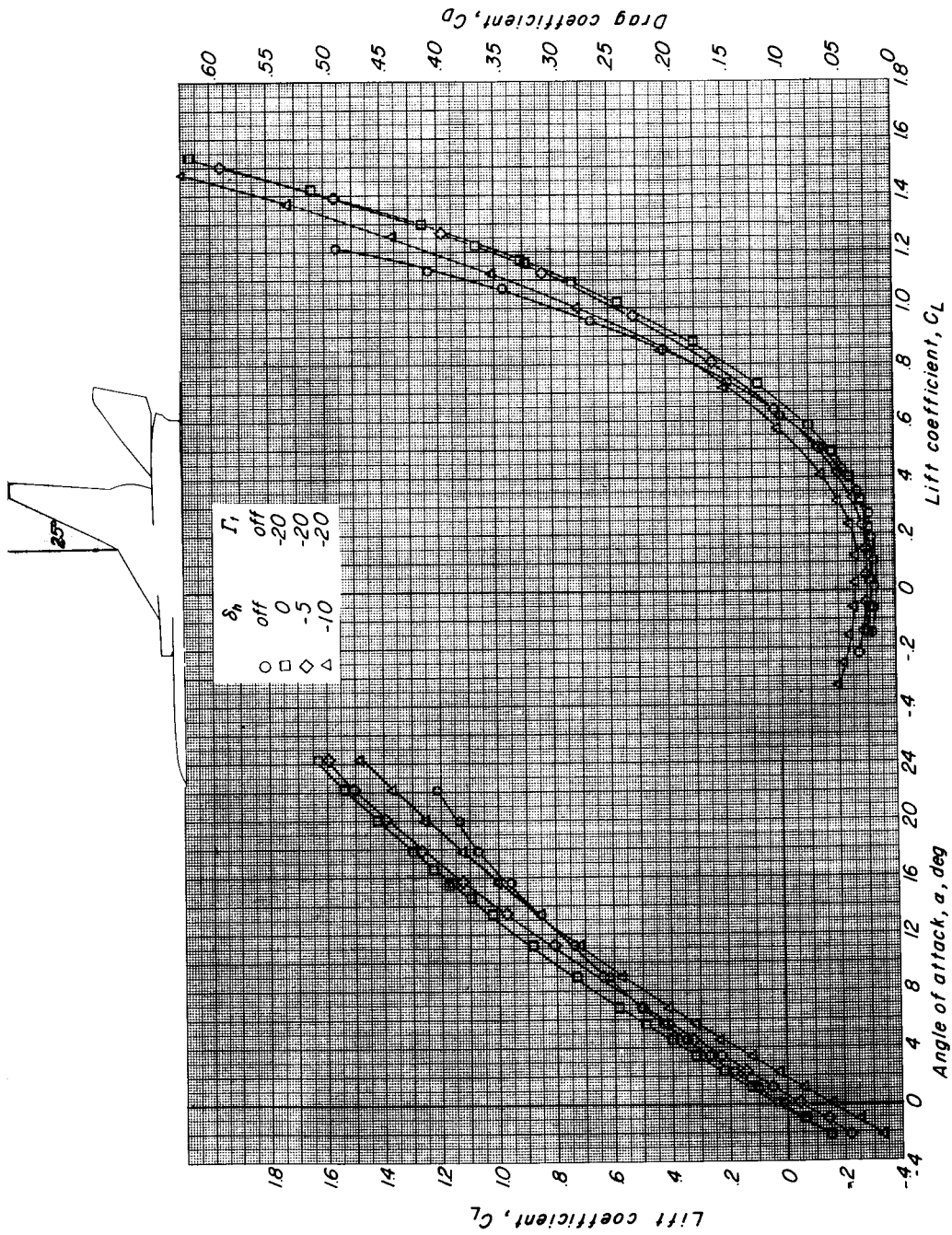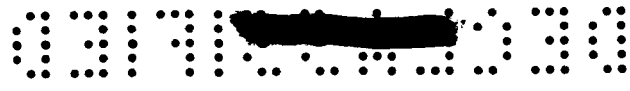
Figure 11.- The effects of horizontal-tail deflection on the longitudinal aerodynamic character-istics of configuration I with canard surface off. $\Lambda_{LE} = 25^\circ$.
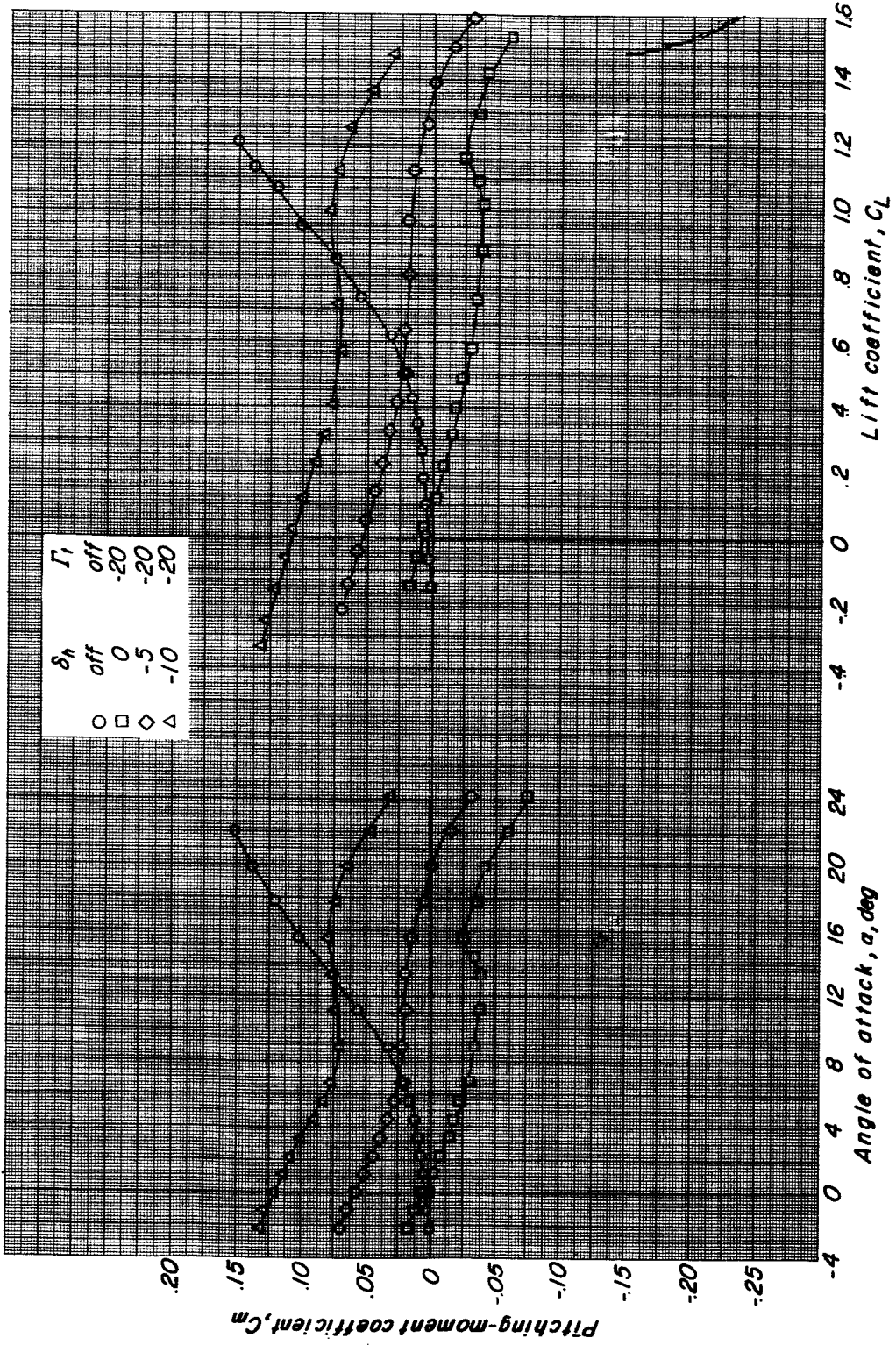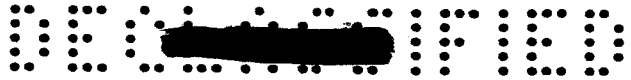
Figure 11.- Concluded.
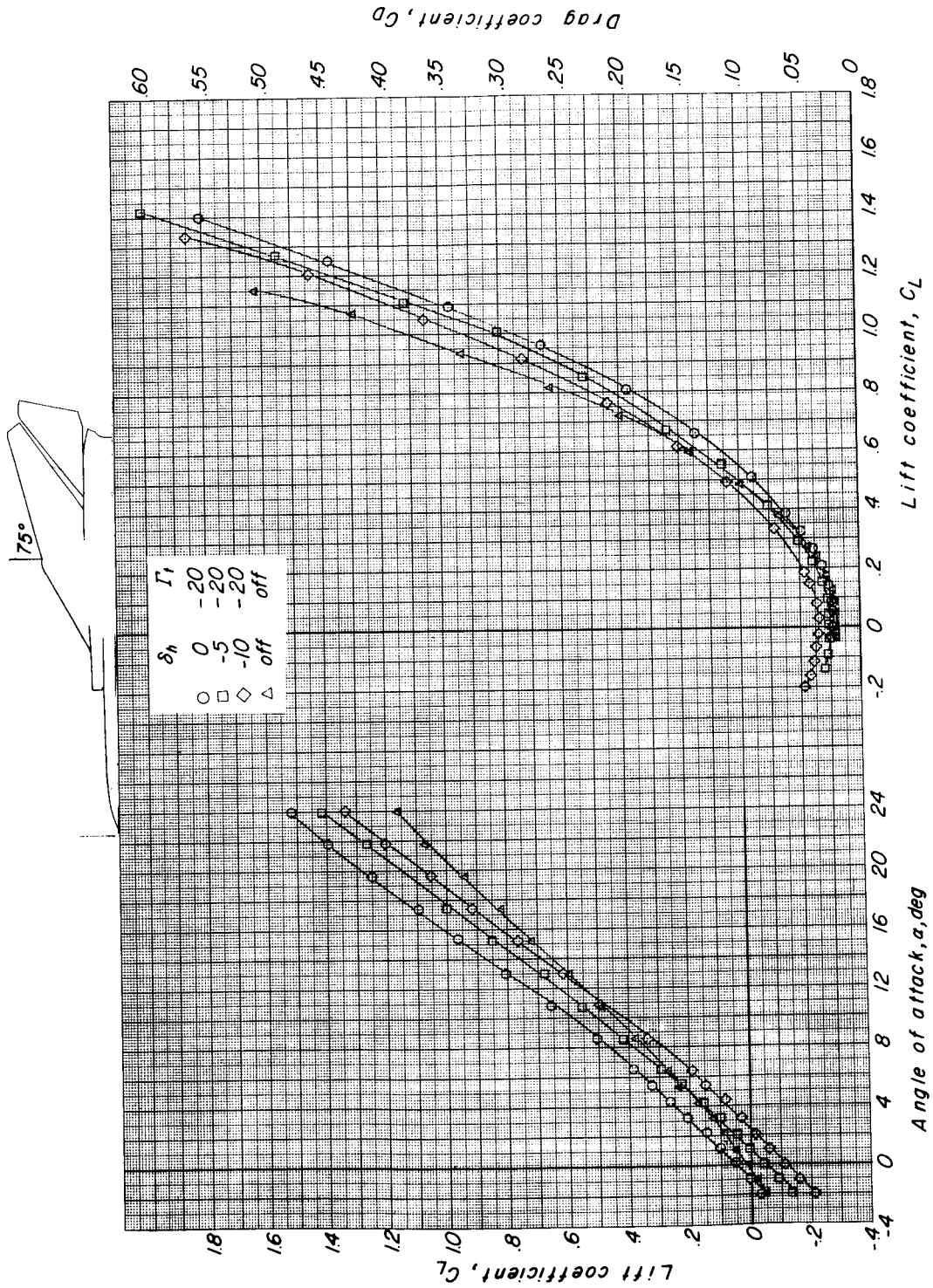
Figure 12.- The effects of horizontal-tail deflection on the longitudinal aerodynamic character-
istics of configuration I with canard surface off. $\Lambda_{LE} = 75°$.

L-1024
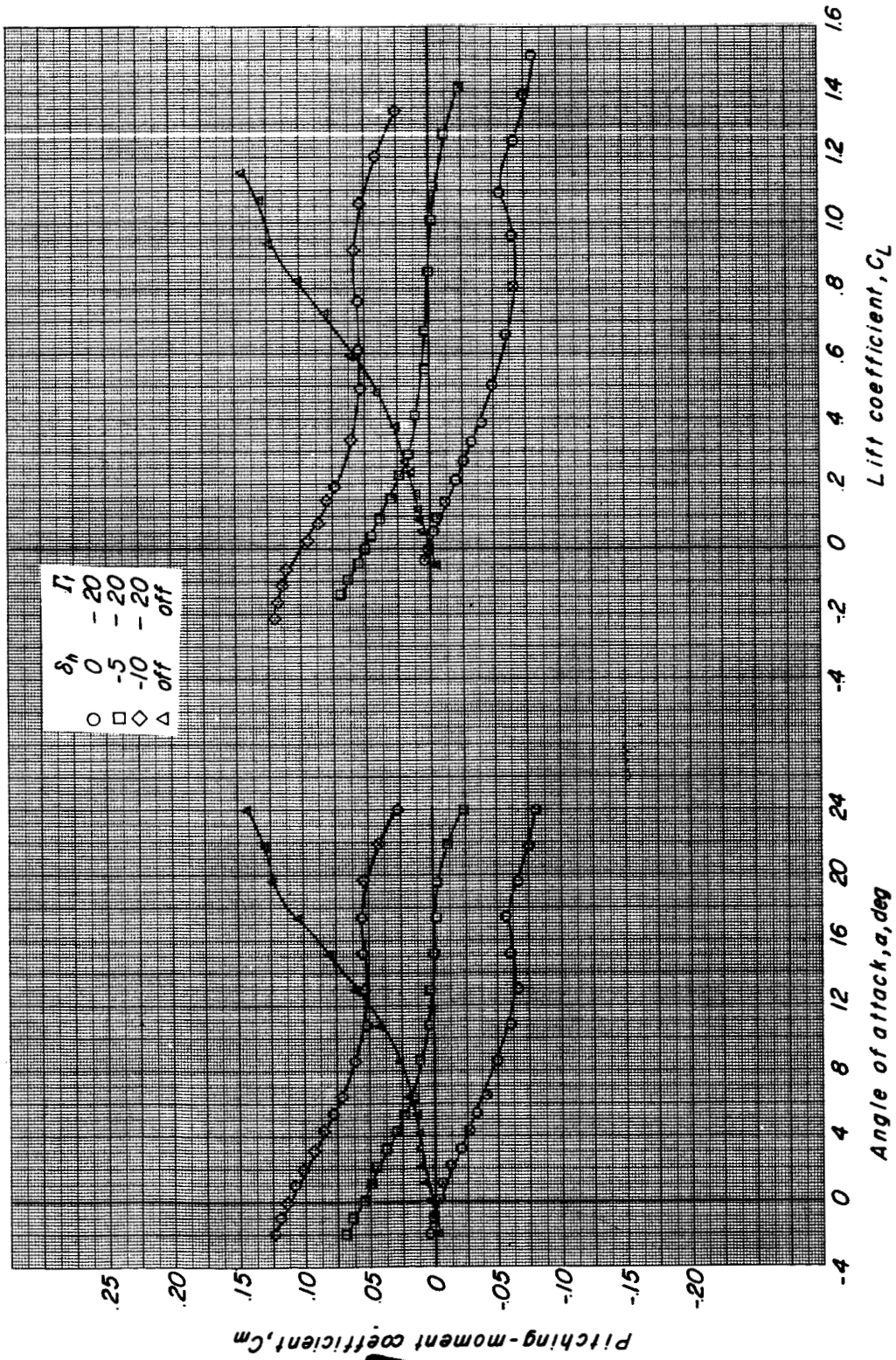
Figure 12.- Concluded.
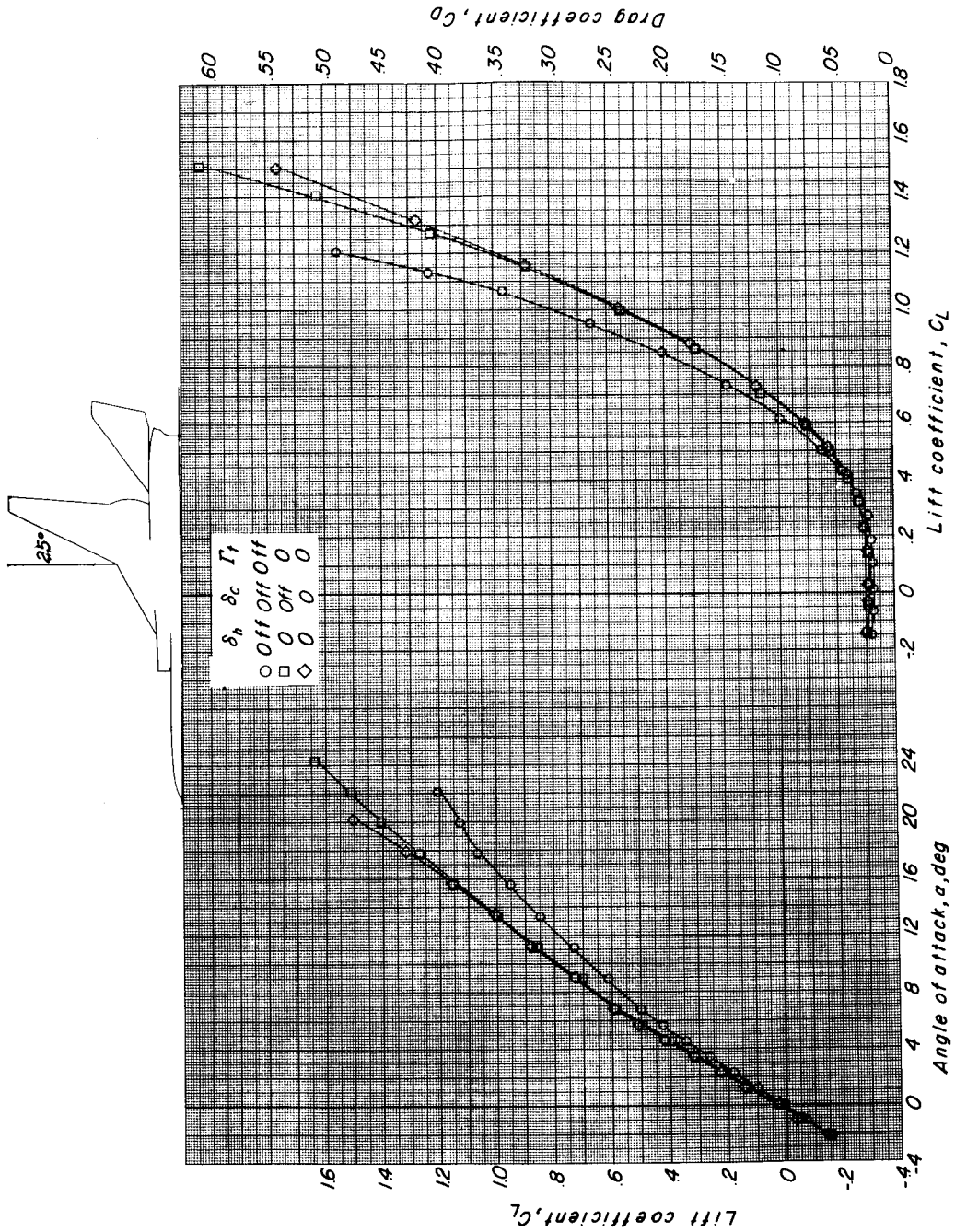
Figure 13.- Longitudinal aerodynamic characteristics of the various component parts of configu-
ration I with 0° control deflection. $\Lambda_{LE} = 25°$.

L-1024
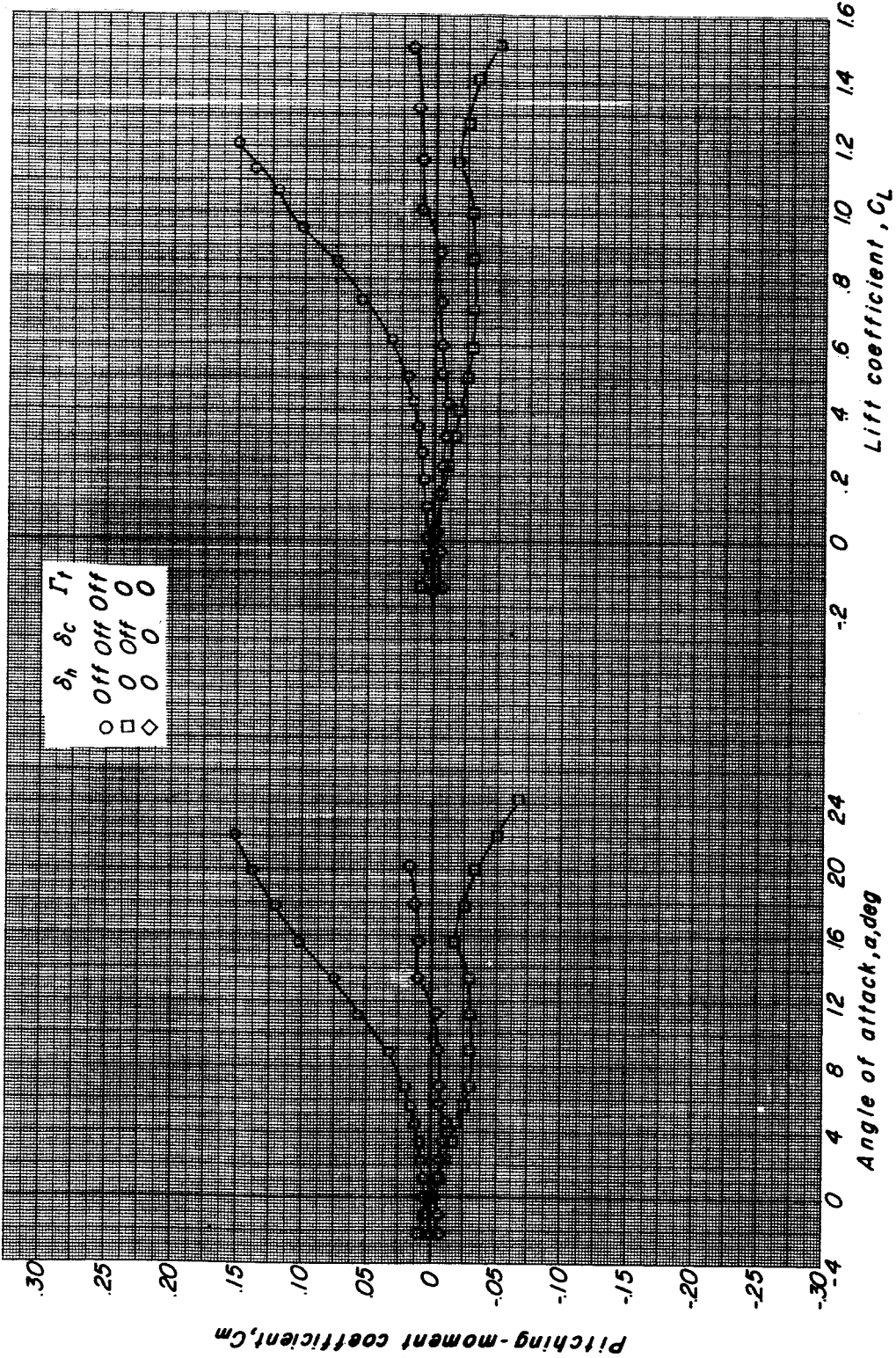
Figure 13.- Concluded.

L-1024
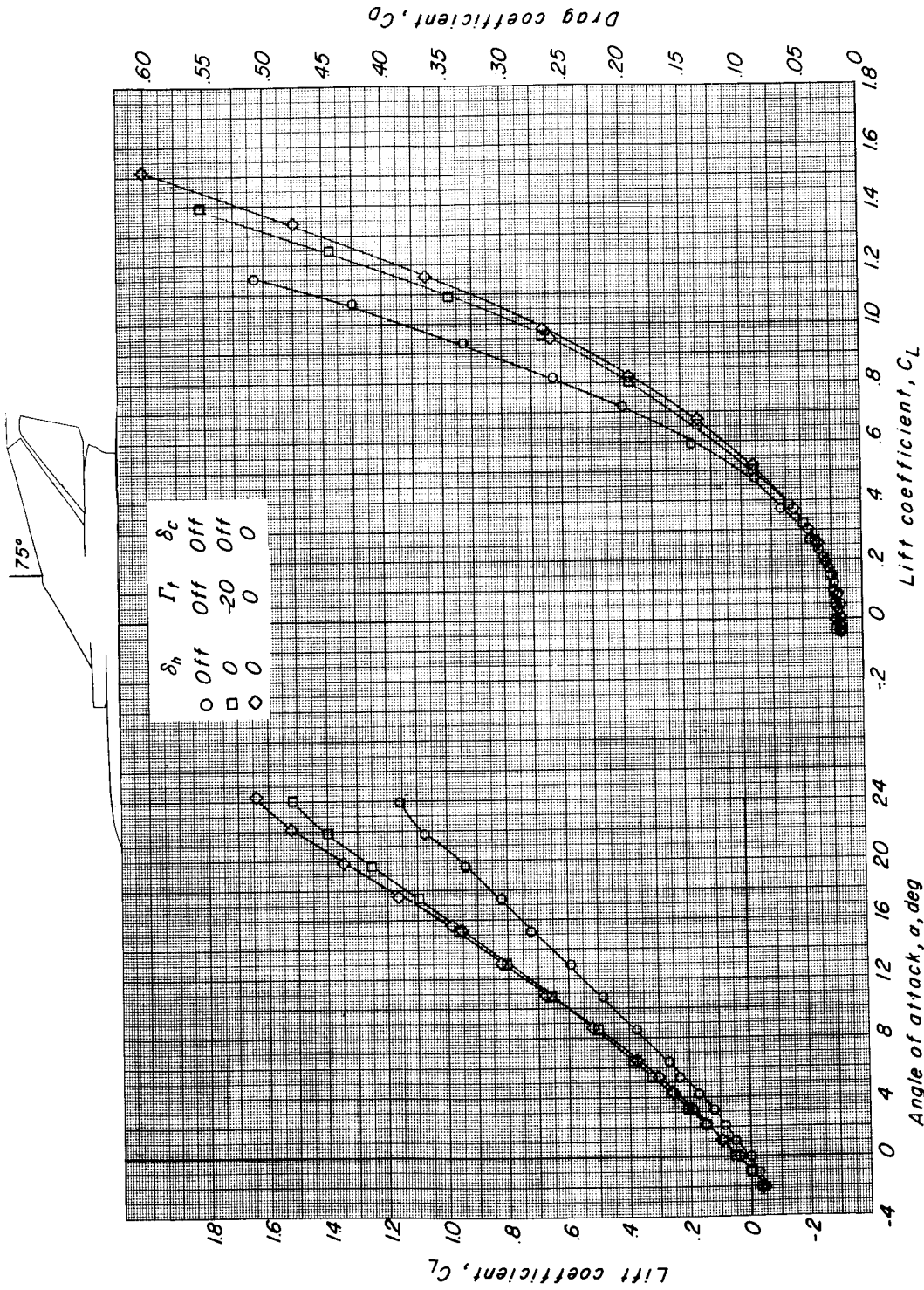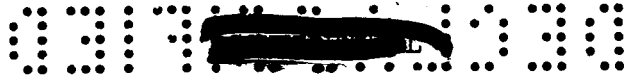
Figure 14.- Longitudinal aerodynamic characteristics of the various component parts of configuration I. $\Lambda_{LE} = 75°$.

L-1024
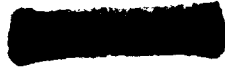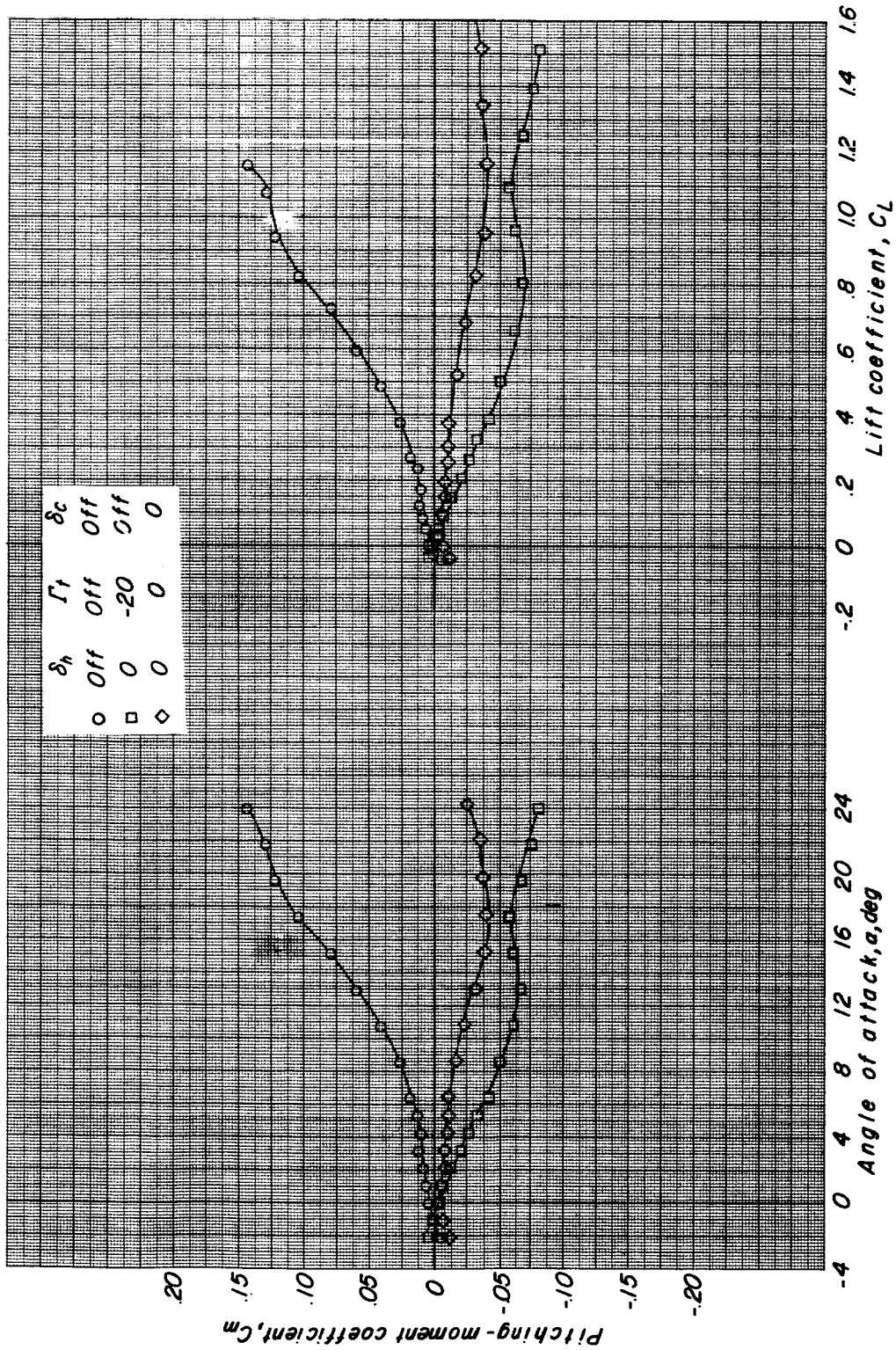
Figure 14.- Concluded.
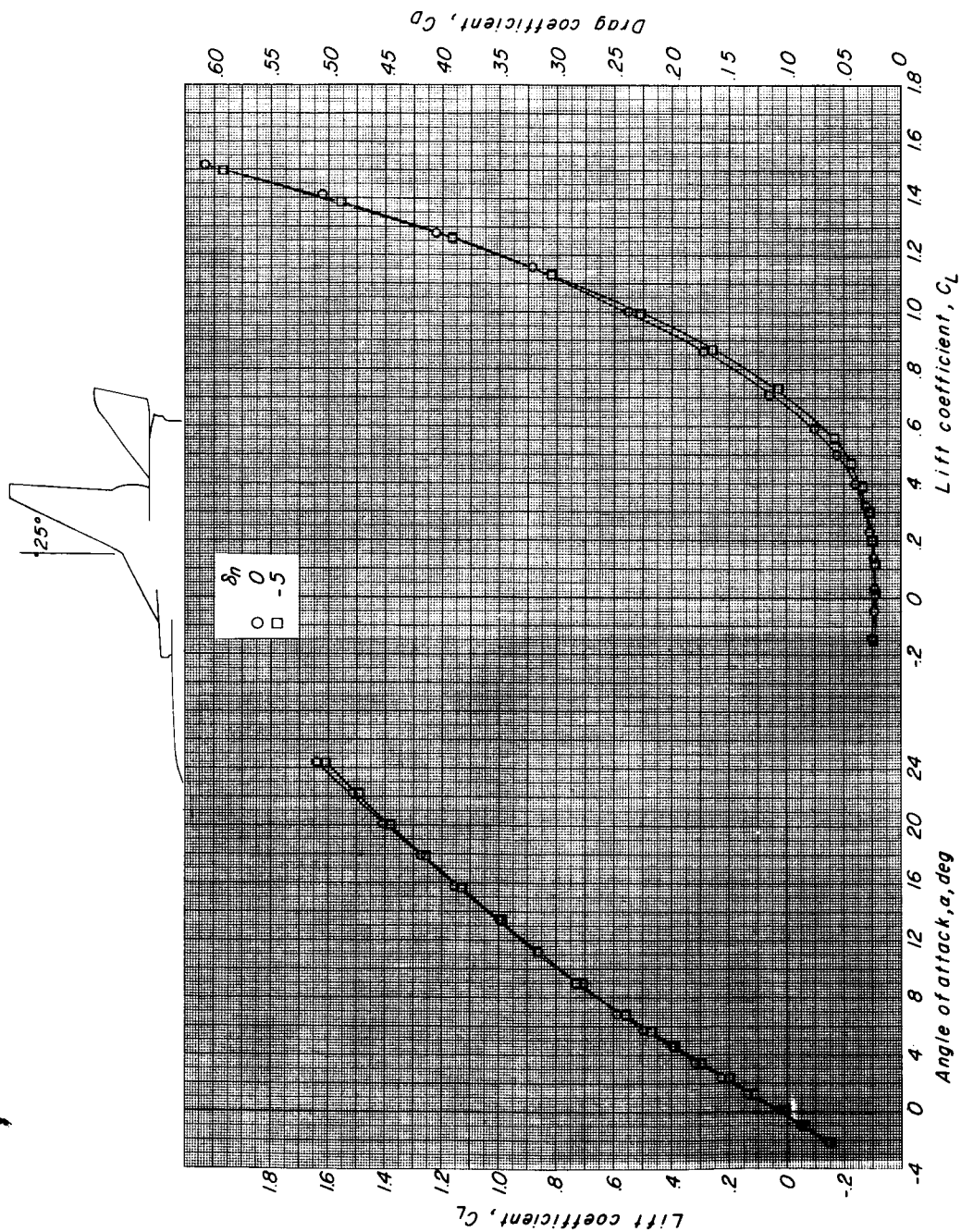
Figure 15.- Longitudinal aerodynamic characteristics of configuration I with canard surface off and horizontal tail on. $\delta_n = 0^\circ$ and -5°; $\delta_h = 0^\circ$; $\Gamma_t = 0^\circ$.
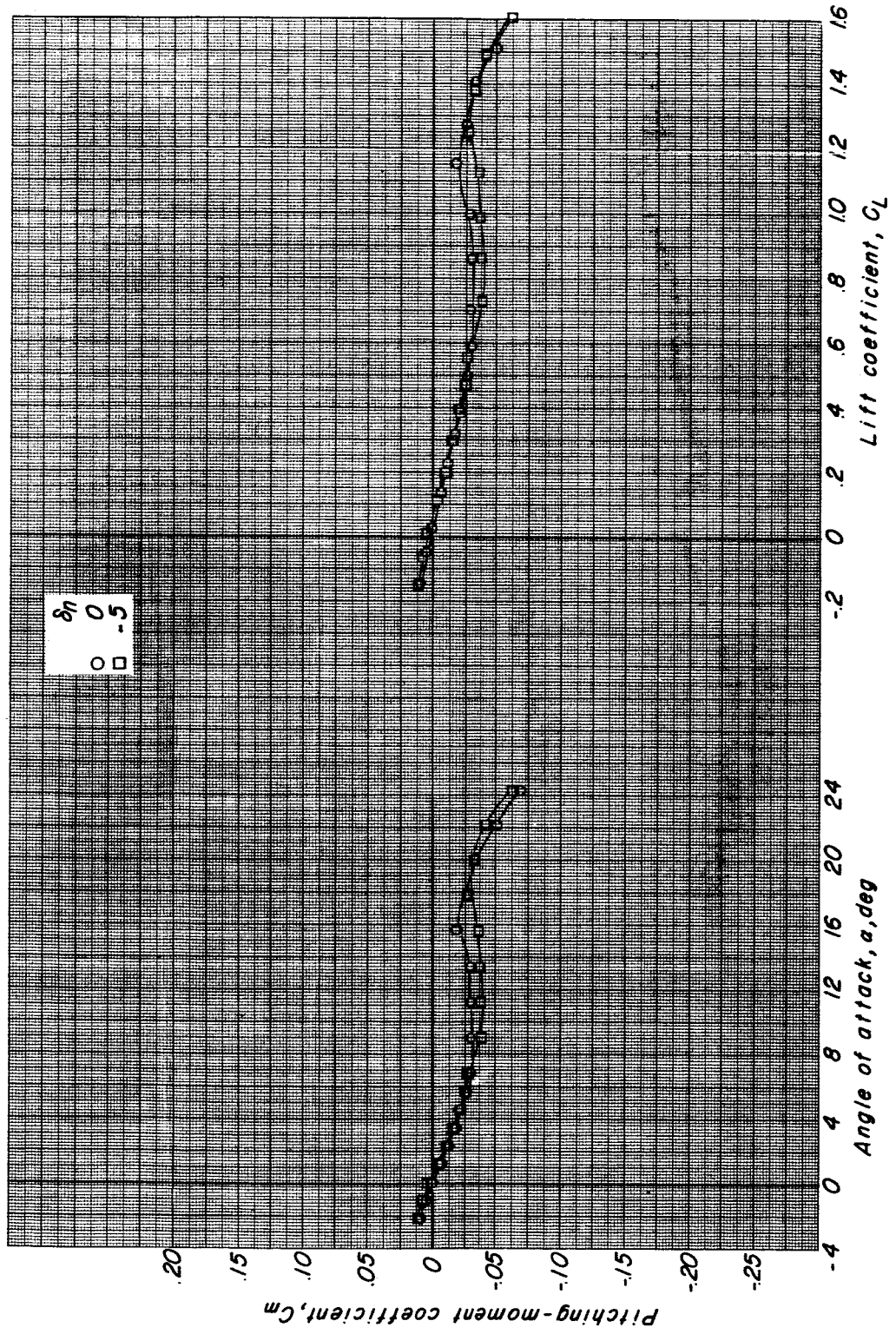
Figure 15.- Concluded.
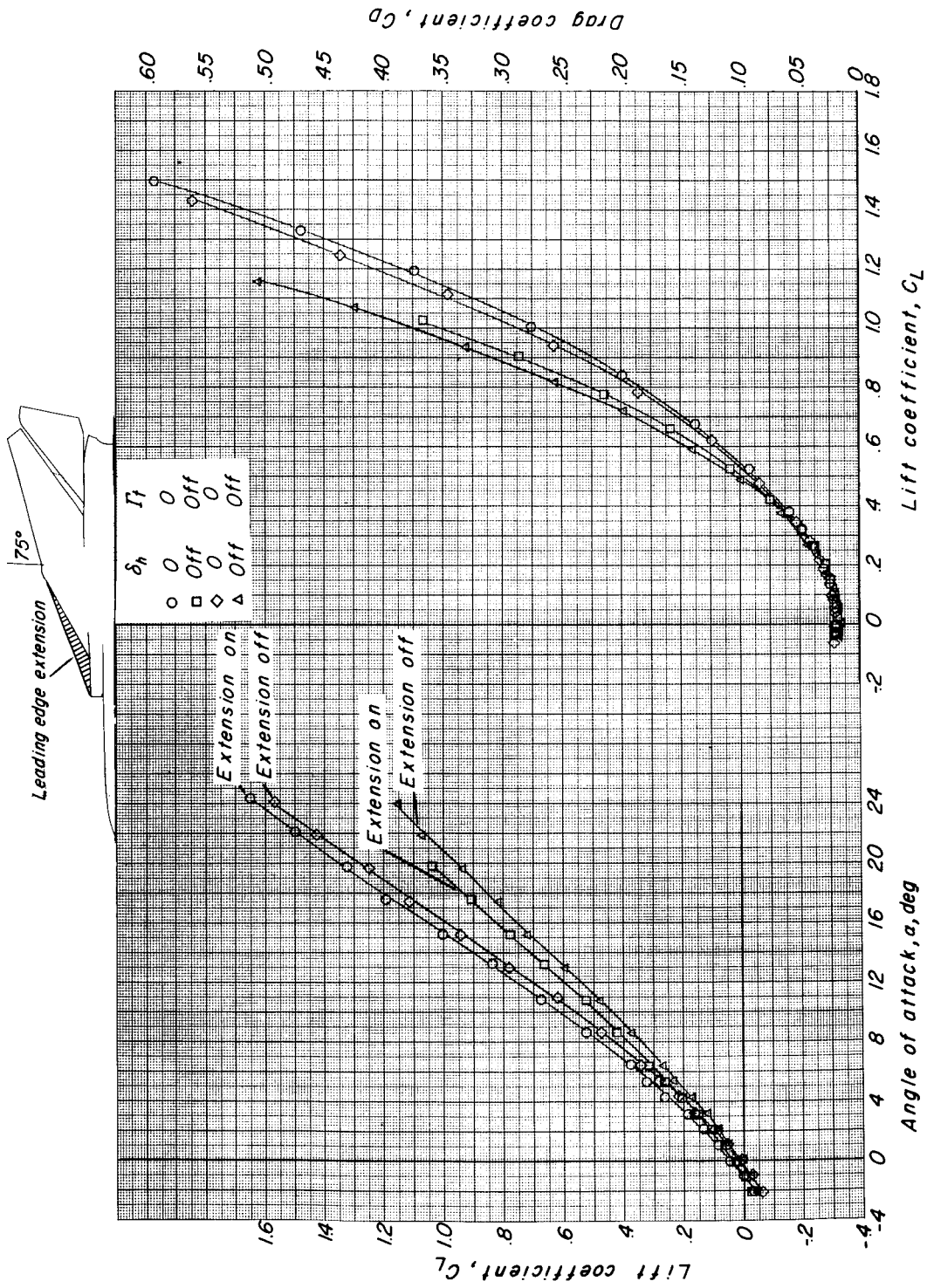
Figure 16.- The effects on the longitudinal aerodynamic characteristics of adding a wing leading-edge extension to the fixed portion of configuration I with canard surface off. $\Lambda_{LE} = 75°$.

L-1024

Figure 16.- Concluded.

		δ_h	Γ_t	δ_c
○	WBT	0	0	Off
◻	WBCT	0	0	0
◇	WBCT	0	0	0
△	WBT	0	0	Off

C_{Y_β}

Vertical tail off

Vertical tail on

C_{n_β}

Vertical tail on

Vertical tail off

C_{l_β}

Vertical tail on

Vertical tail off
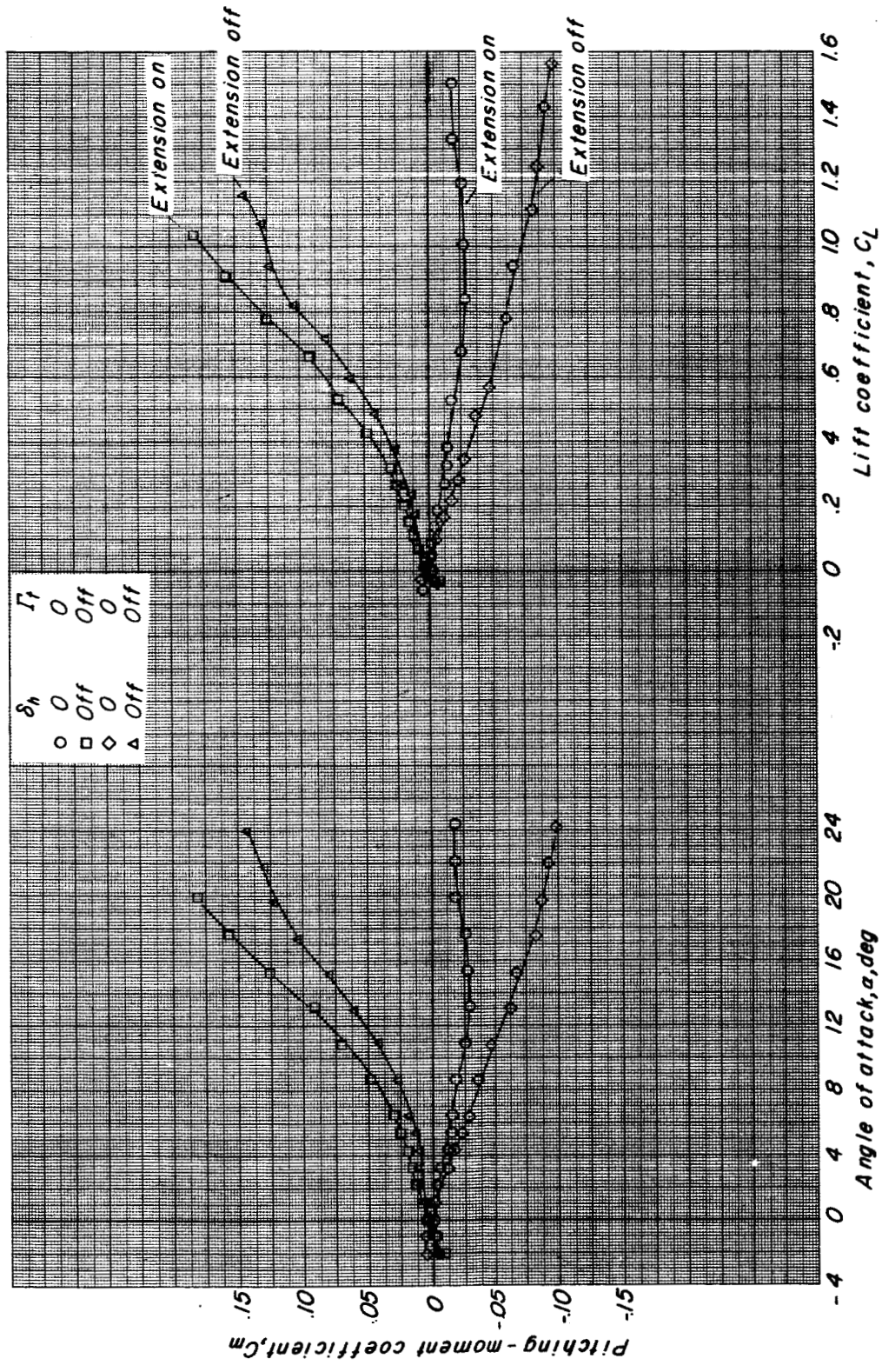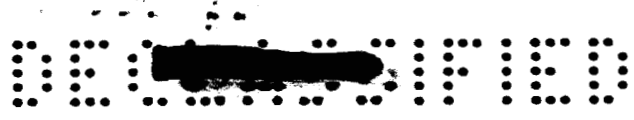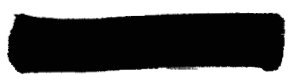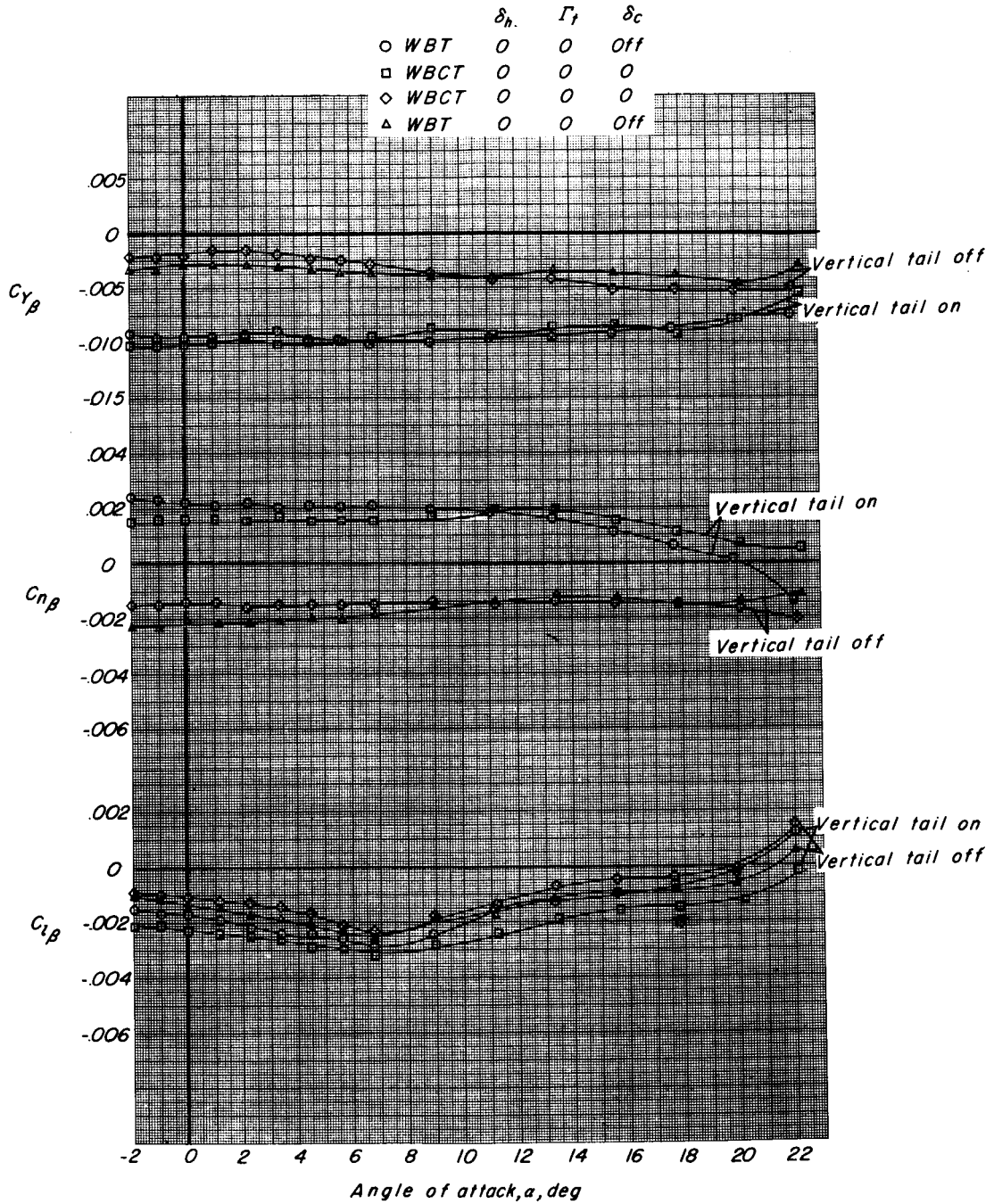
Angle of attack, a, deg

Figure 17.- Variation of sideslip derivatives with angle of attack for the various parts of configuration I. $\Lambda_{LE} = 25^o$.

L-1024

	δ_h	Γ_t	δ_c
○ WBT	0	0	Off
□ WBCT	0	0	0
◇ WBCT	0	0	0
△ WBT	0	0	Off
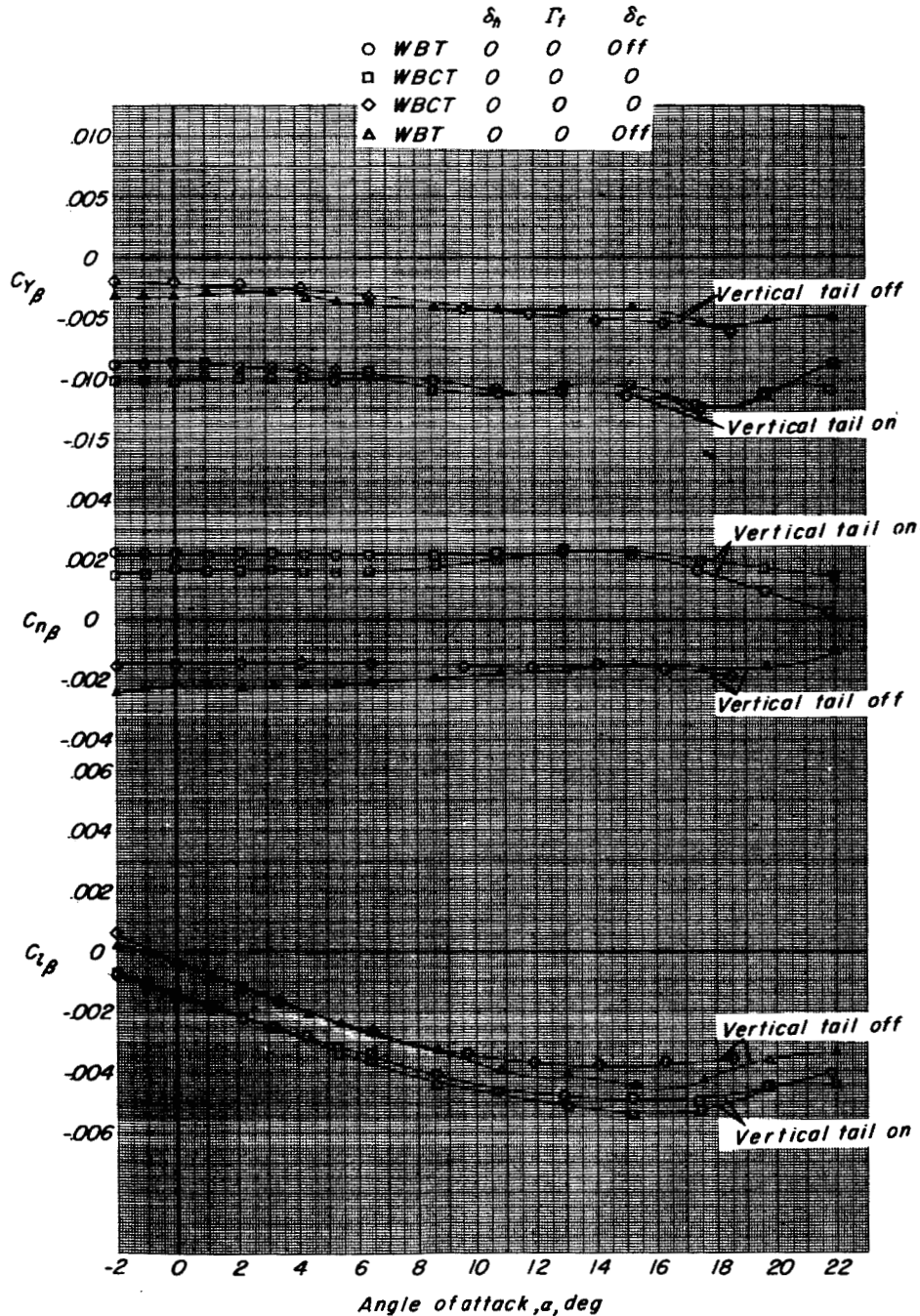
Figure 18.- Variation of sideslip derivatives with angle of attack for the various component parts of configuration I. $\Lambda_{LE} = 75°$.

I-1024
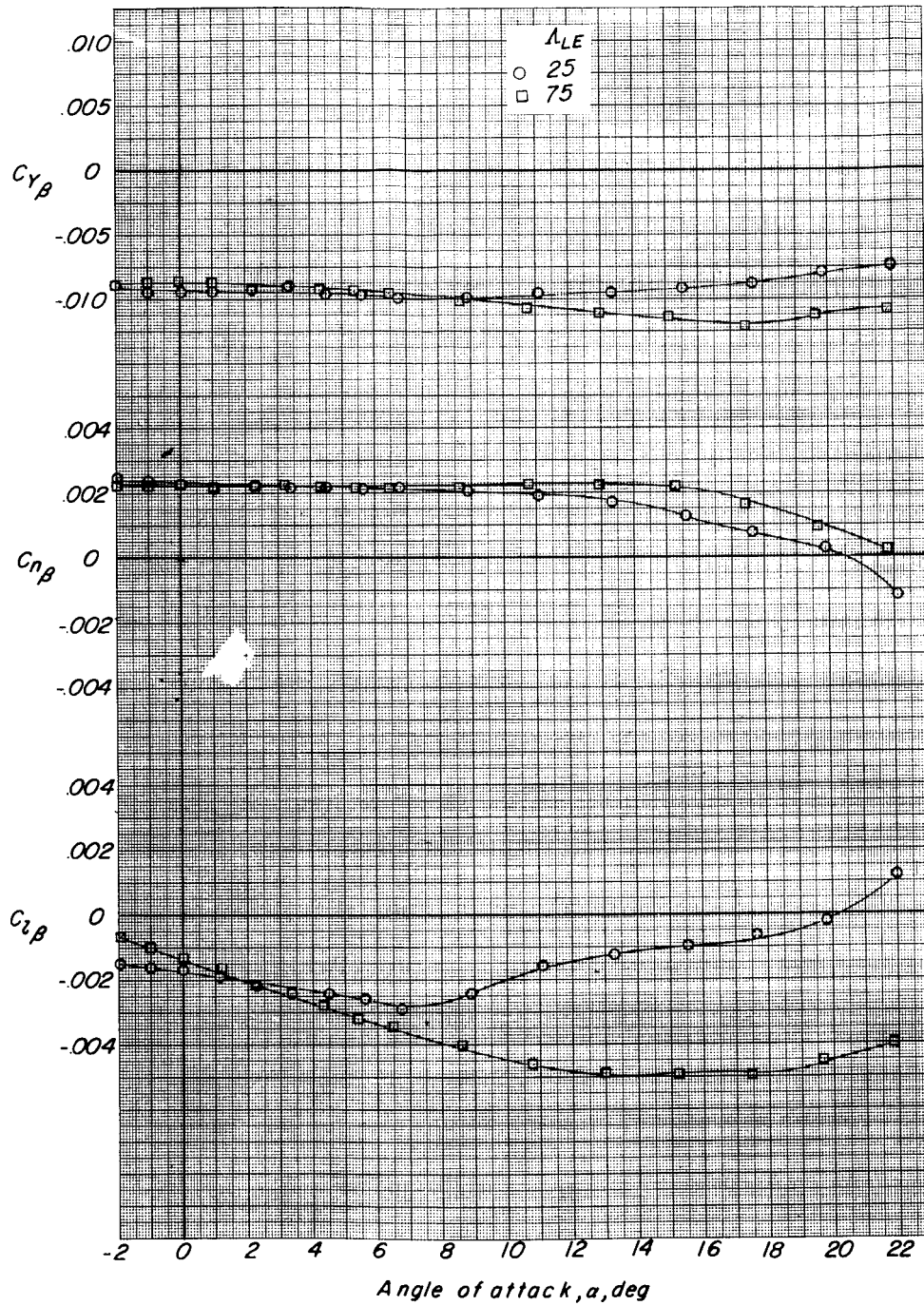
Figure 19.- Variation of sideslip derivatives with angle of attack for configuration I with canard surface off and horizontal tail on. $\Lambda_{LE} = 25^\circ$ and 75°.
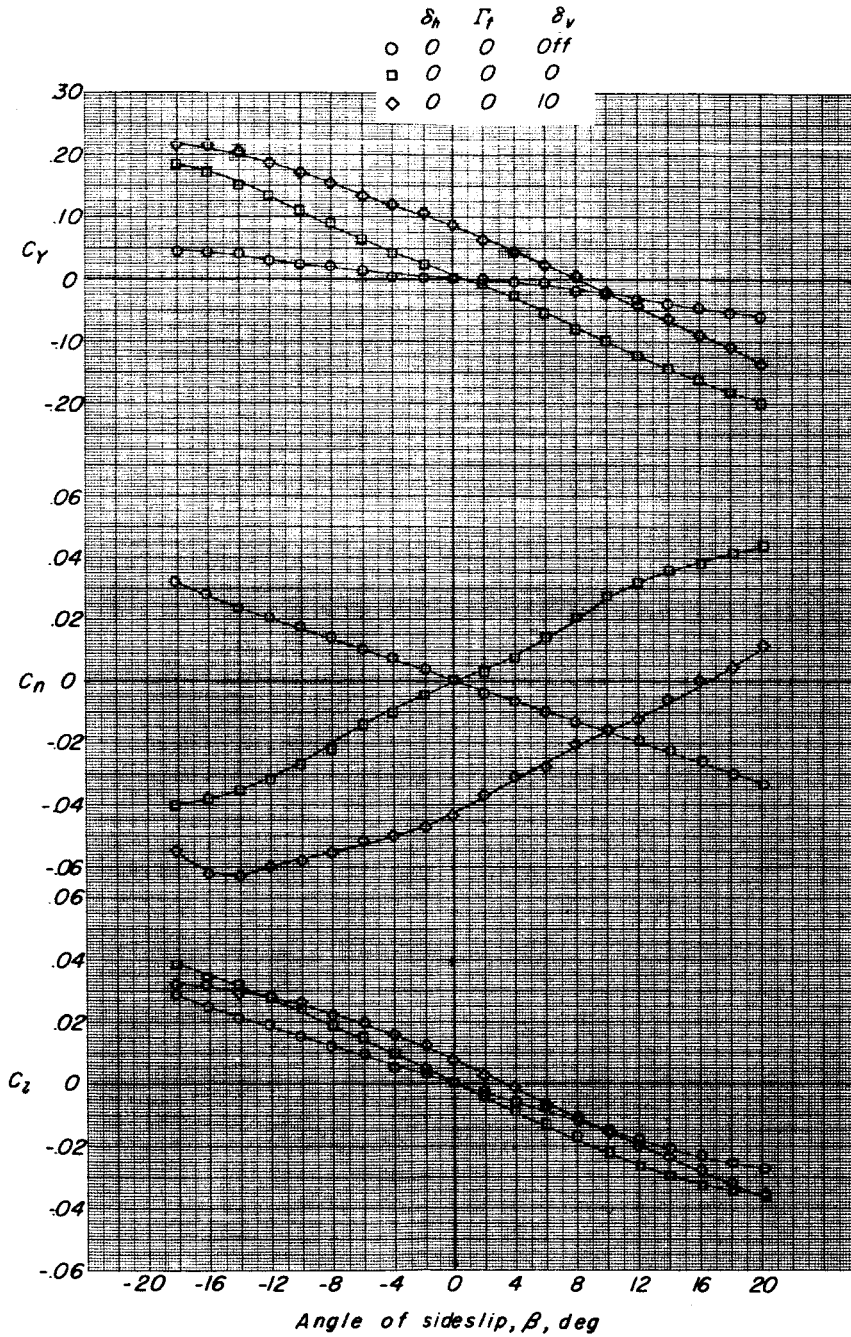
Figure 20.- Effect of vertical tail on the lateral aerodynamic characteristics of configuration I with canard surface off; $\Lambda_{LE} = 75^{\circ}$; $\alpha \approx 4.0^{\circ}$.
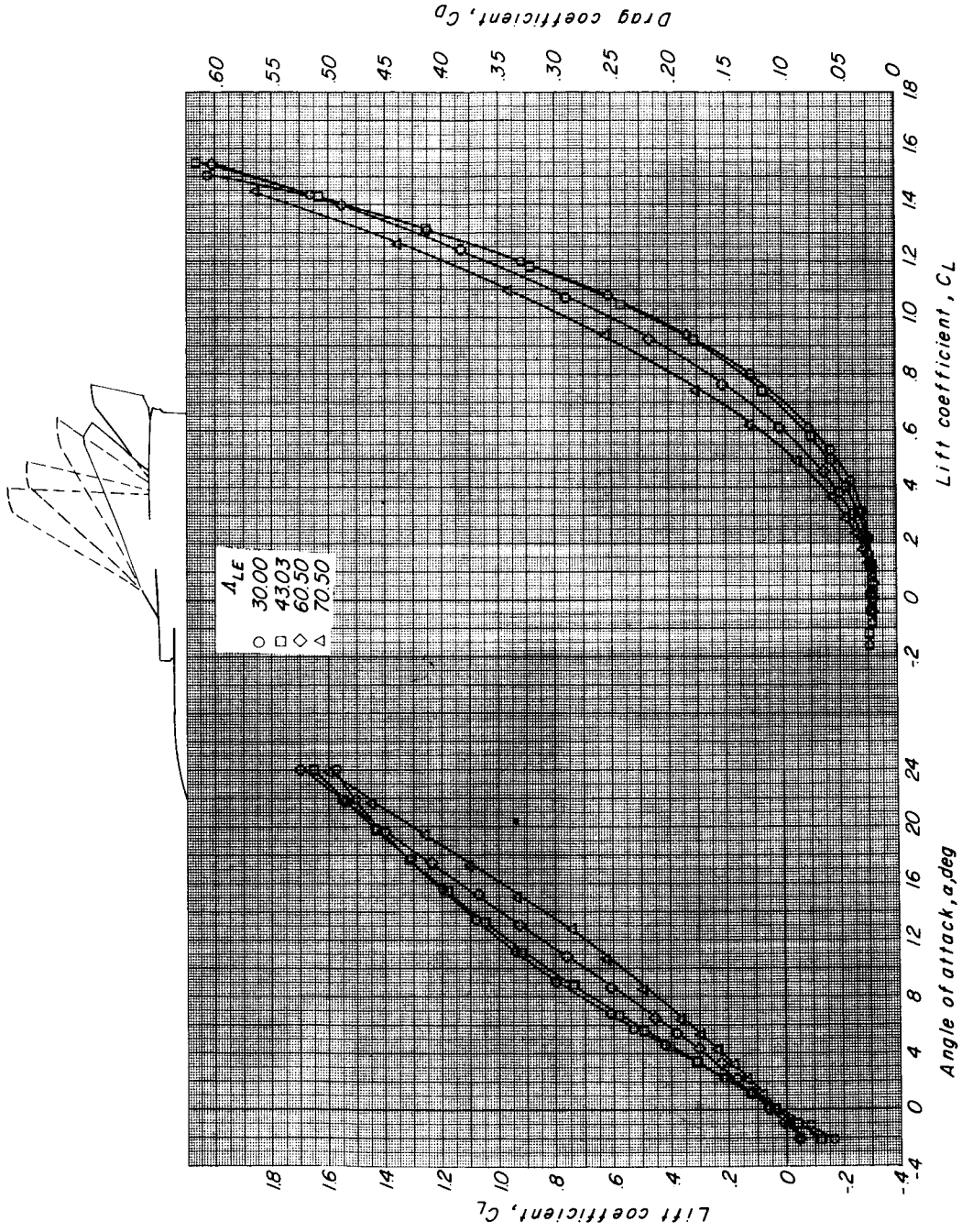
Figure 21.- The effects of wing sweep on the longitudinal aerodynamic characteristics of configuration II with canard surface off and horizontal tail on. $\Gamma_t = 0^\circ$; $\delta_h = 0^\circ$.
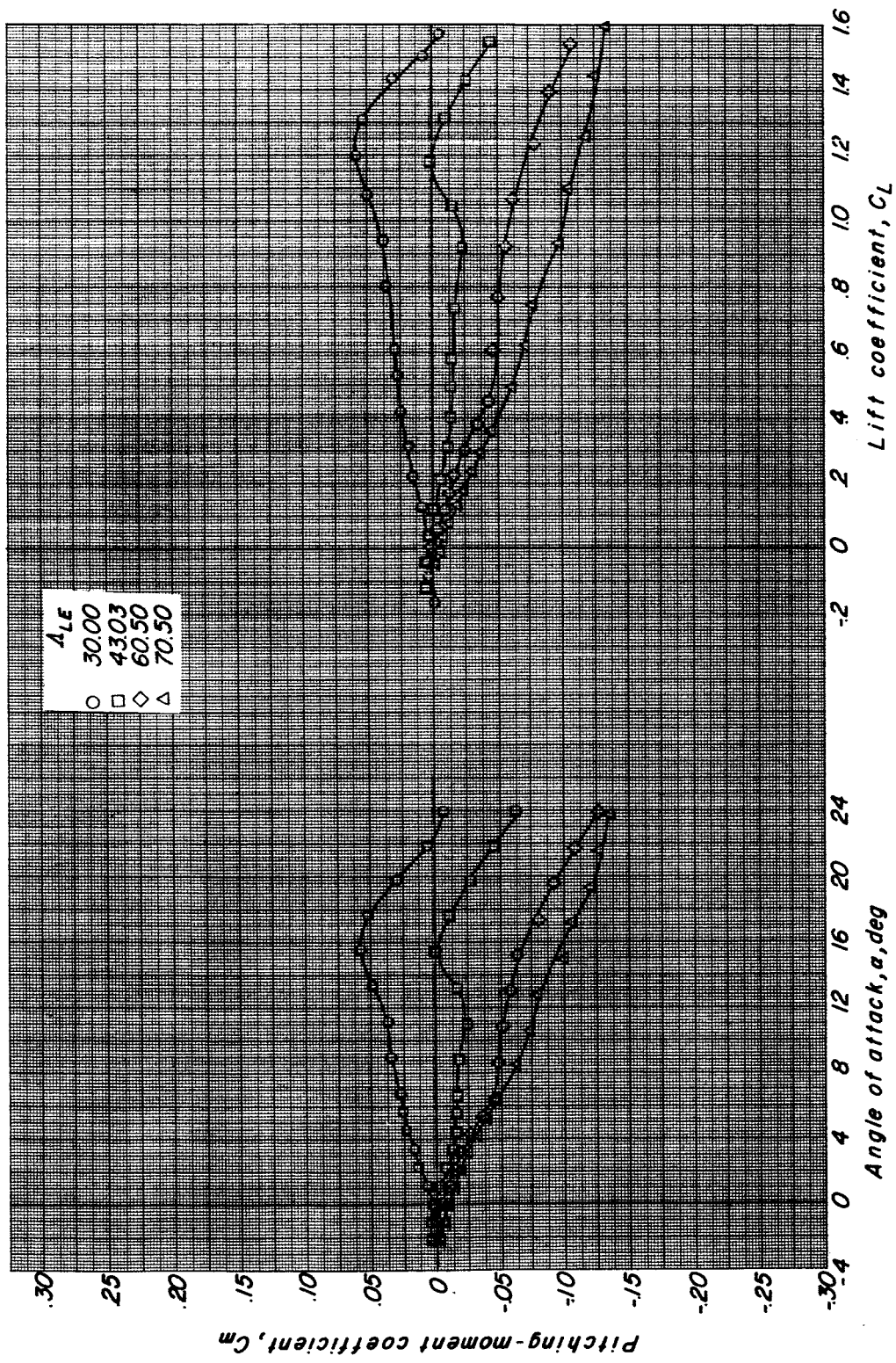
Figure 21.- Concluded.
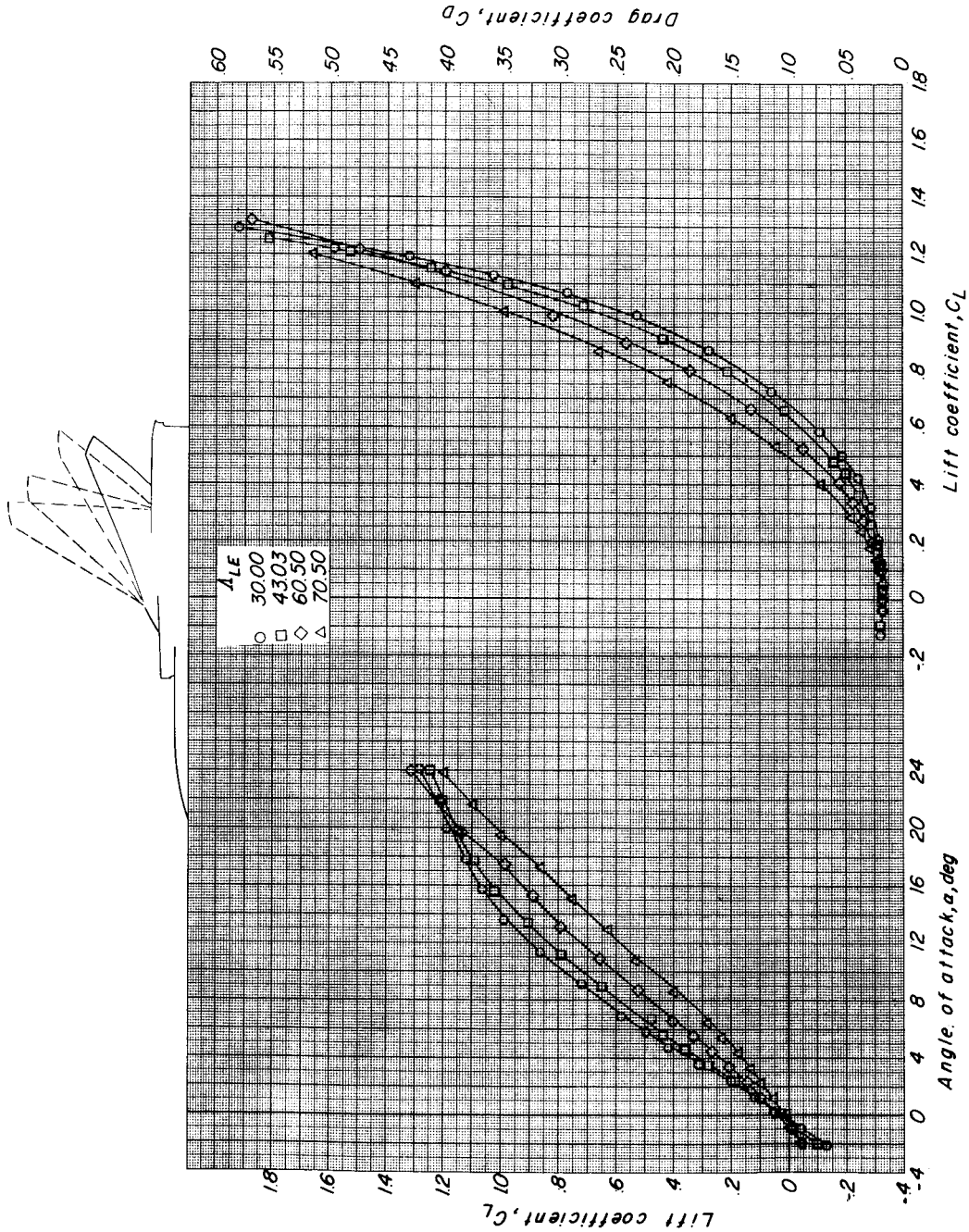
Figure 22.- The effects of wing sweep on the longitudinal aerodynamic characteristics of configuration II with both canard surface and horizontal tail off.
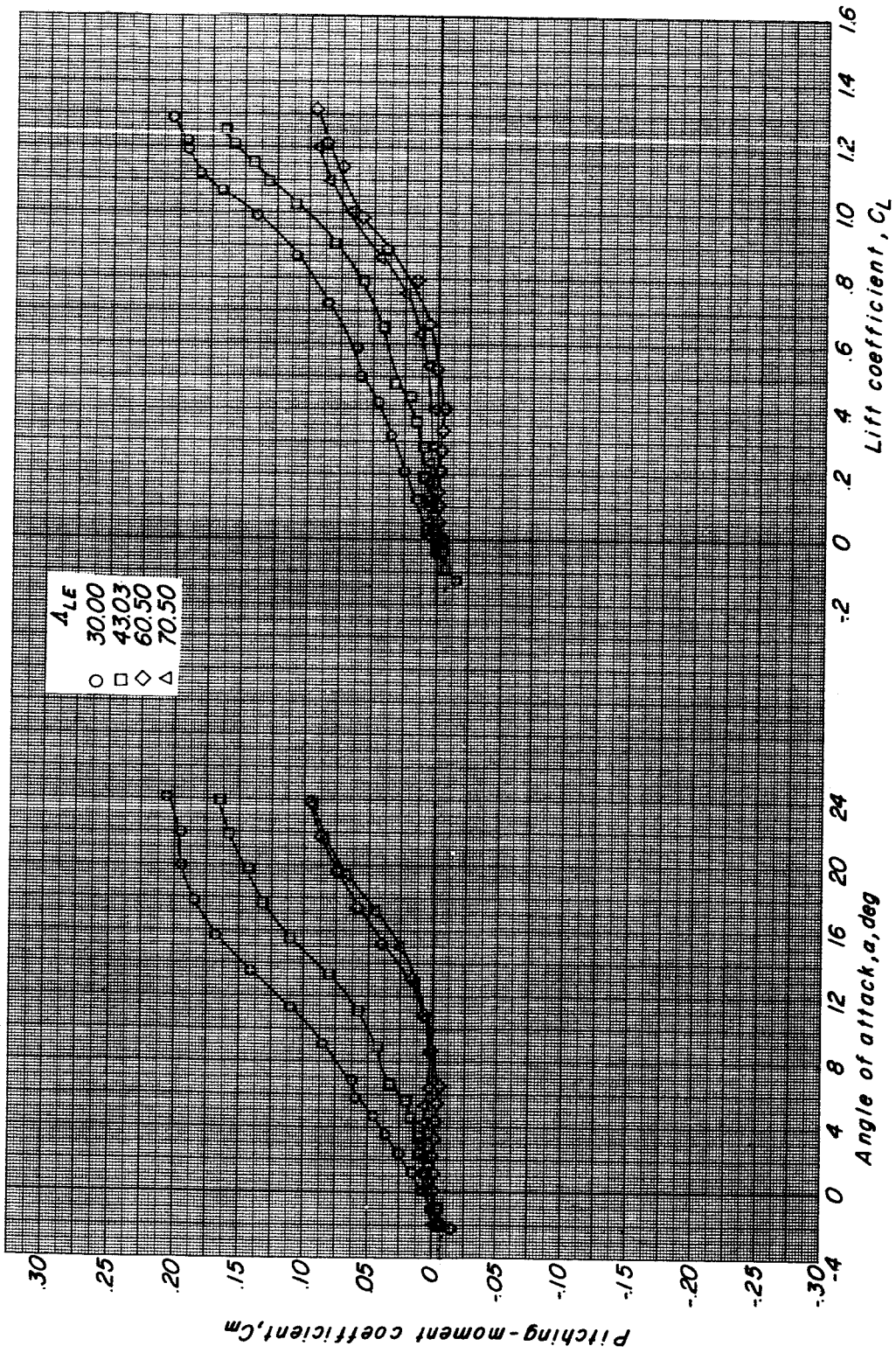
Figure 22.- Concluded.
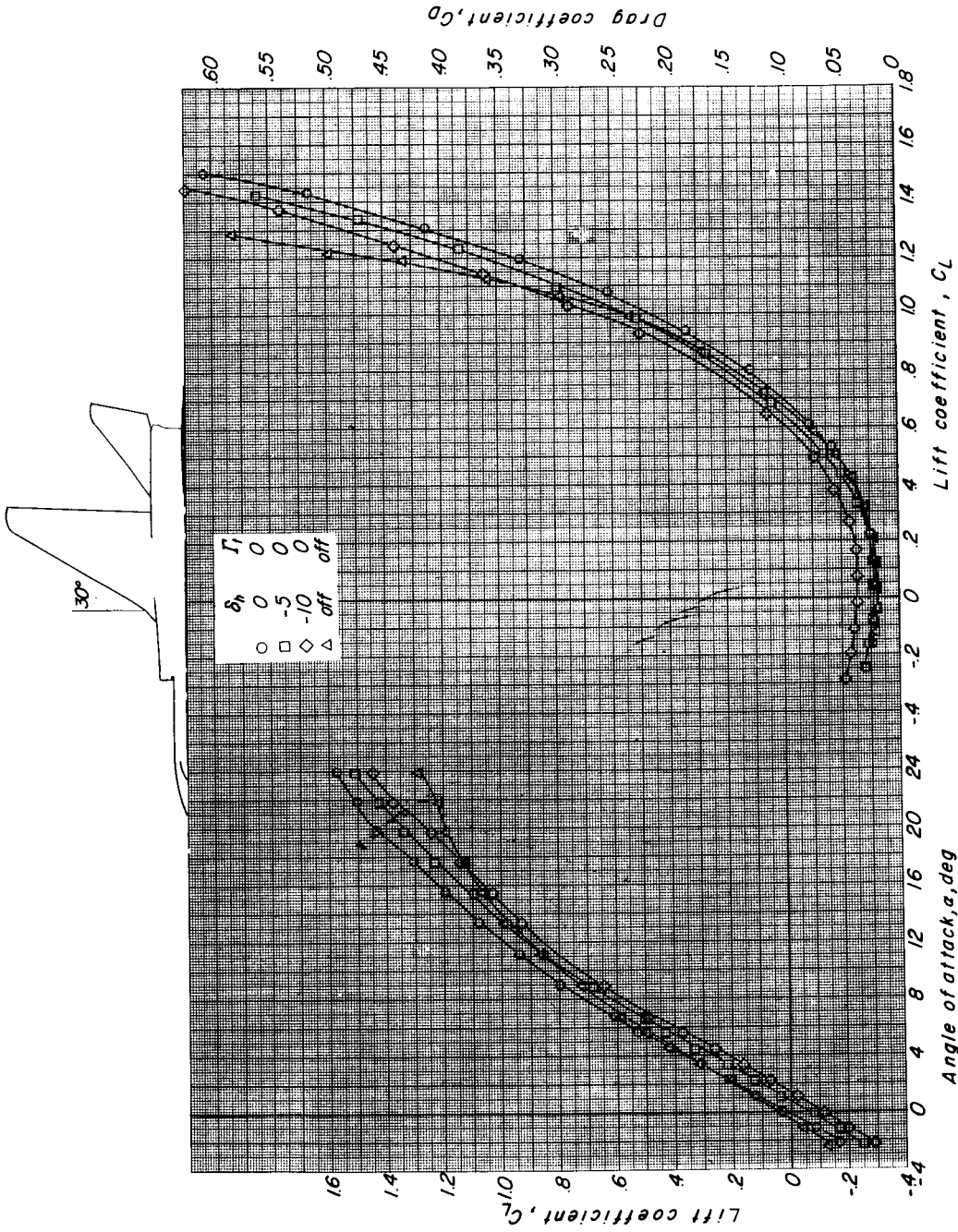
Figure 23.- The effects of horizontal-tail deflection on the longitudinal aerodynamic character-
istics of configuration II with canard surface off. Λ_{LE} = 30.00°.
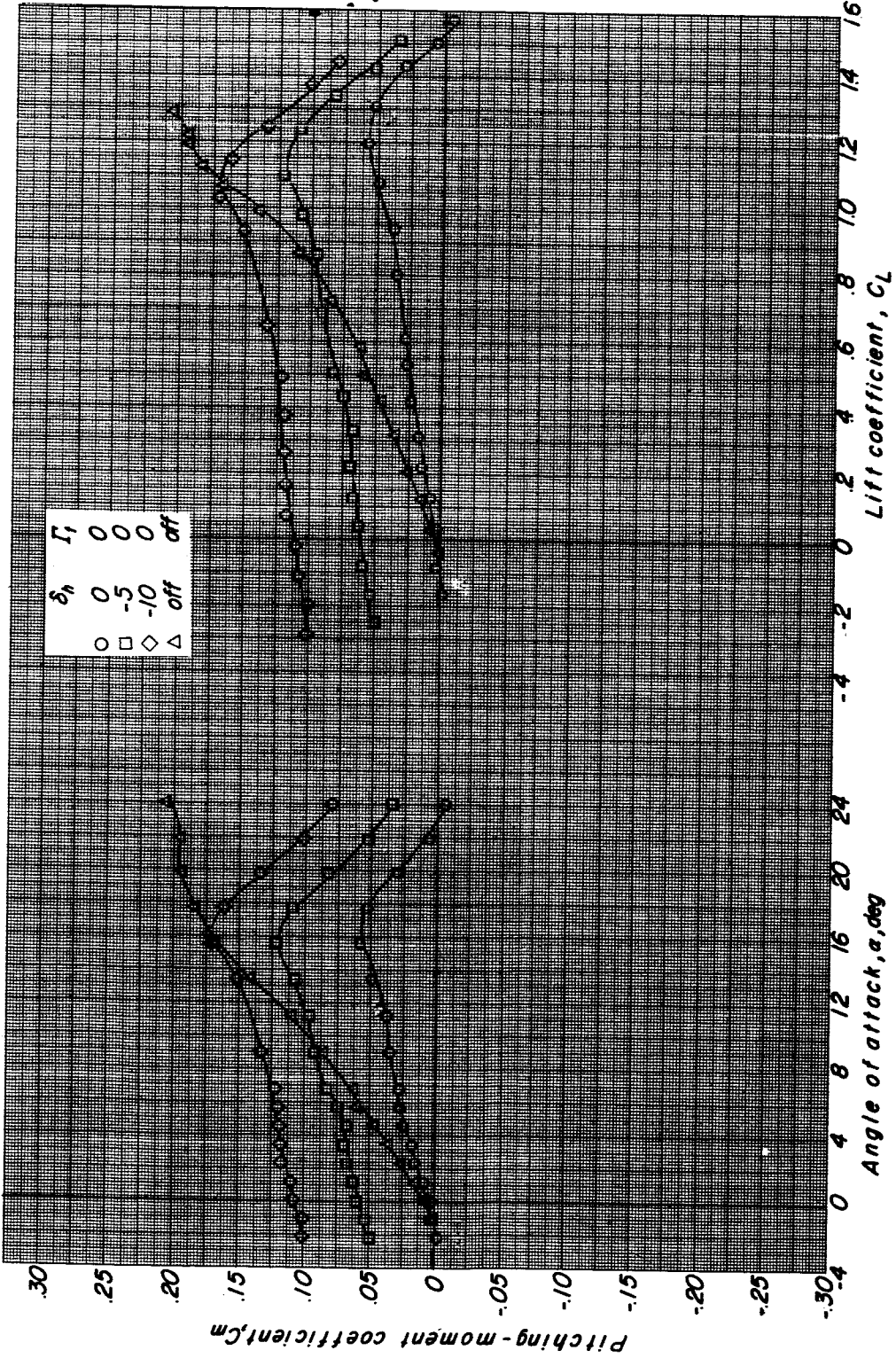
Figure 23.- Concluded.
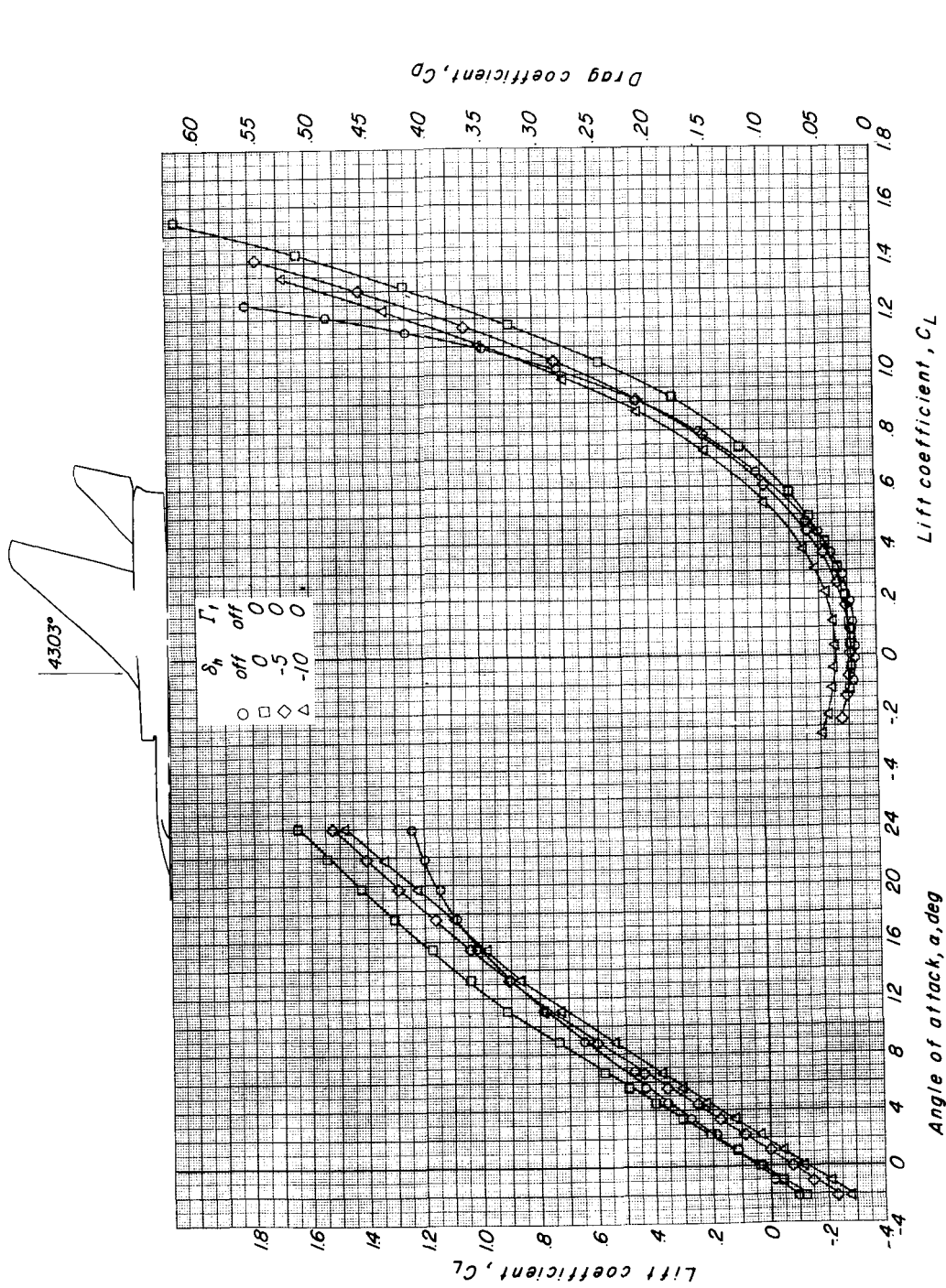
Figure 24.- The effects of horizontal-tail deflection on the longitudinal aerodynamic character-istics of configuration II with canard surface off. $\Lambda_{LE} = 43.03^\circ$.

L-1024
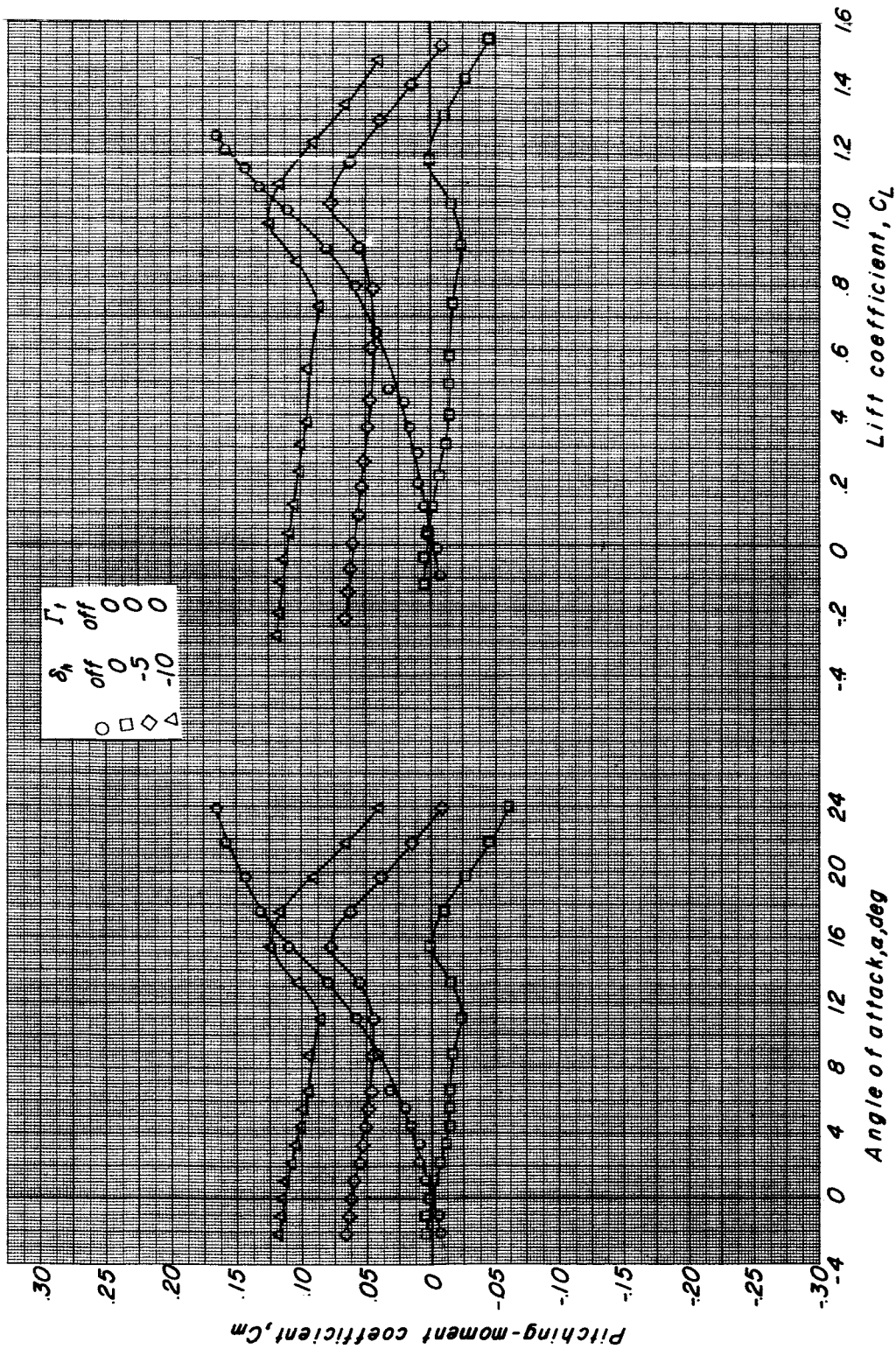
Figure 24.- Concluded.
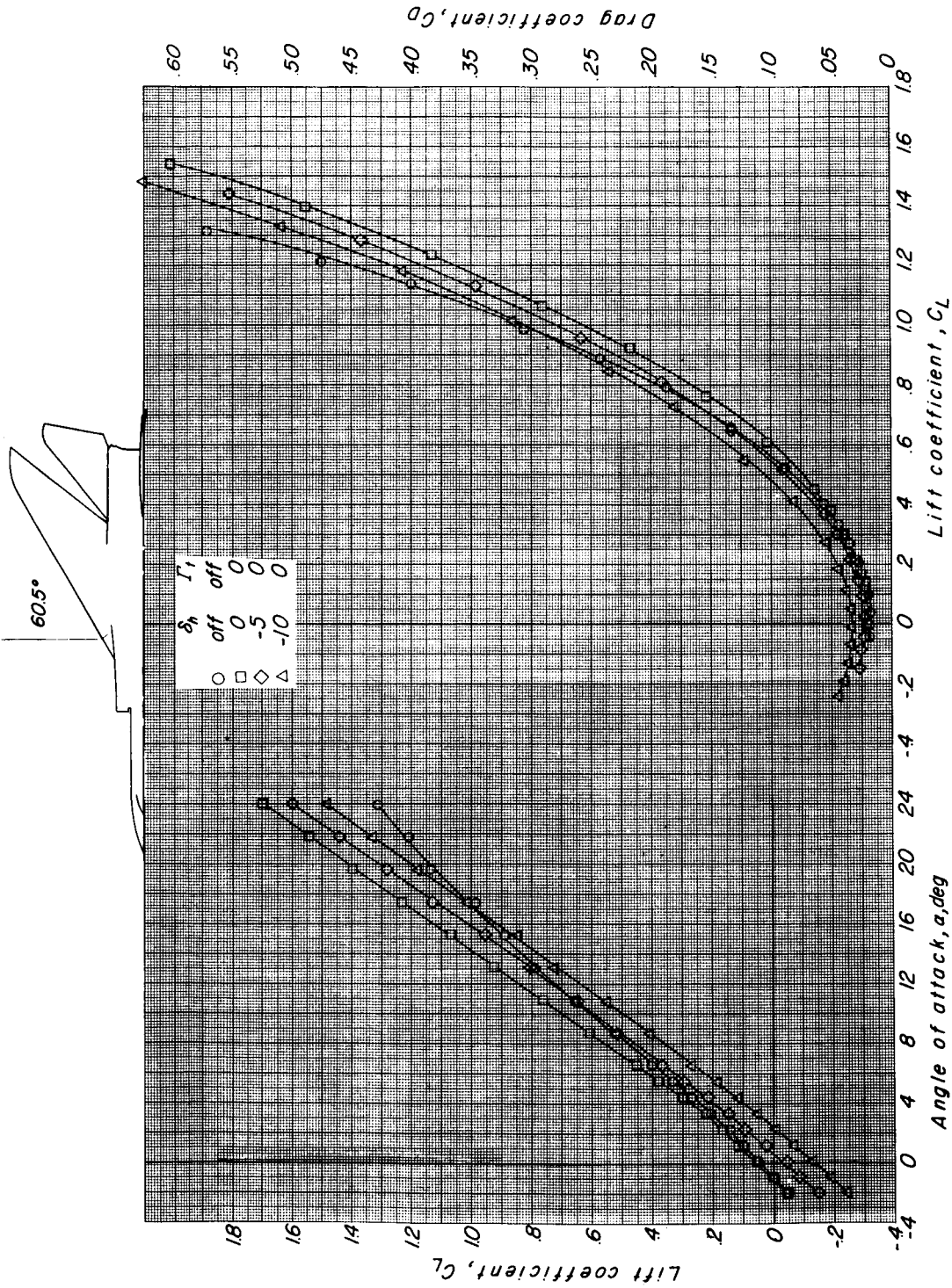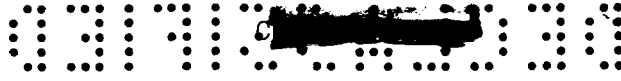
Figure 25.- The effects of horizontal-tail deflection on the longitudinal aerodynamic characteristics of configuration II with canard surface off. $\Lambda_{LE} = 60.50°$; $\Gamma_t = 0°$.
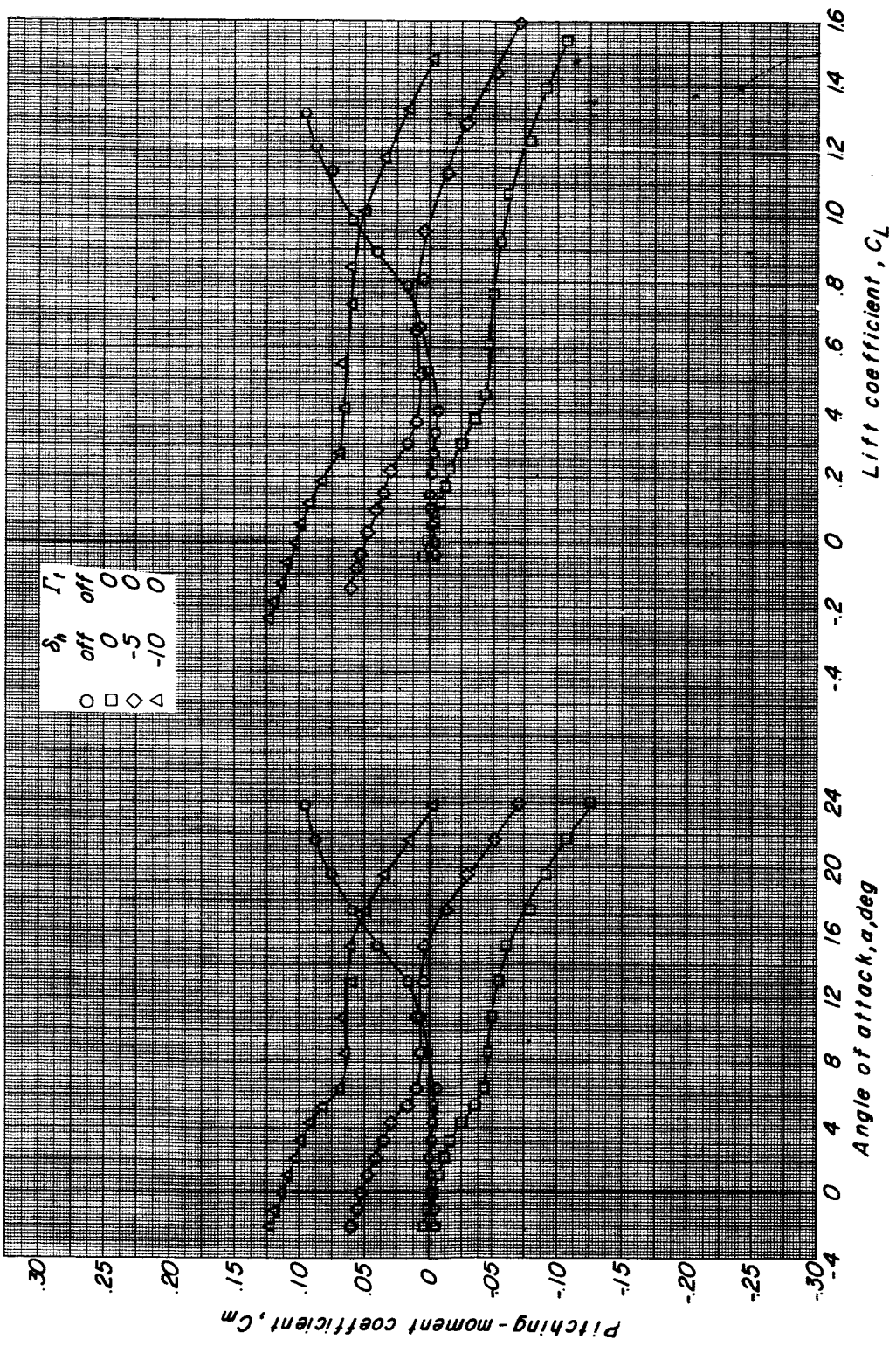
Figure 25.- Concluded.
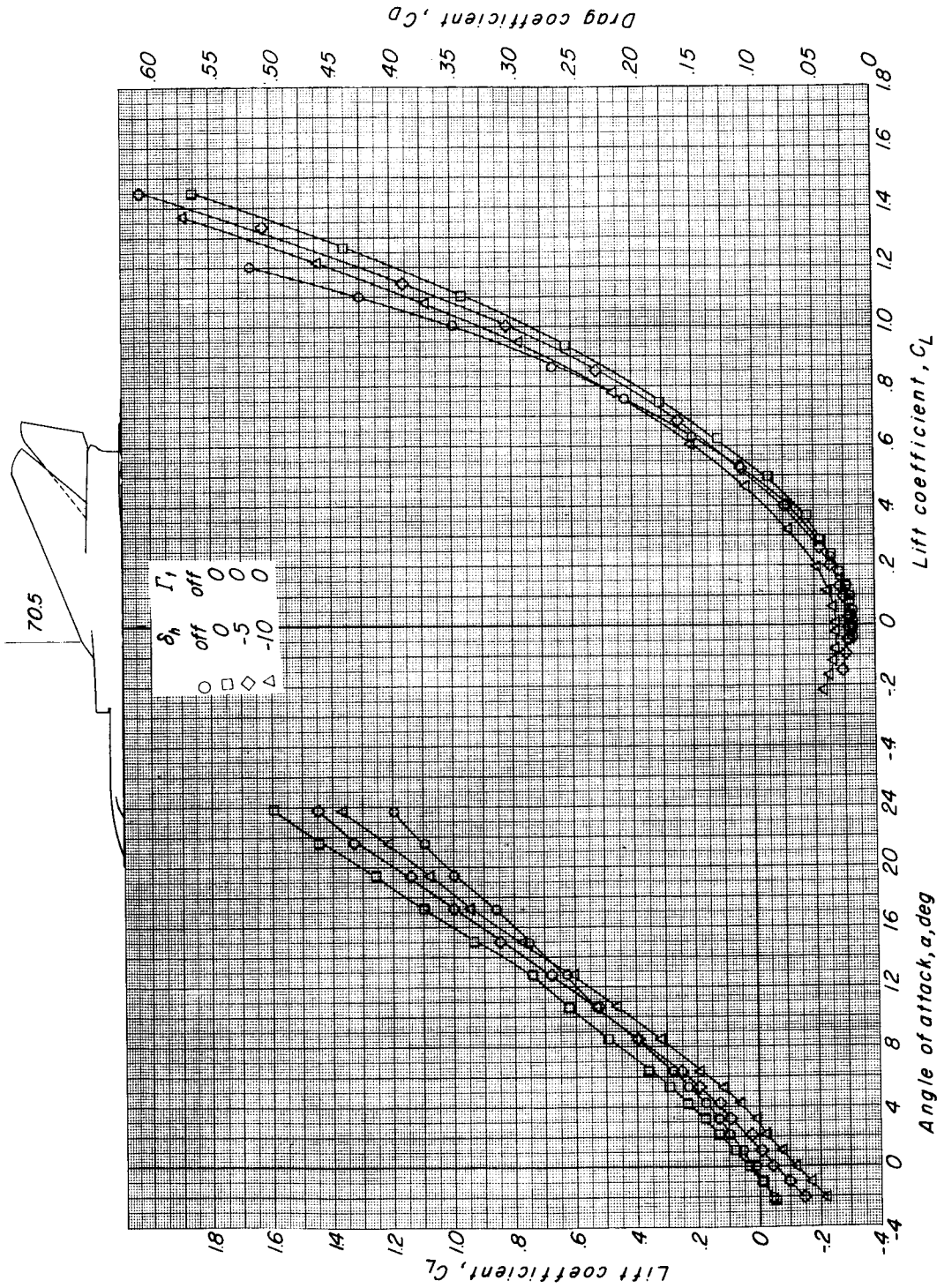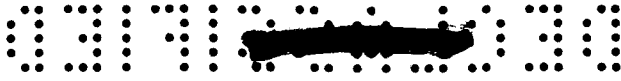
Figure 26.- The effects of horizontal-tail deflection on the longitudinal aerodynamic character-istics of configuration II with canard surface off. $\Lambda_{LE} = 70.50°$; $\Gamma_t = 0°$.
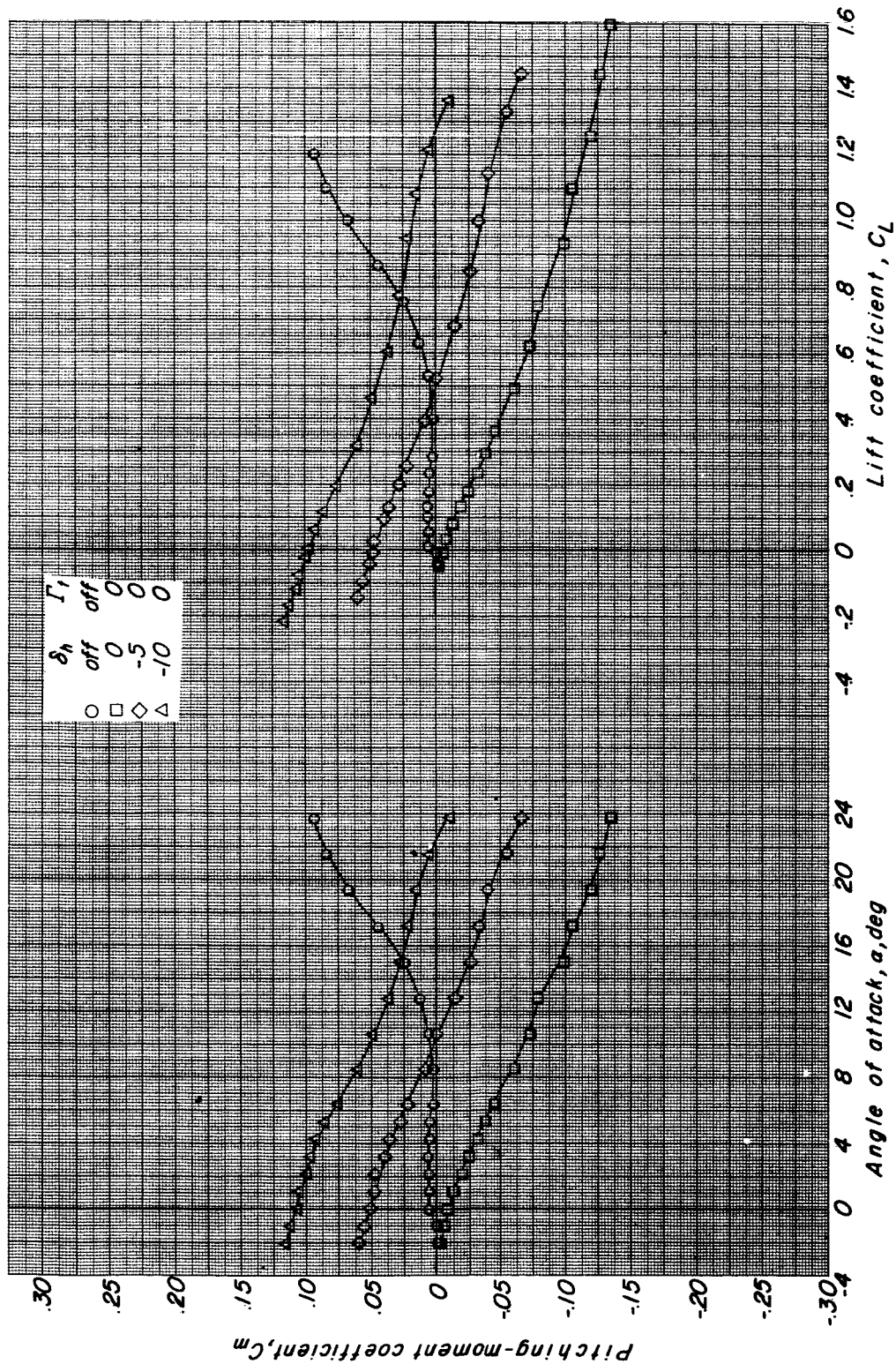
Figure 26.- Concluded.
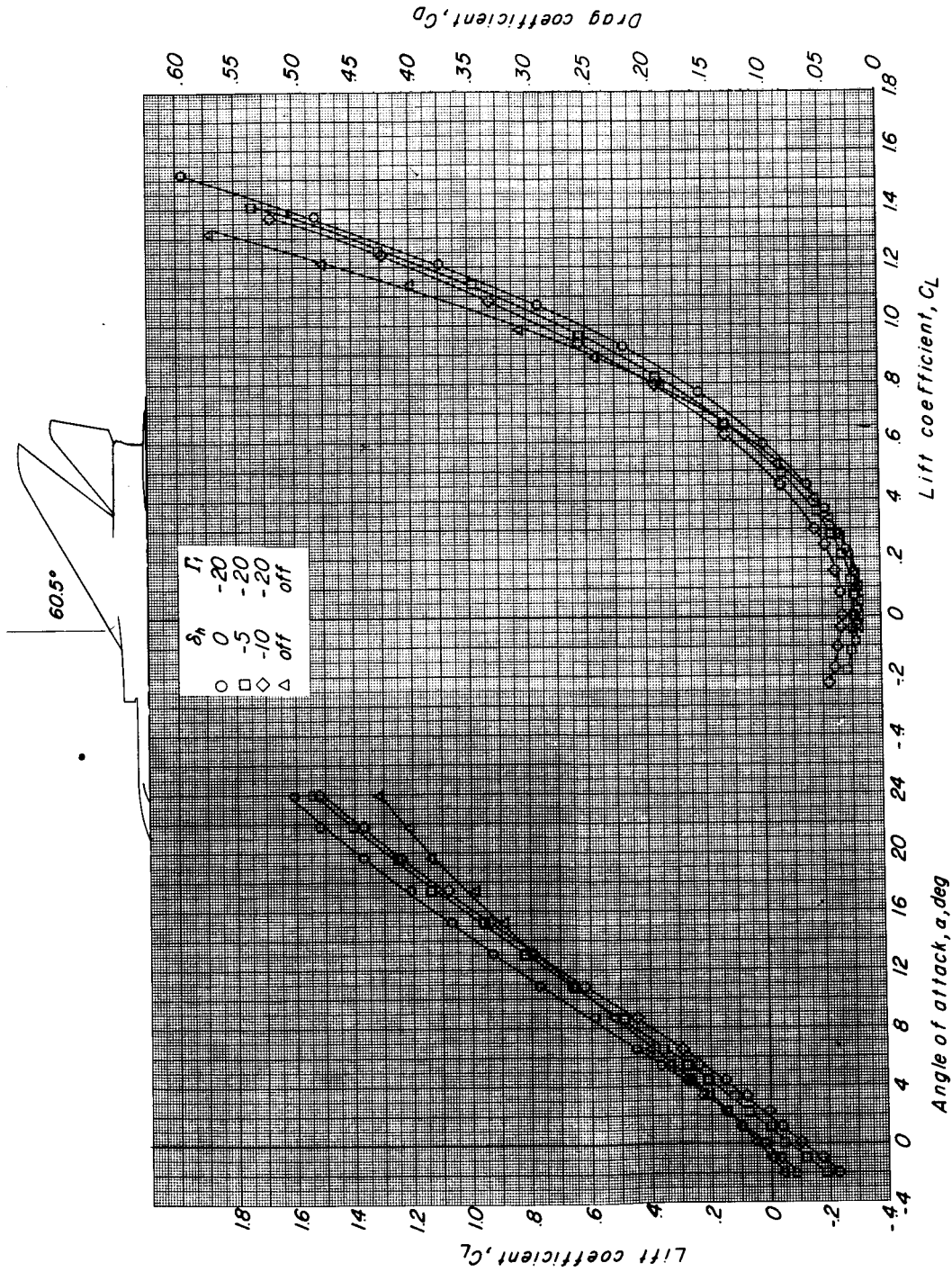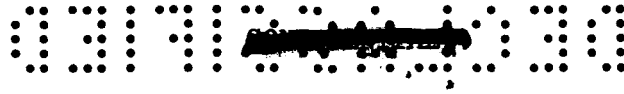
Figure 27.- The effects of horizontal-tail deflection on the longitudinal aerodynamic characteristics of configuration II with canard surface off. $\Lambda_{LE} = 60.50°$; $\Gamma_t = -20°$.

L-1024
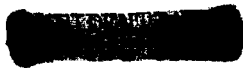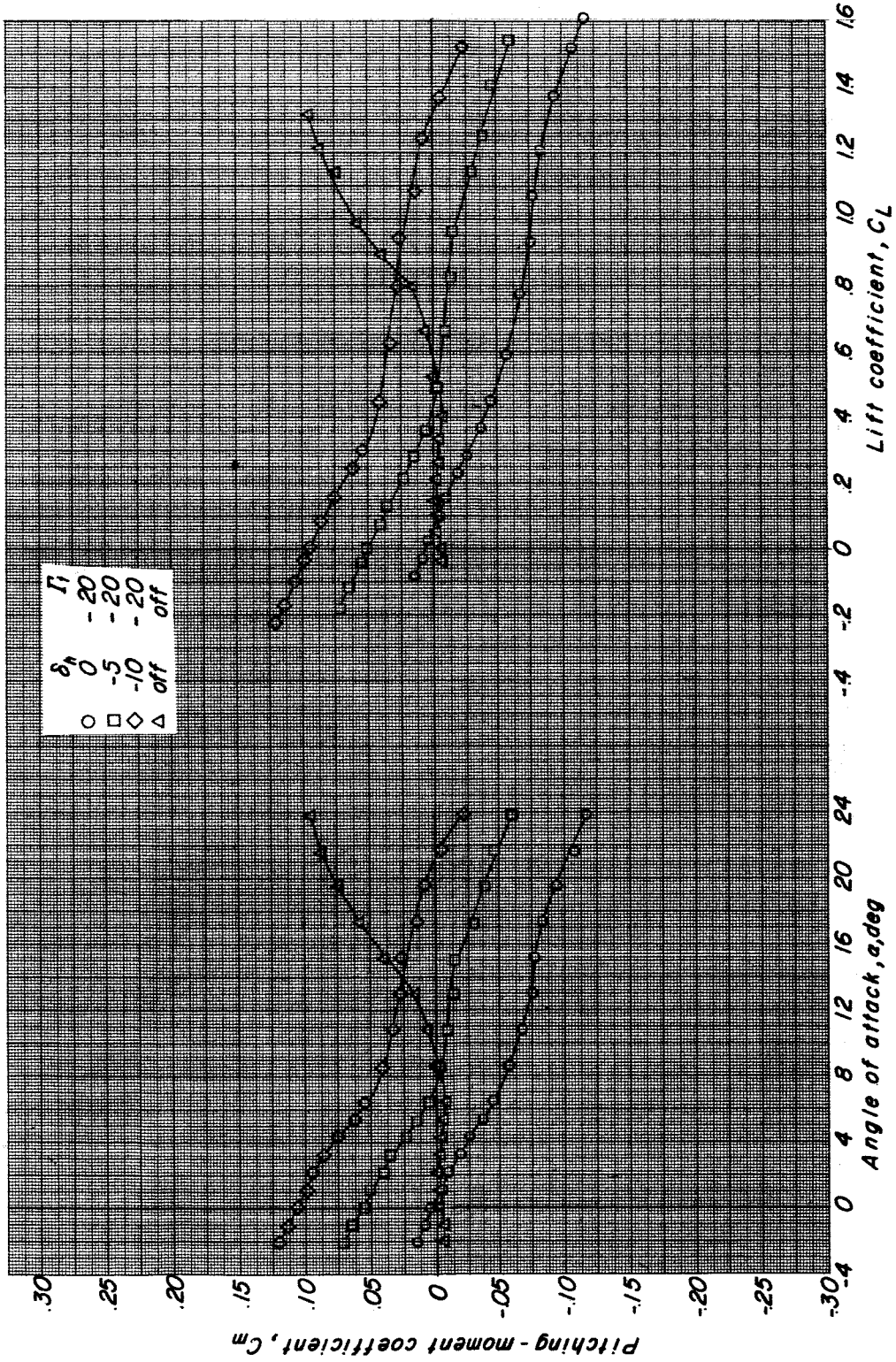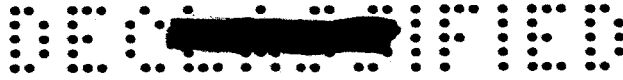
Figure 27.- Concluded.
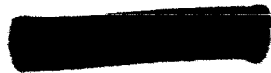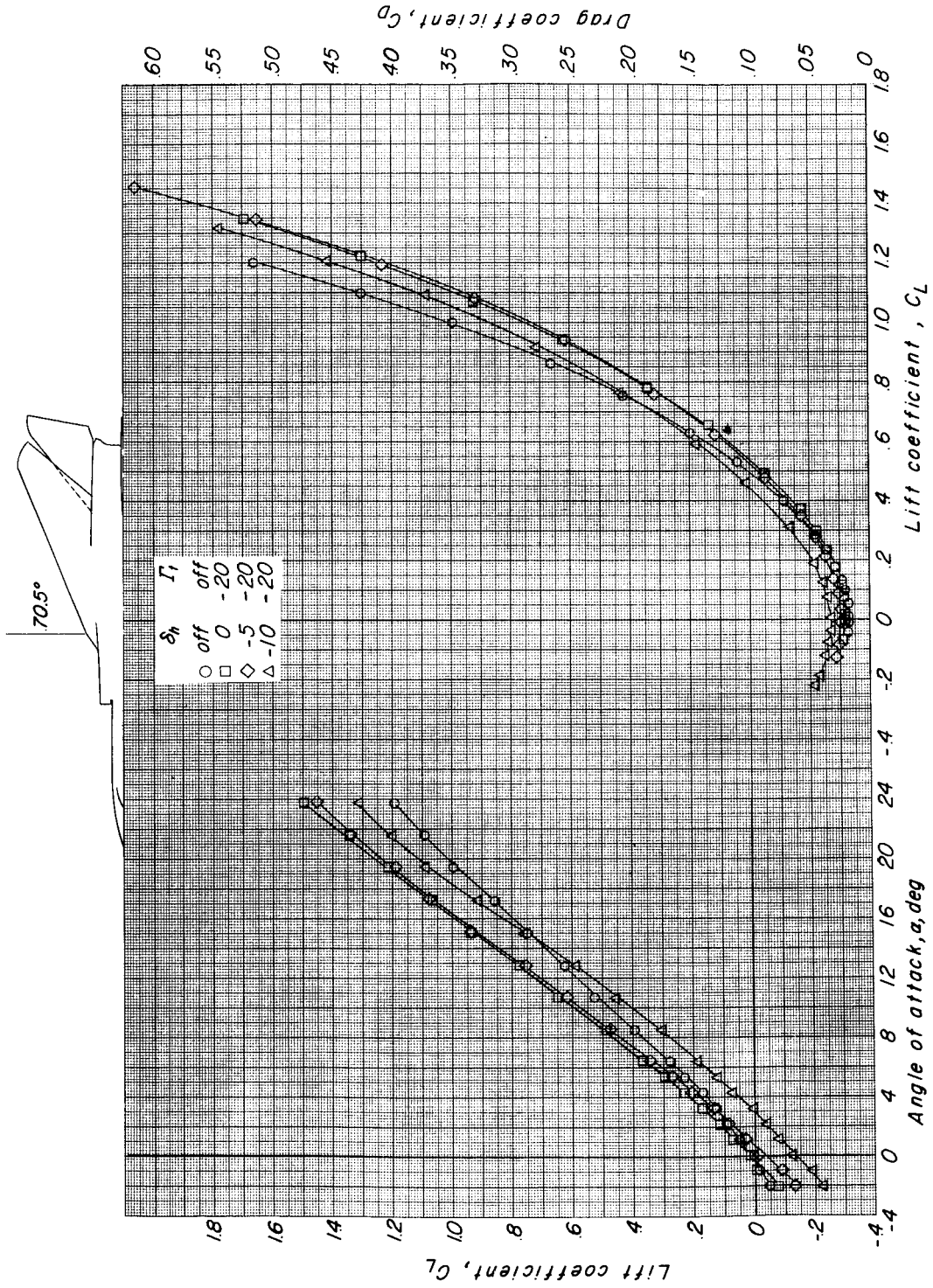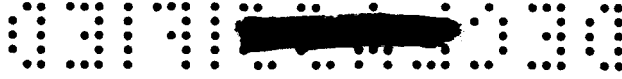
Figure 28.- The effects of horizontal-tail deflection on the longitudinal aerodynamic characteristics of configuration II with canard surface off. $\Lambda_{LE} = 70.50°$; $\Gamma_t = -20°$.
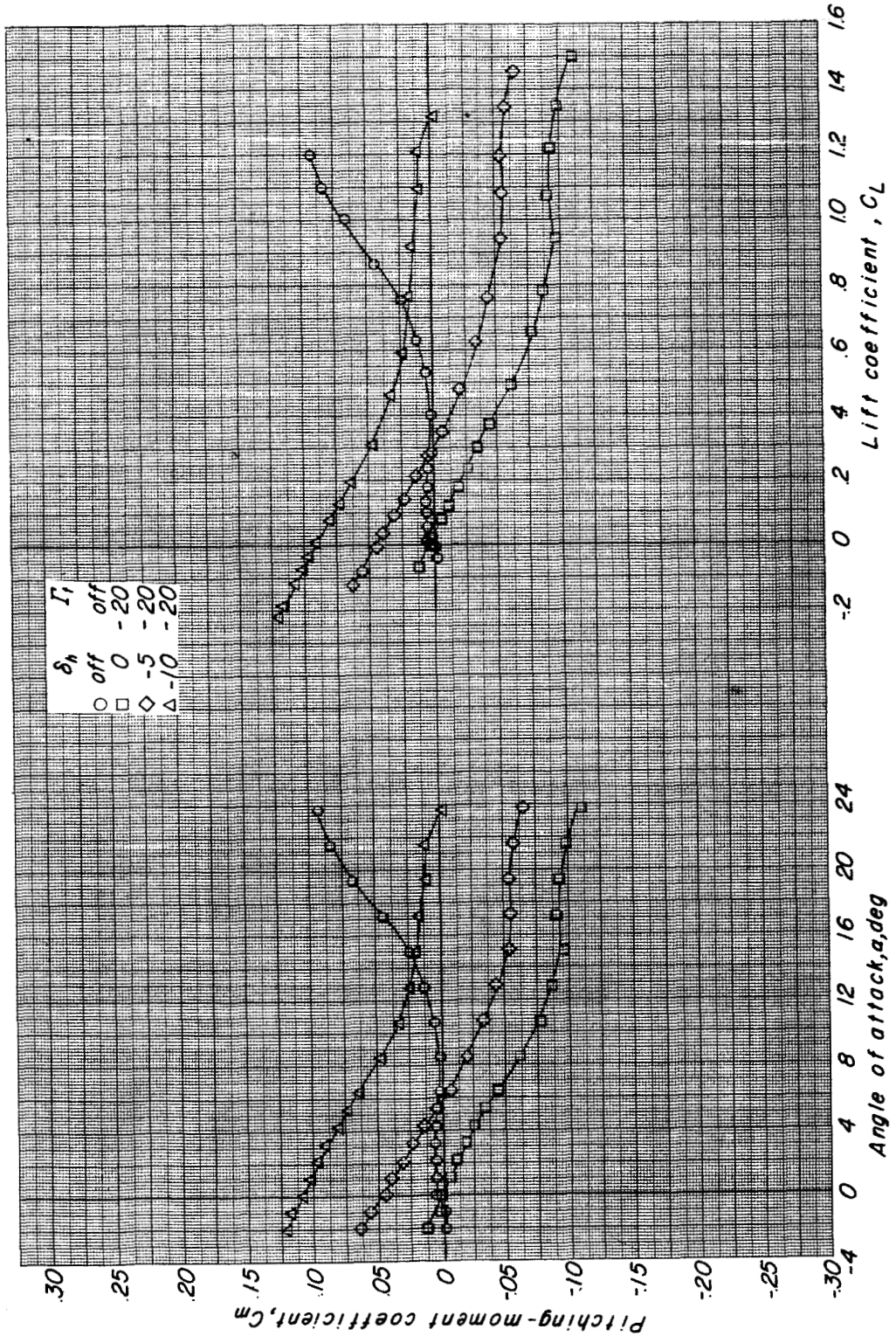
Figure 28.- Concluded.
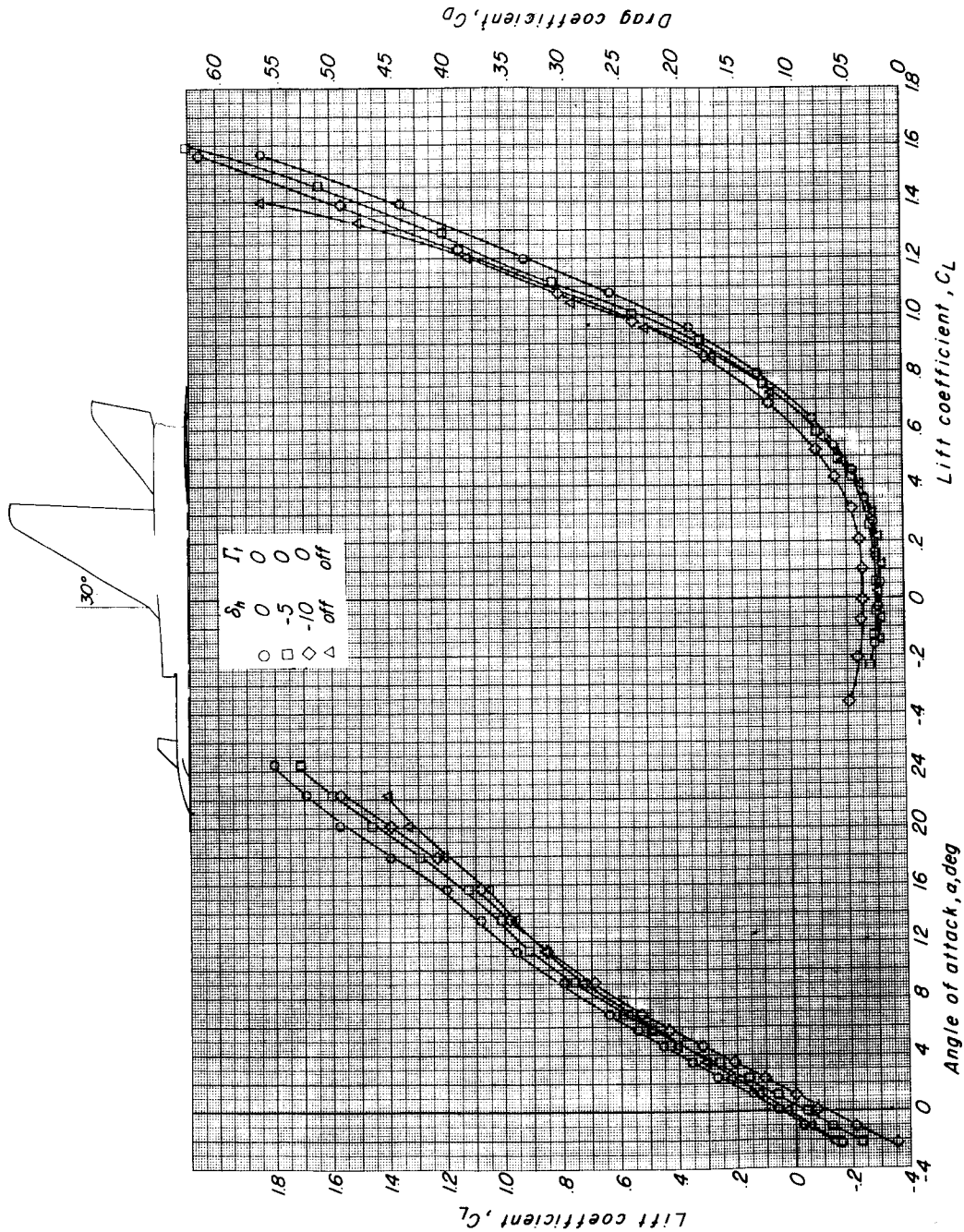
Figure 29.- The effects of horizontal-tail deflection on the longitudinal aerodynamic character-
istics of configuration II with canard surface on. $\Lambda_{LE} = 30.00°$.

L-1024
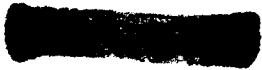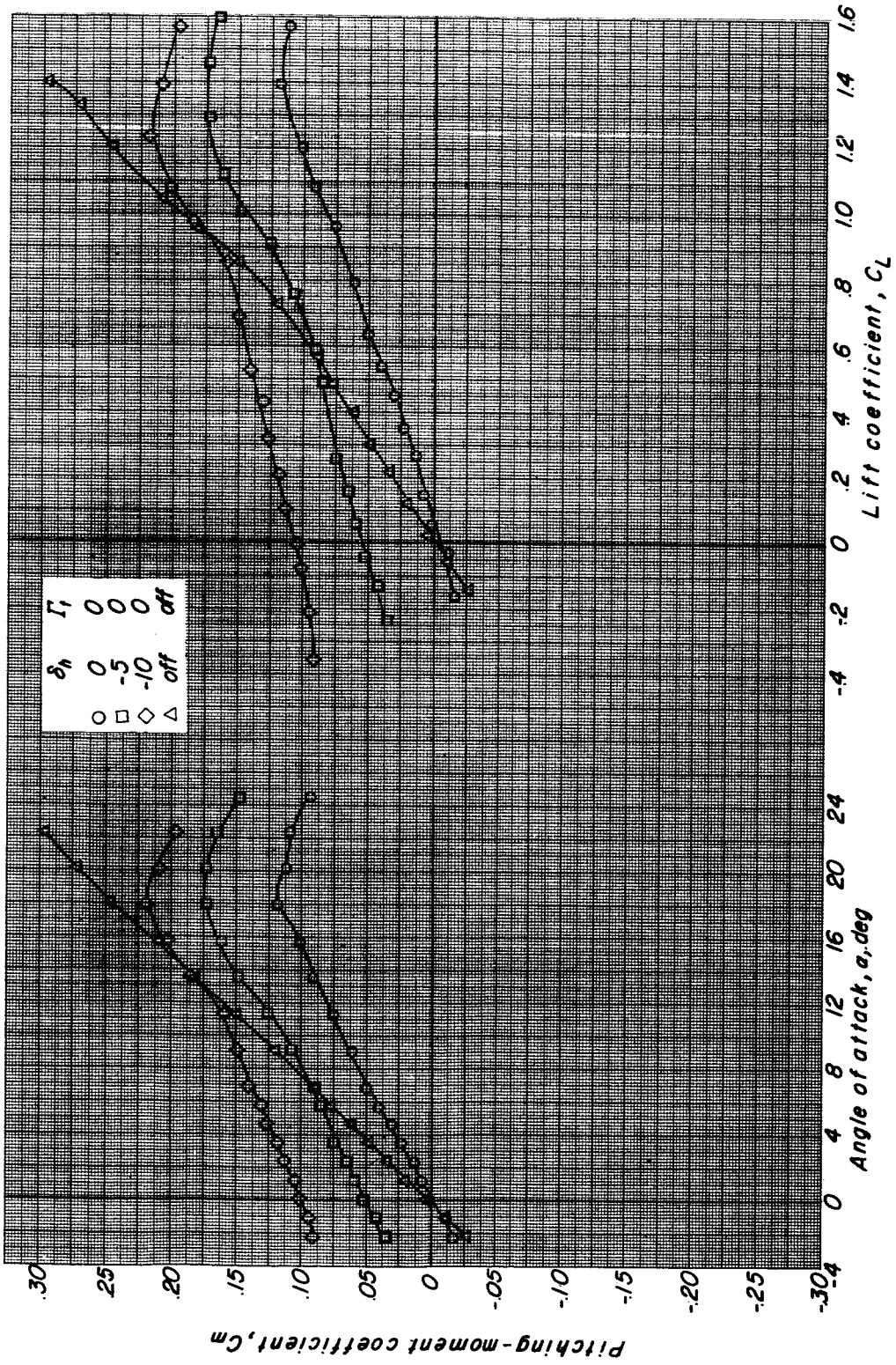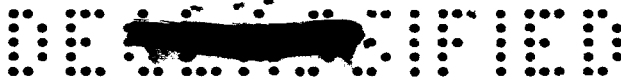
Figure 29.- Concluded.
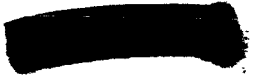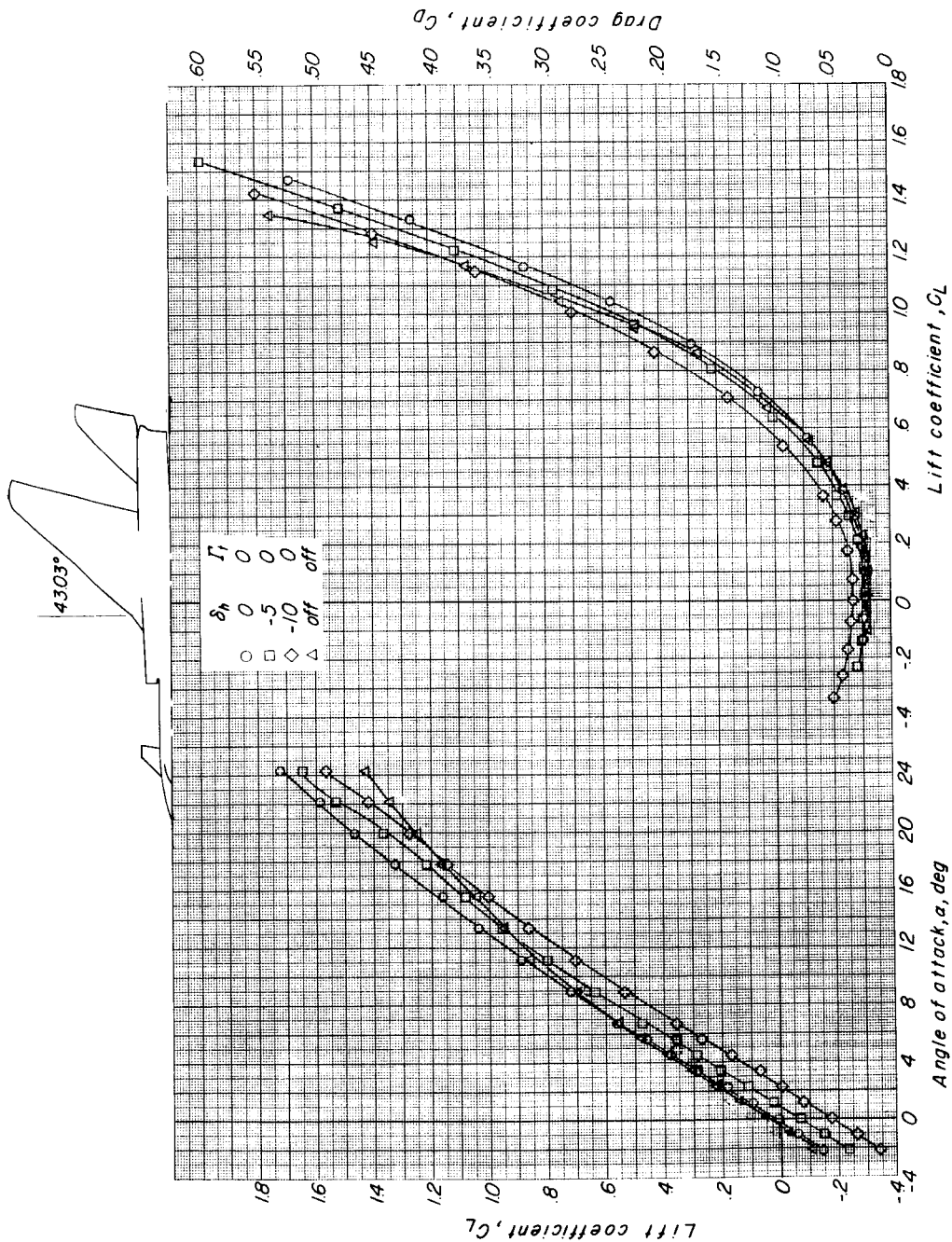
Figure 30.- The effects of horizontal-tail deflection on the longitudinal aerodynamic character-
istics of configuration II with canard surface on. $\Lambda_{LE} = 43.03°$.

L-1024
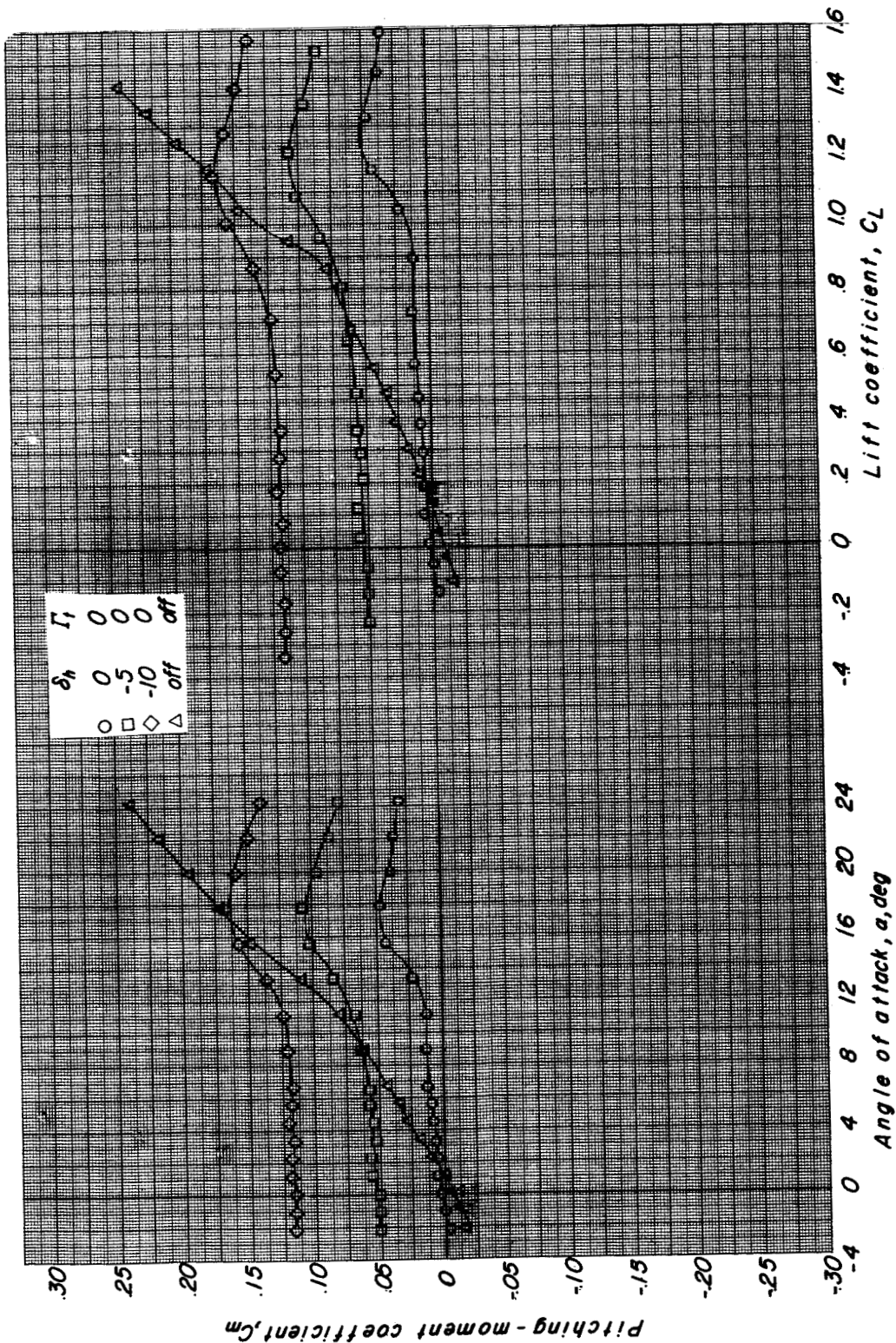
Figure 30.- Concluded.
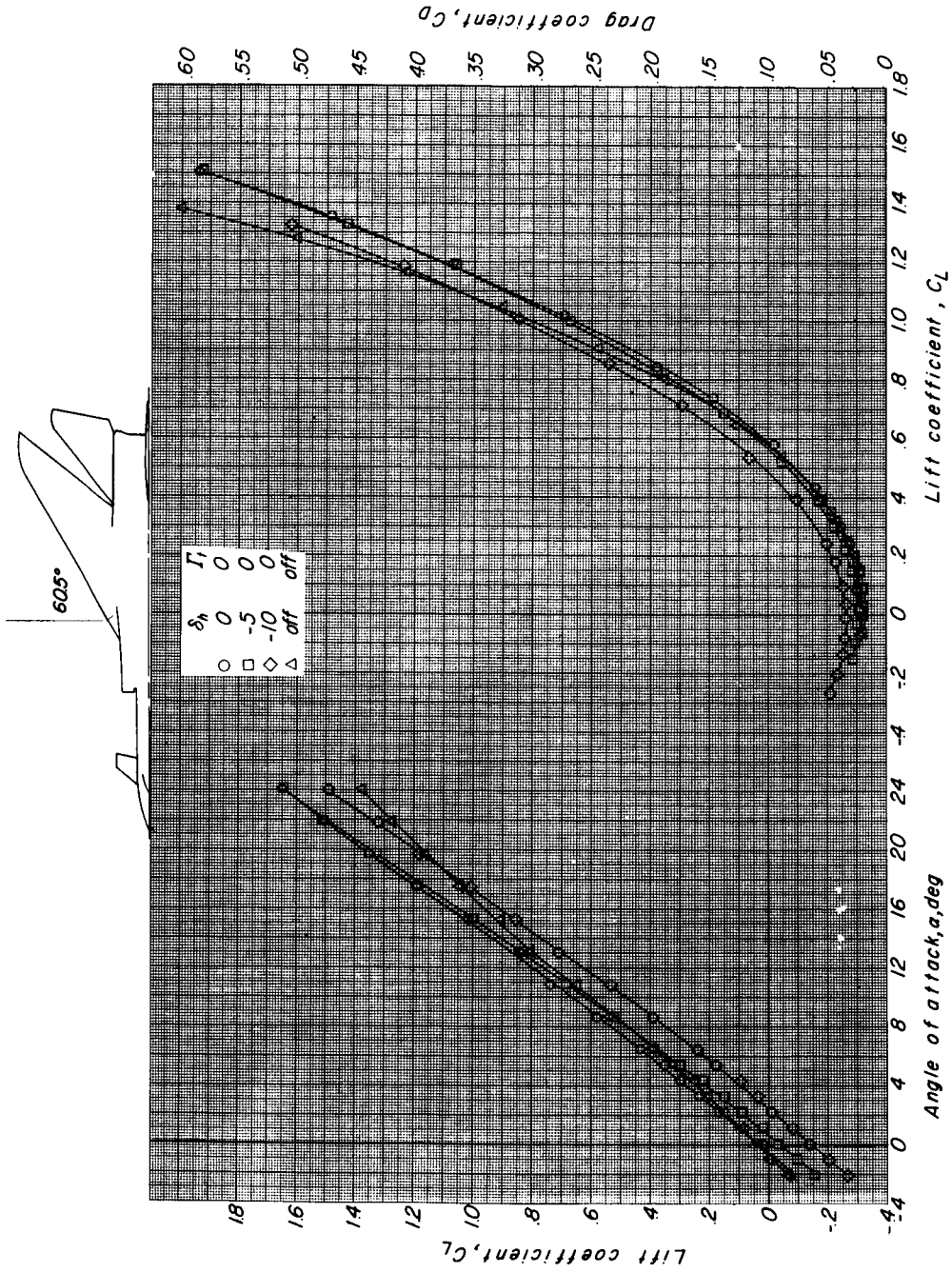
Figure 31.- The effects of horizontal-tail deflection on the longitudinal aerodynamic characteristics of configuration II with canard surface on. $\Lambda_{LE} = 60.50°$.
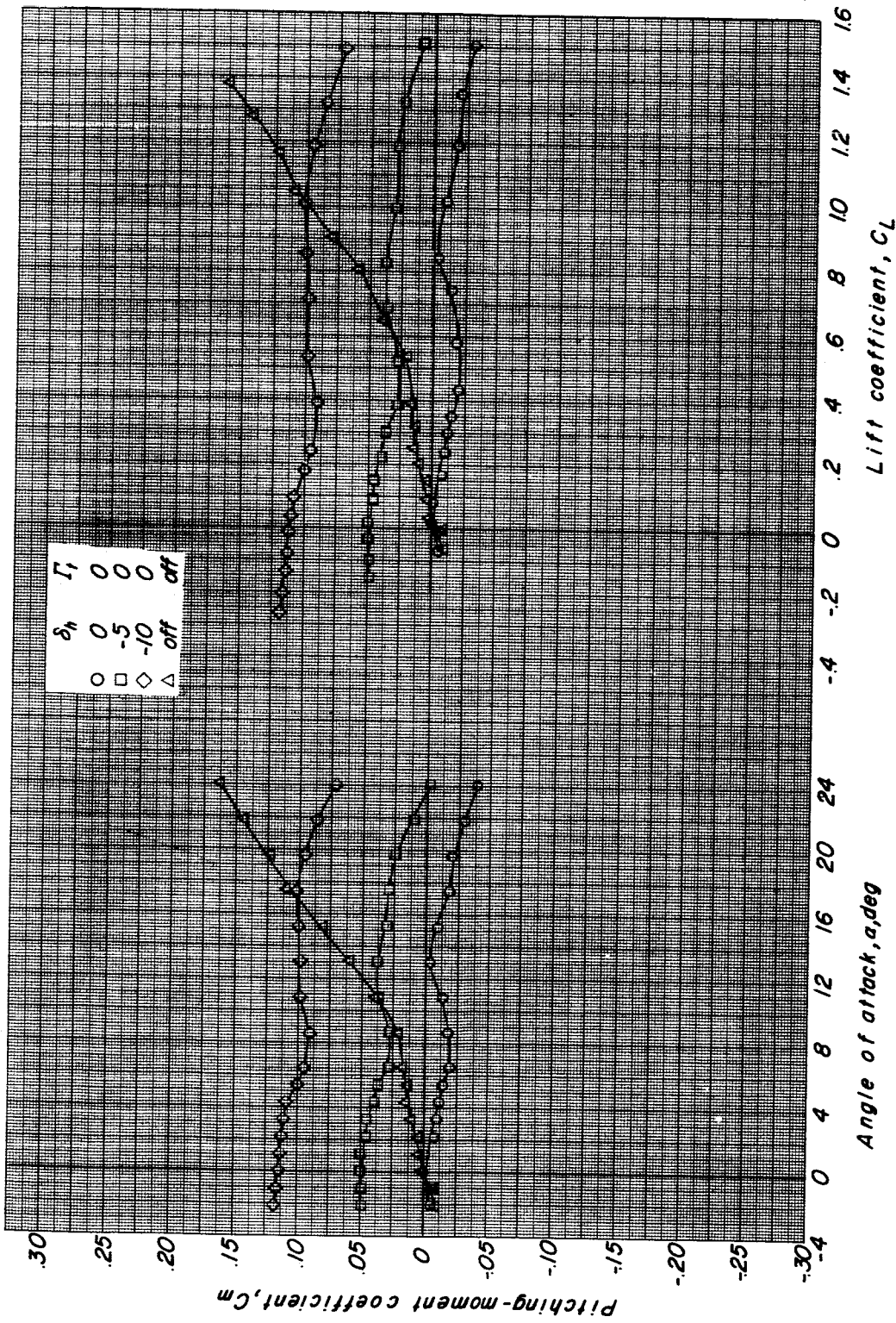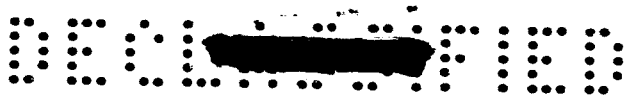
Figure 31.- Concluded.
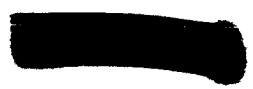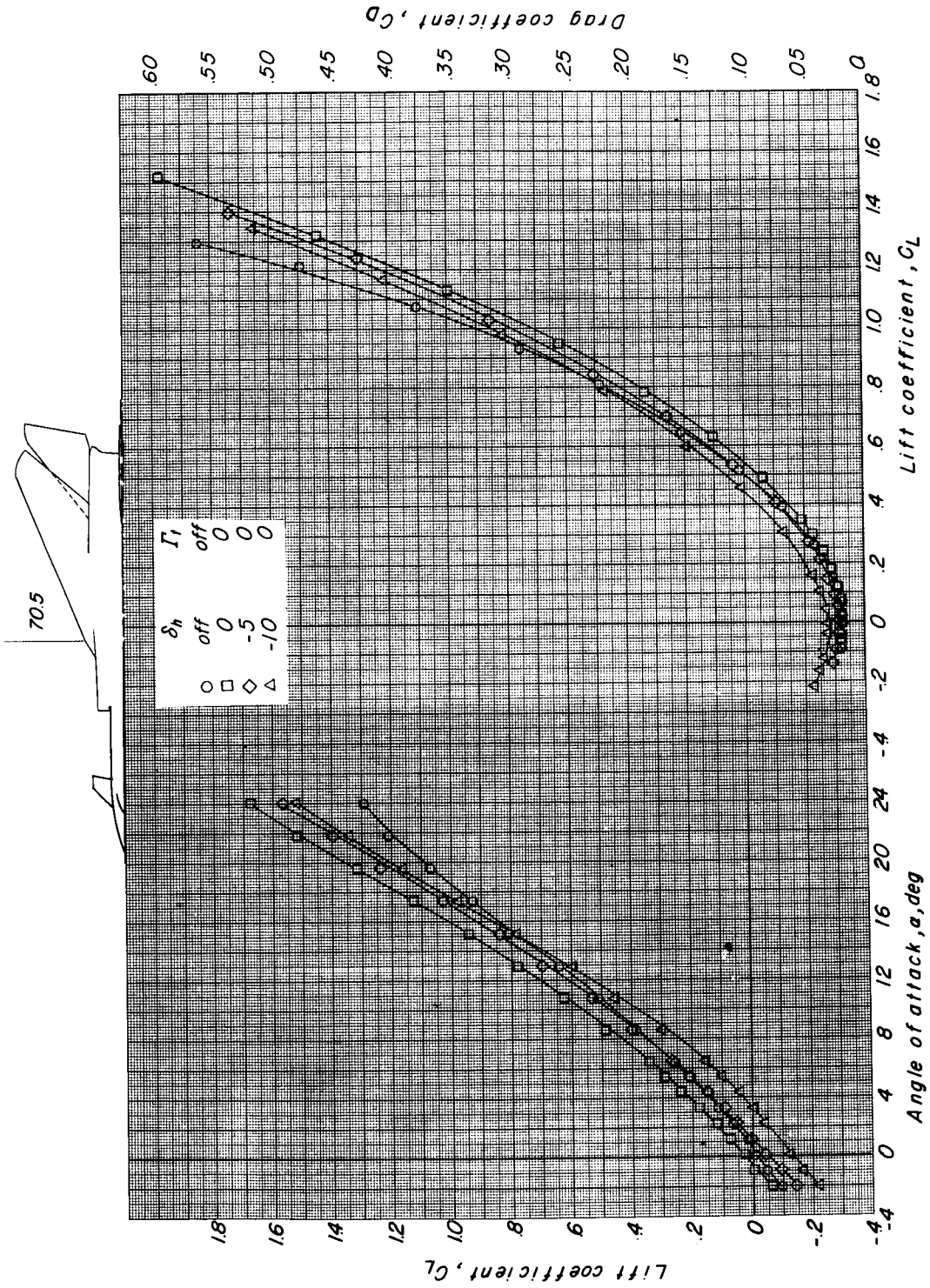
Figure 32.- The effects of horizontal-tail deflection on the longitudinal aerodynamic character-istics of configuration II with canard surface on. $\Lambda_{LE} = 70.50^\circ$.
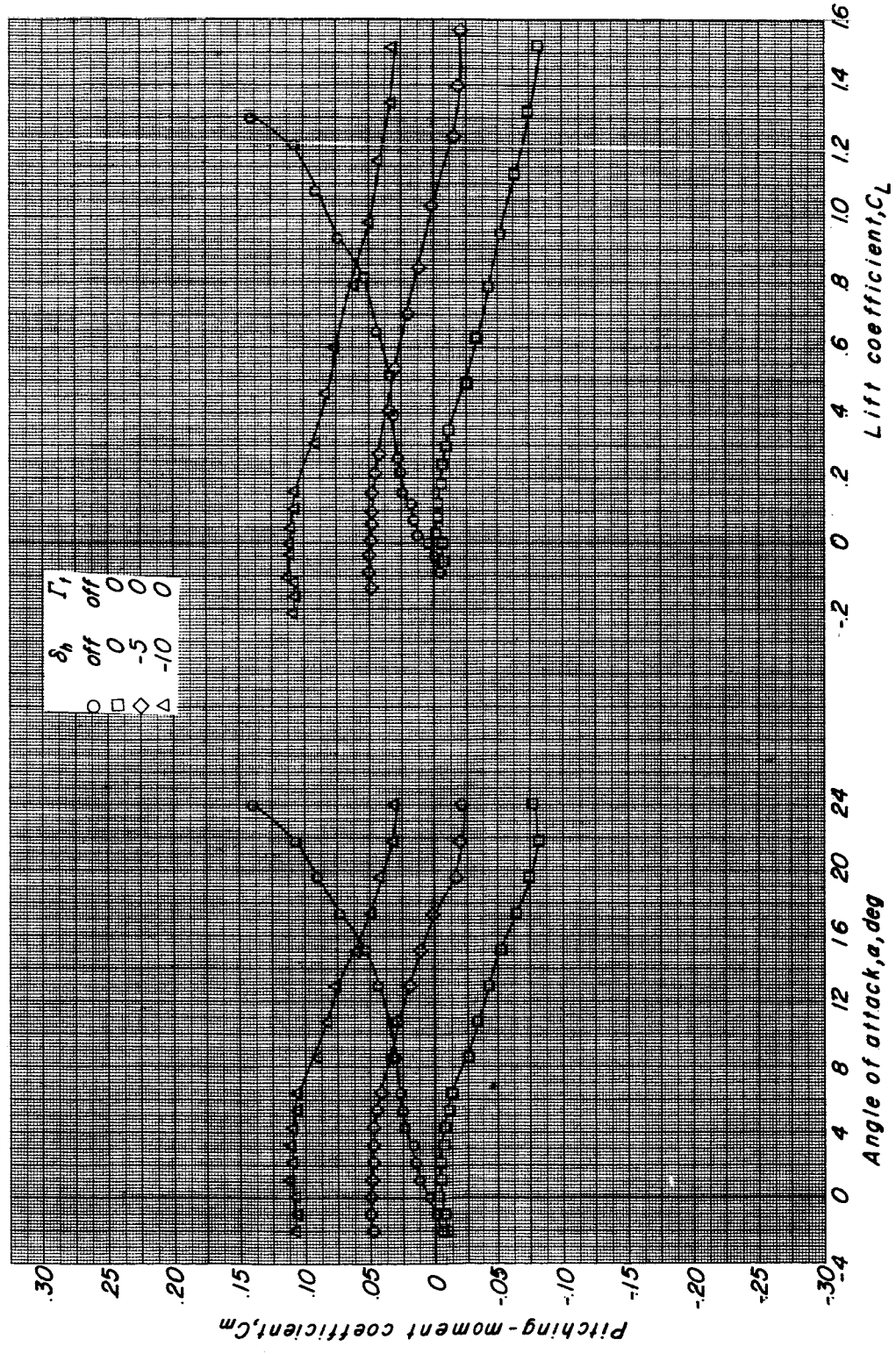
Figure 32.- Concluded.
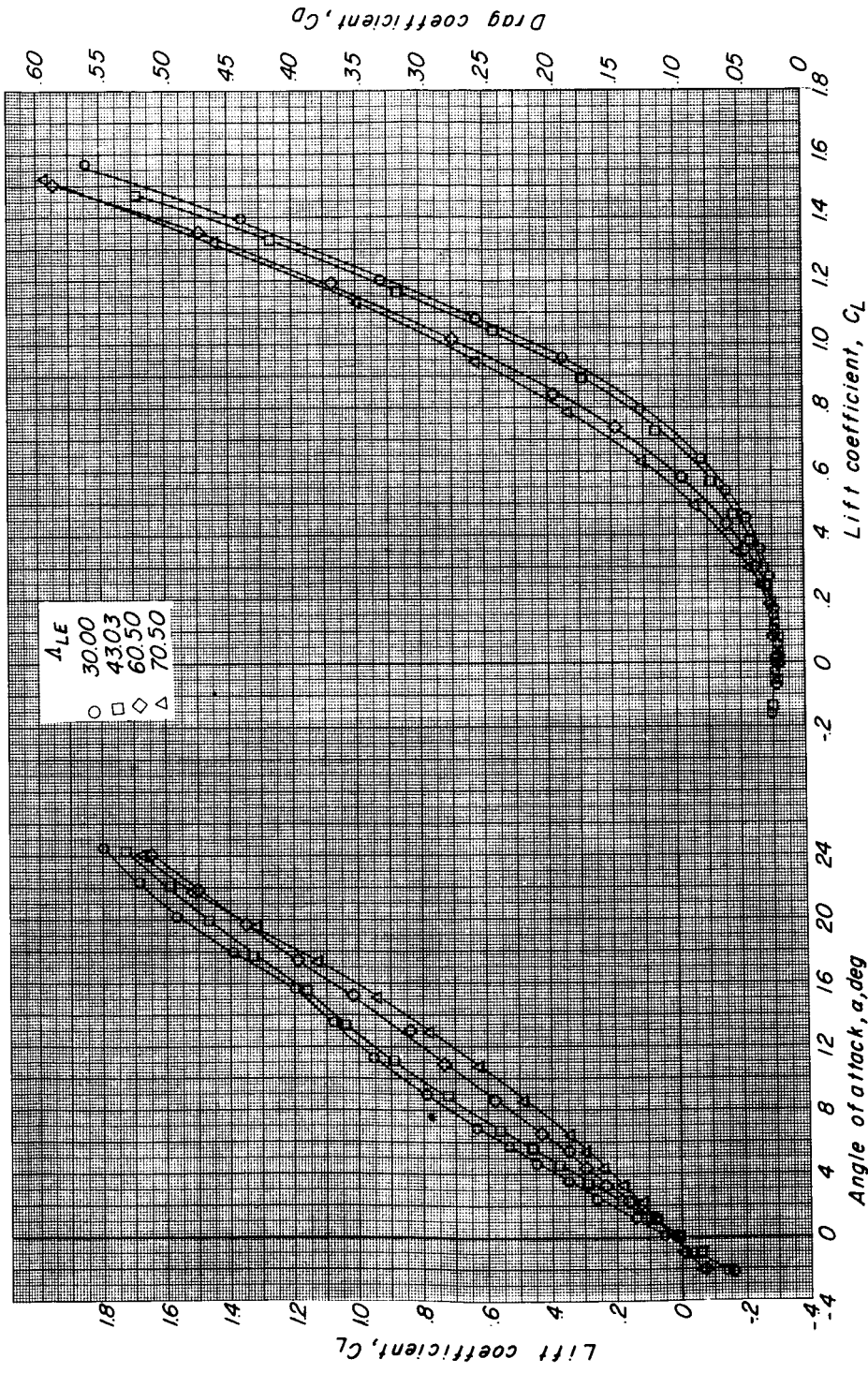
Figure 33.- The effects of wing sweep on the longitudinal aerodynamic characteristics of configuration II with both canard surface and horizontal tail on. $\Gamma_t = 0°$.
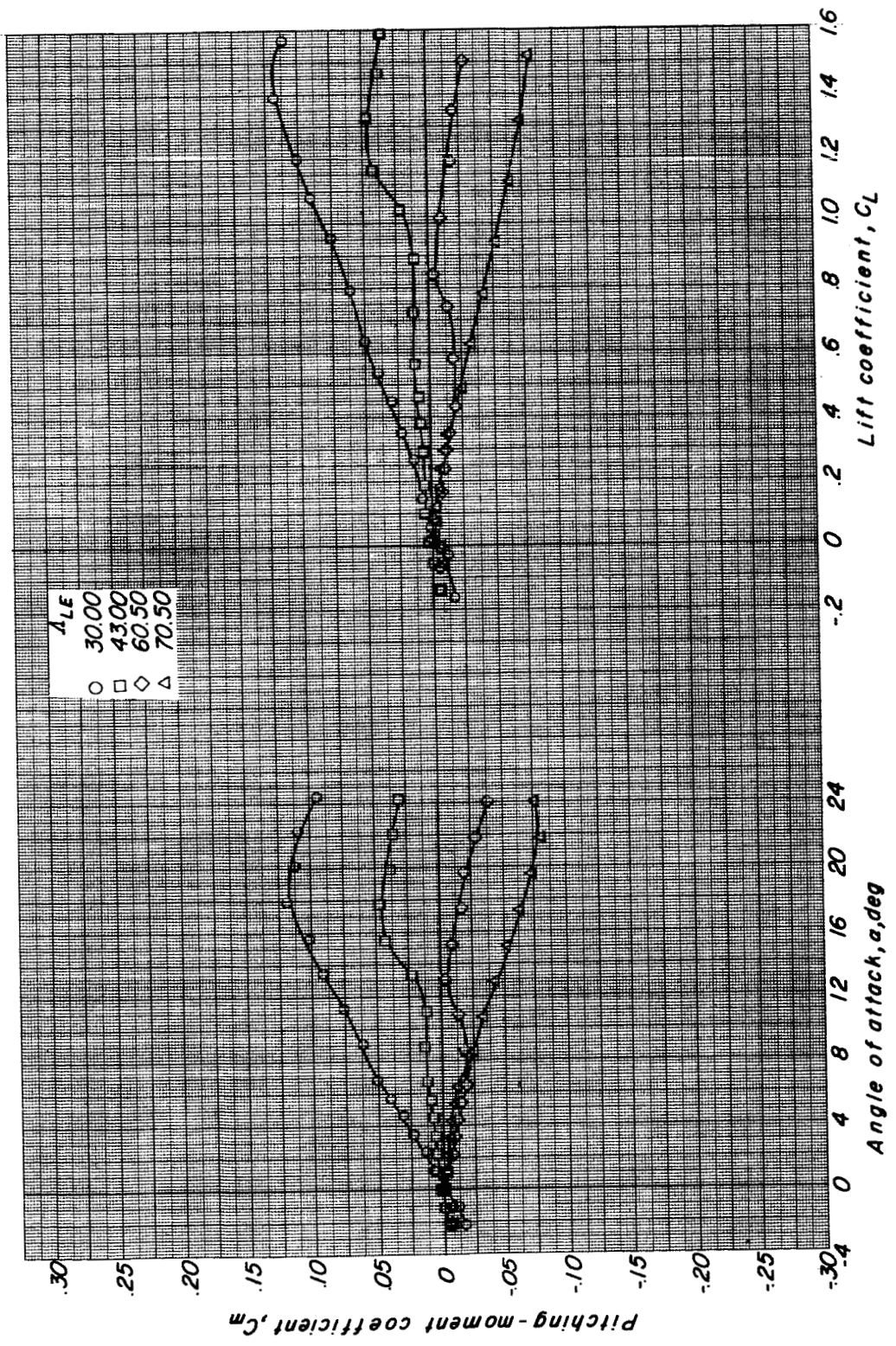
Figure 33.- Concluded.
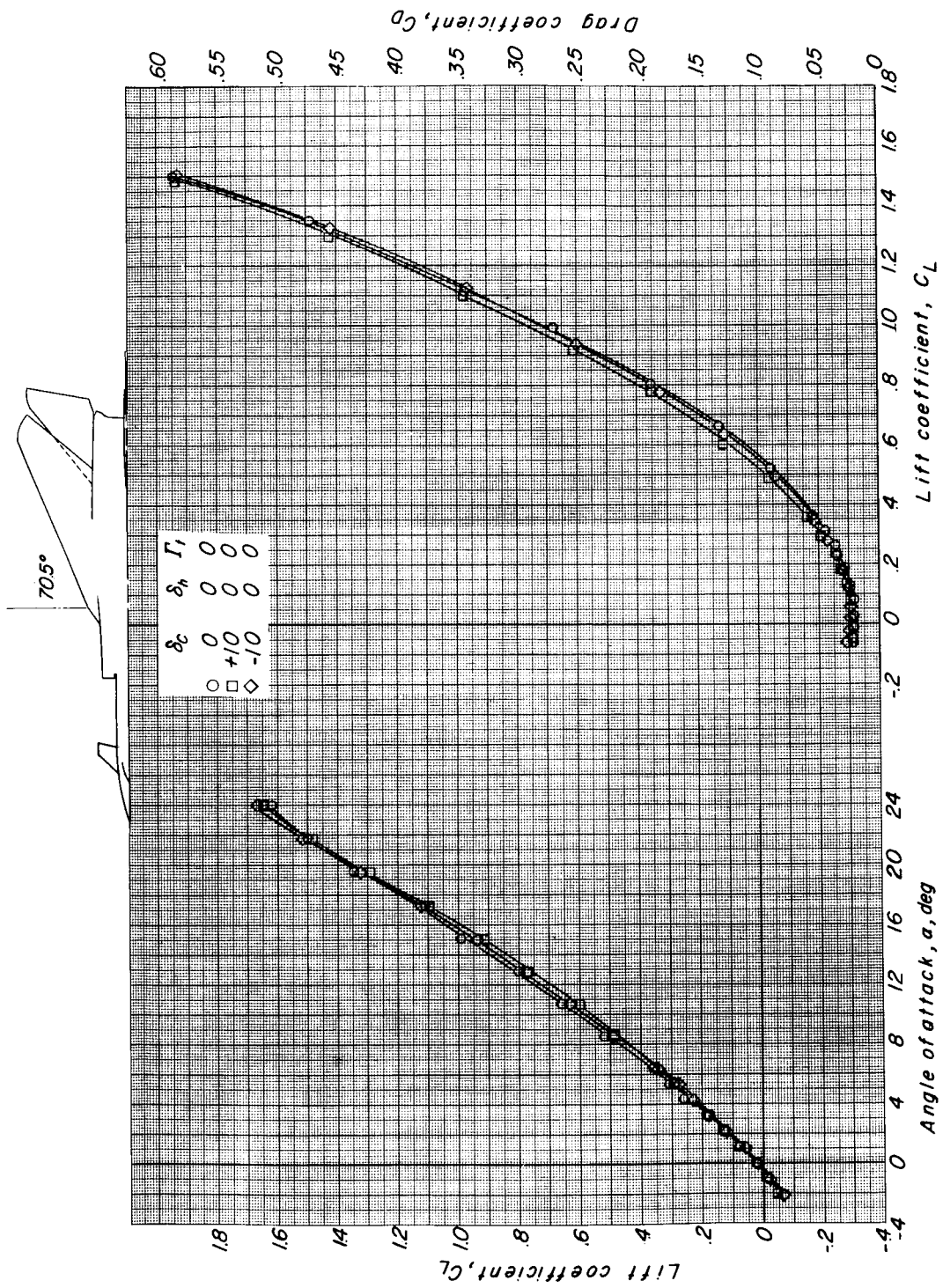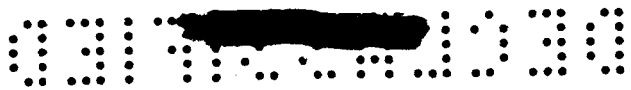
Figure 34.- The effects of canard-surface deflection on the longitudinal aerodynamic character-istics of configuration II with horizontal tail on. $\Lambda_{LE} = 70.50°$.

L-1024
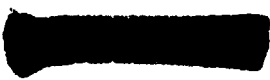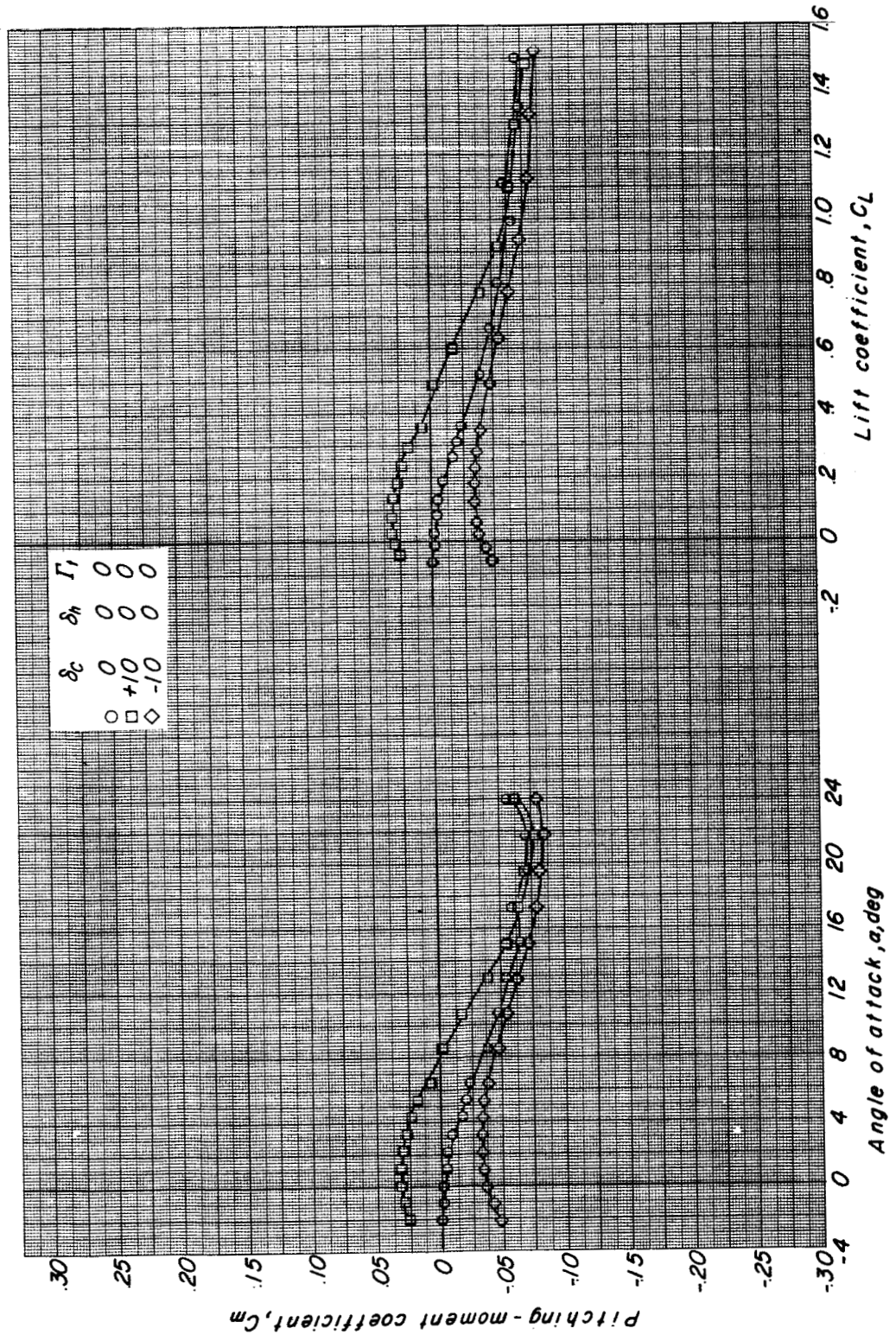
Figure 34.- Concluded.
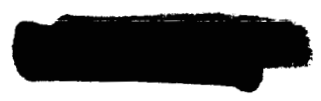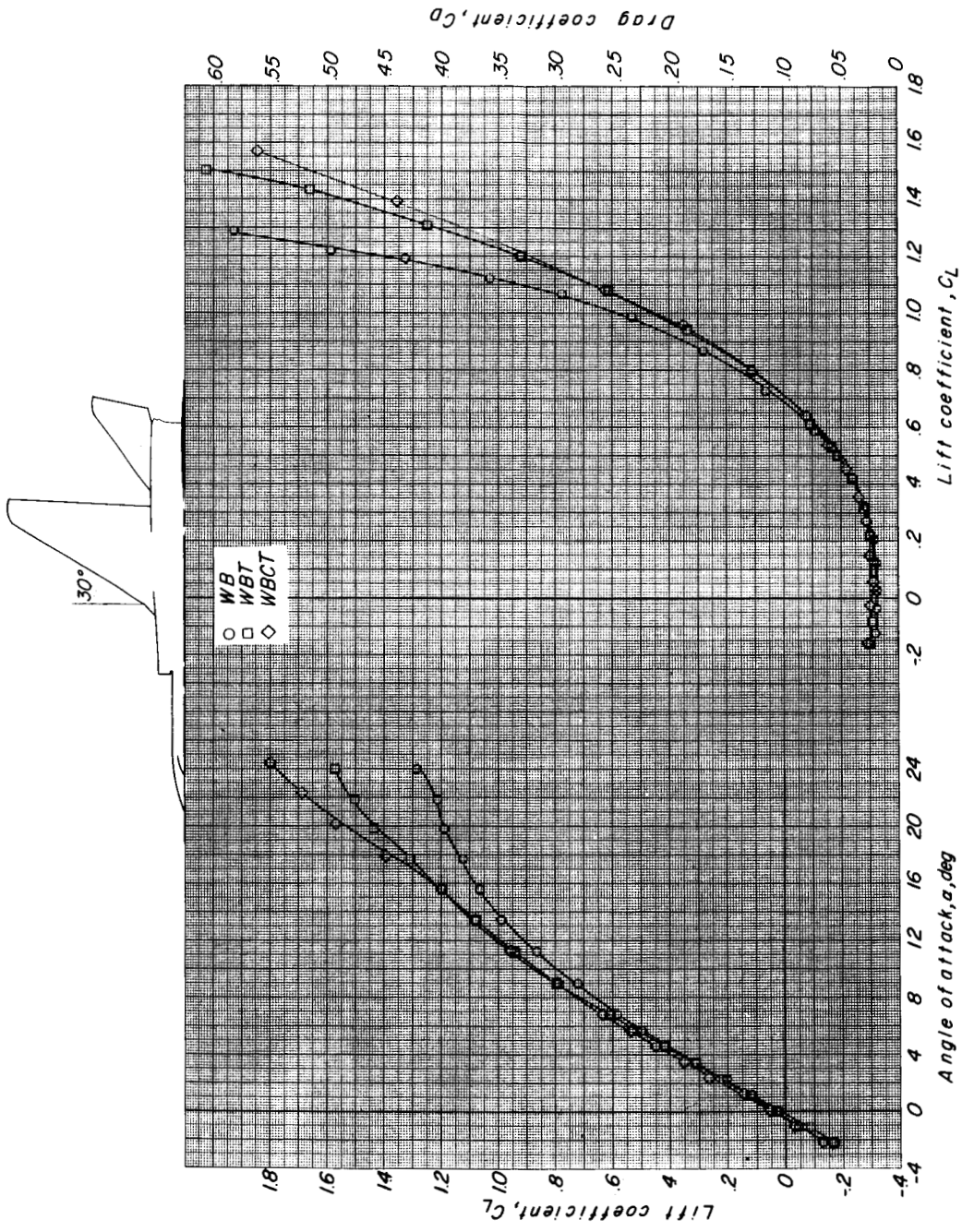
Figure 35.- Longitudinal aerodynamic characteristics of the various component parts for configuration II at 0° control deflection. $\Lambda_{LE} = 30.00°$.

I-1024

L-1024
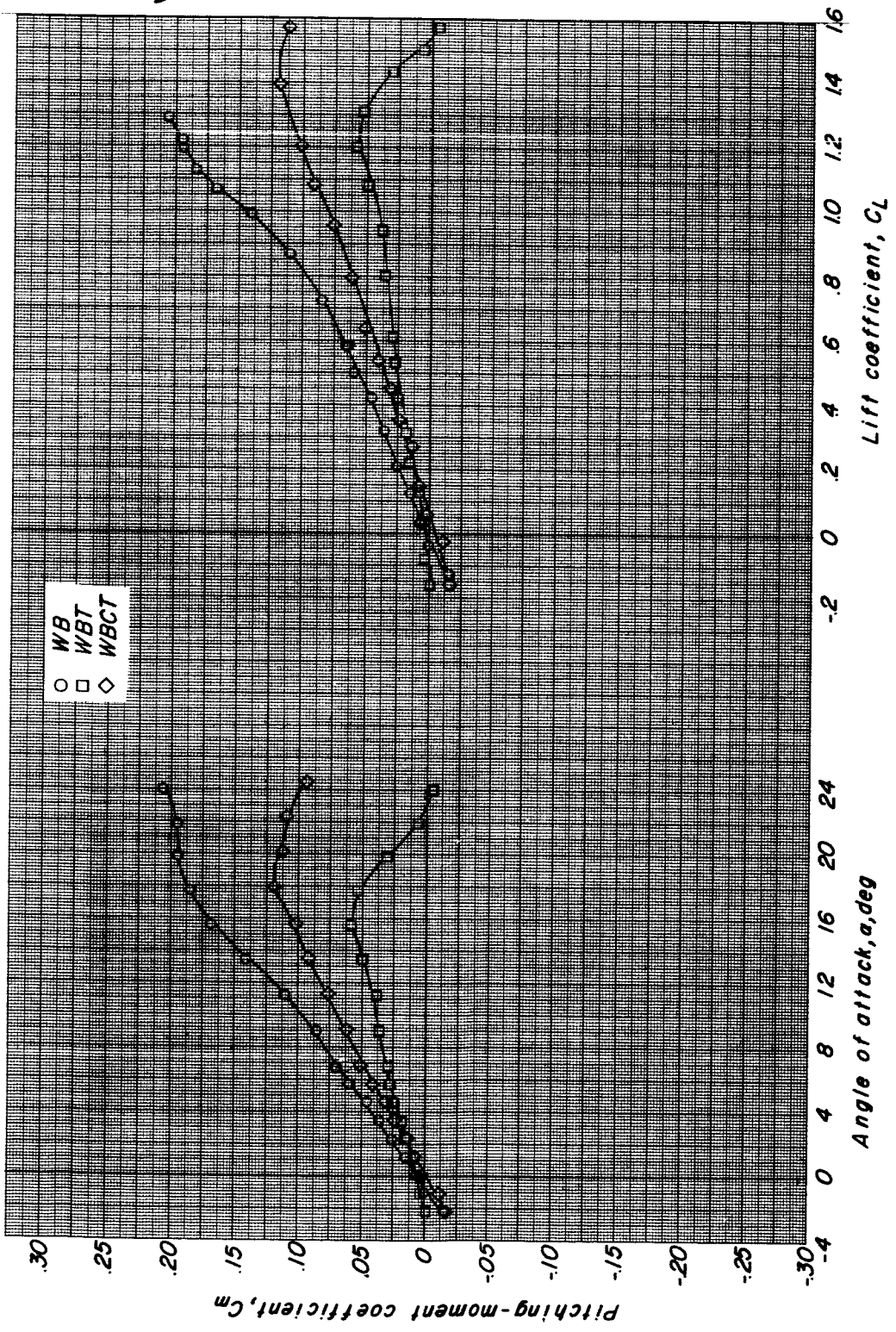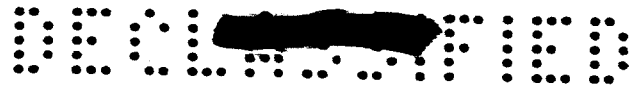
Figure 35.- Concluded.
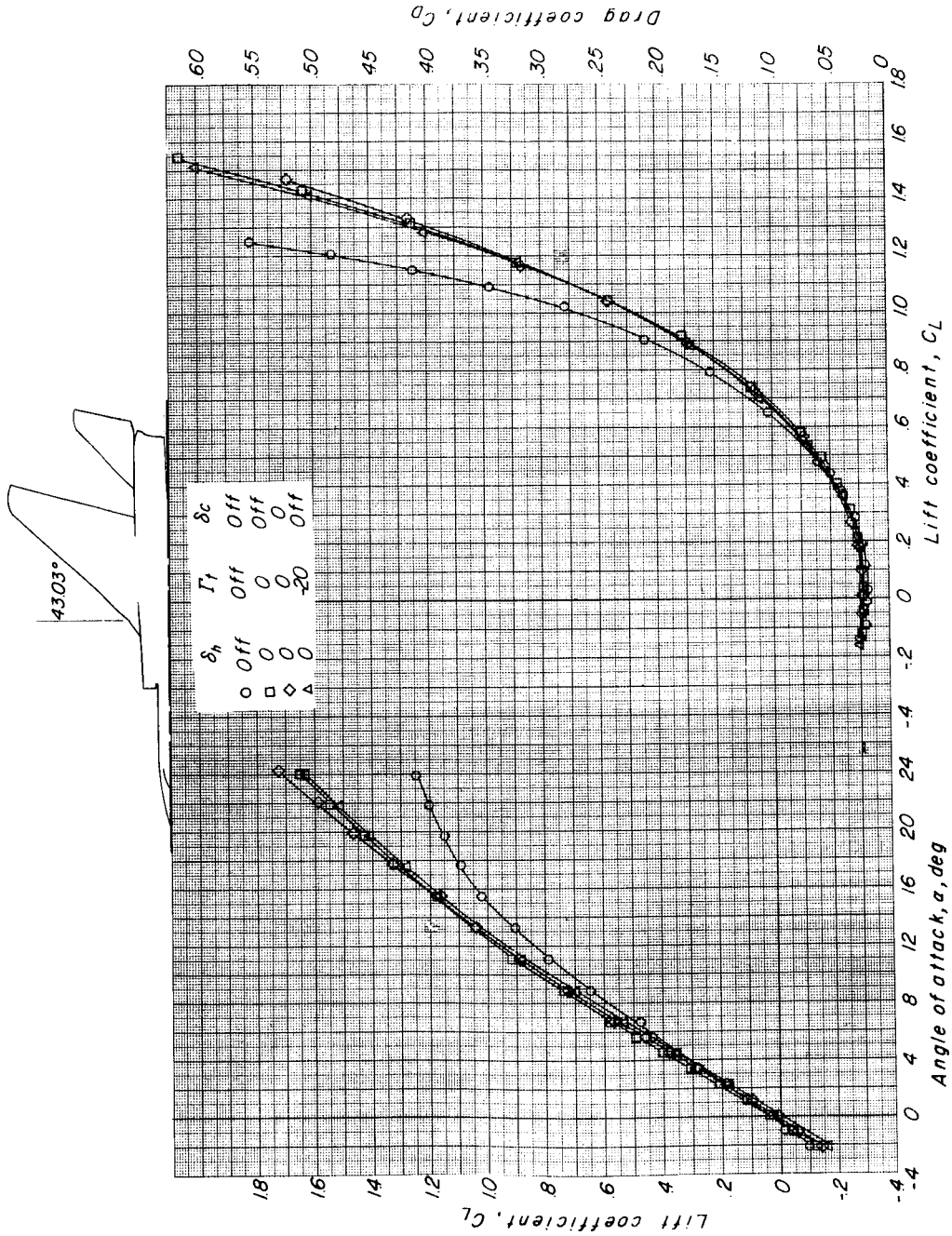
Figure 36.- Longitudinal aerodynamic characteristics of the various component parts of configuration II at 0° control deflection. $\Lambda_{LE} = 43.03°$.
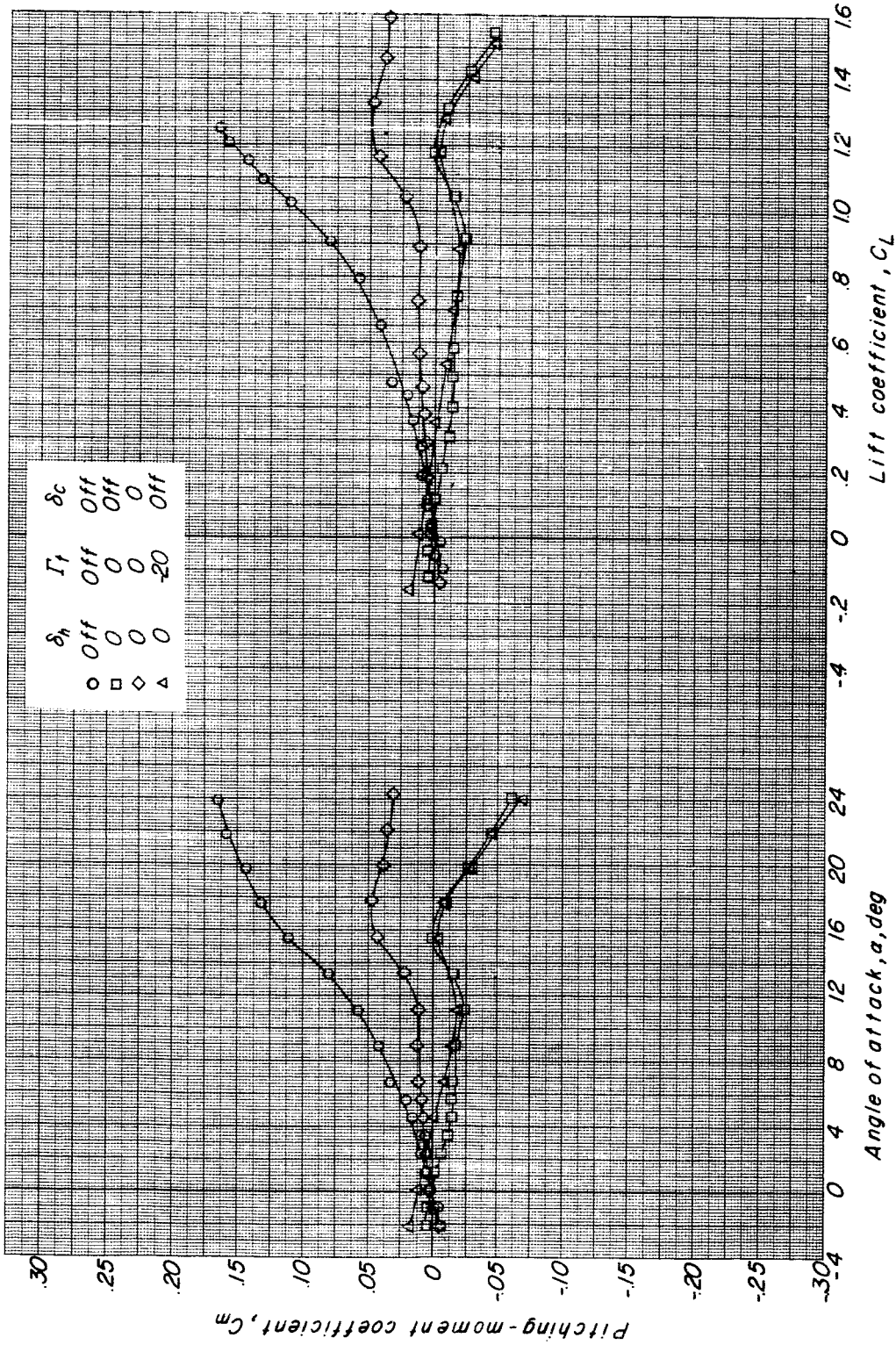
Figure 36.- Concluded.
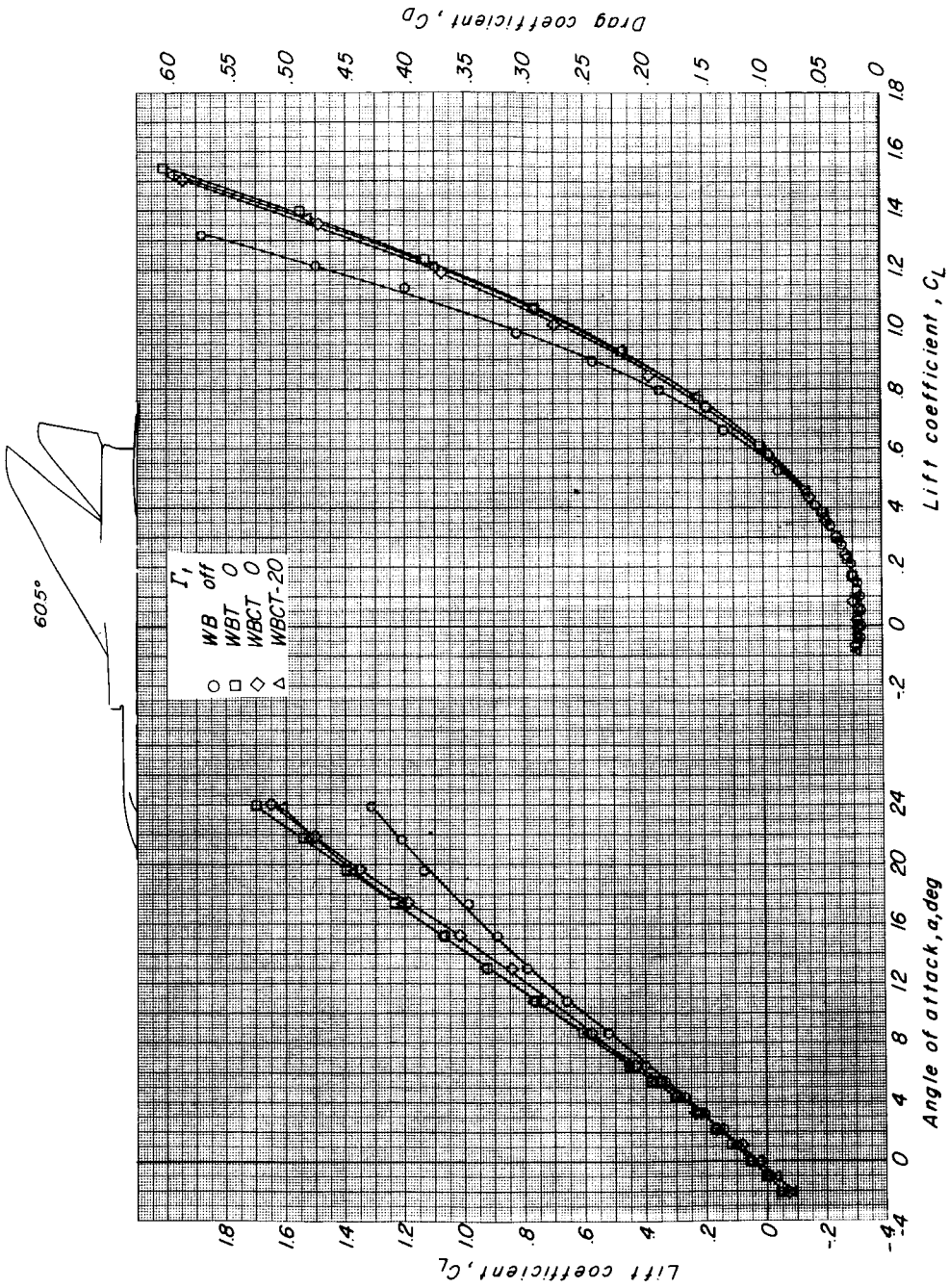
Figure 37.- Longitudinal aerodynamic characteristics of the various component parts of configuration II at 0° control deflection. $\Lambda_{LE} = 60.50°$.
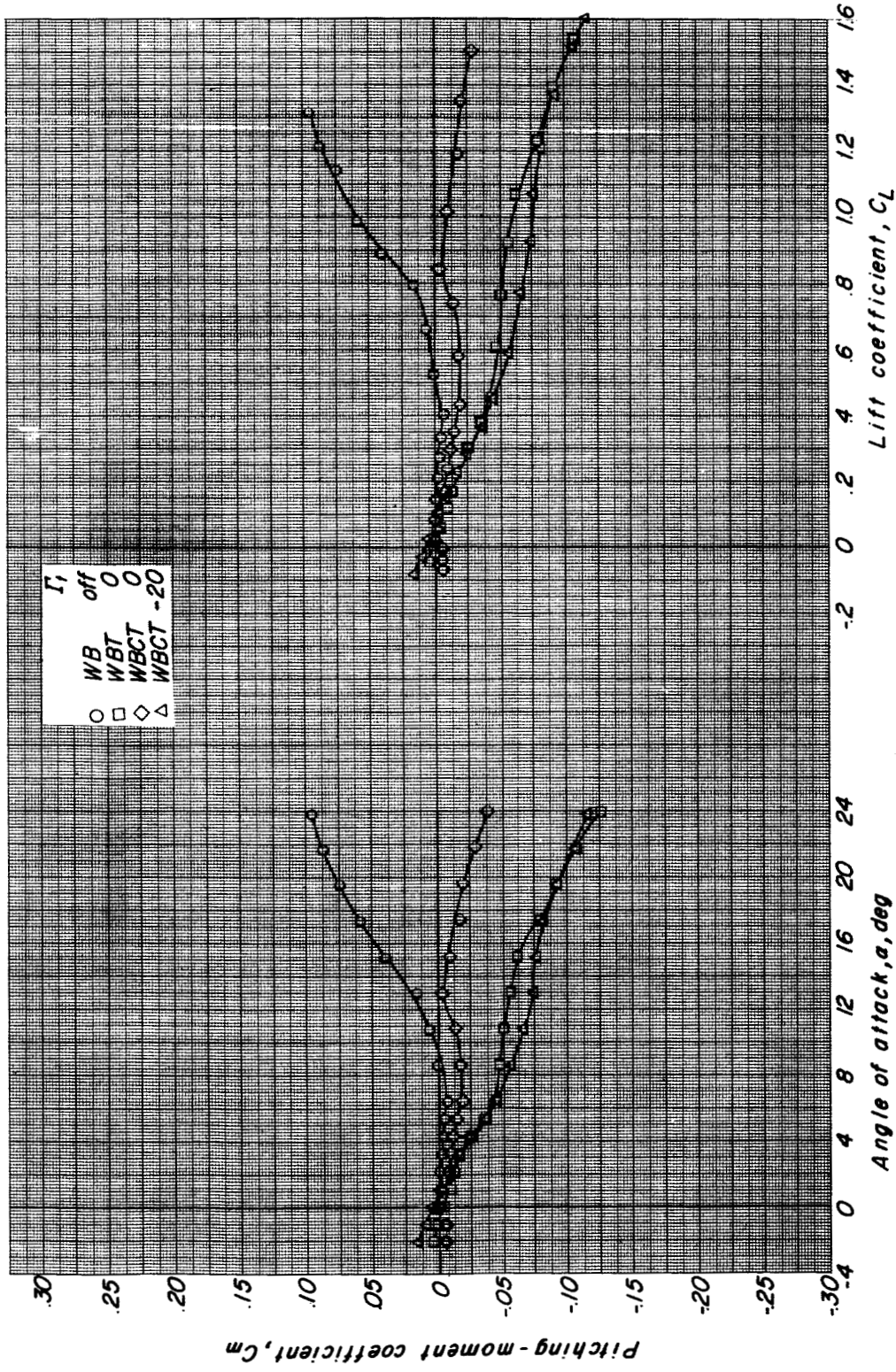
Figure 37.- Concluded.
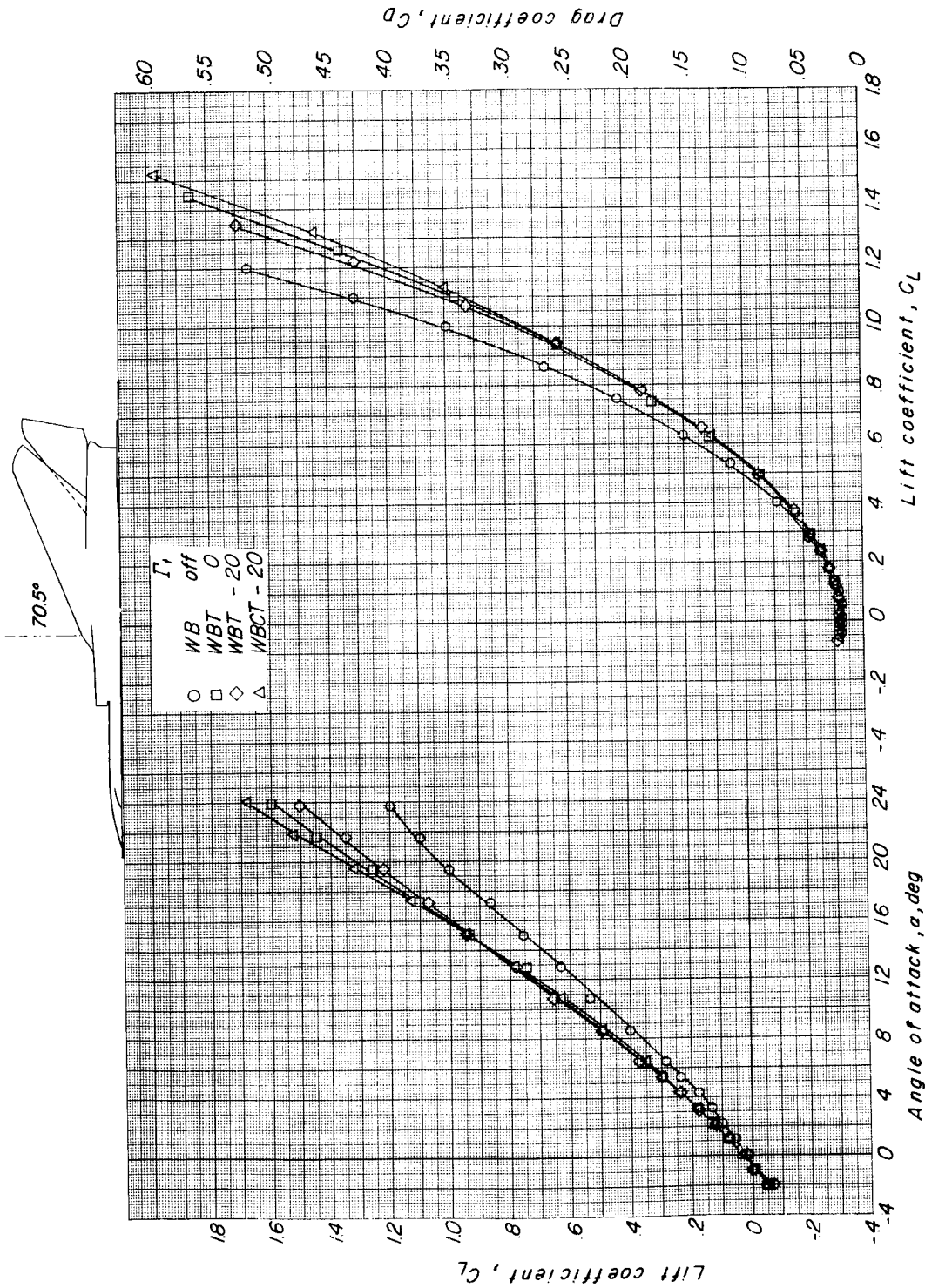
Figure 38.- Longitudinal aerodynamic characteristics of the various component parts of configuration II at 0° control deflection. $\Lambda_{LE} = 70.5°$.
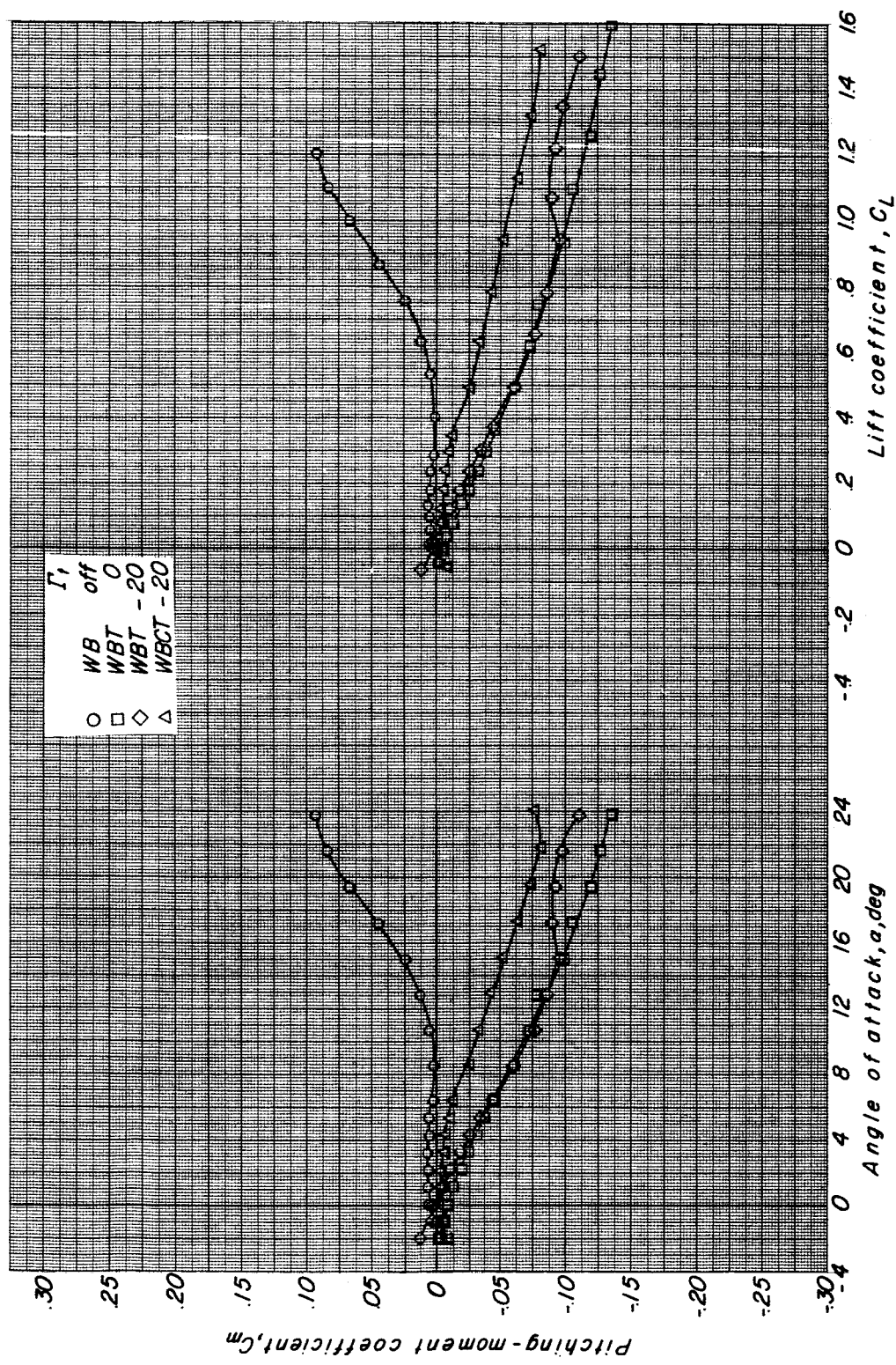
Figure 38.- Concluded.
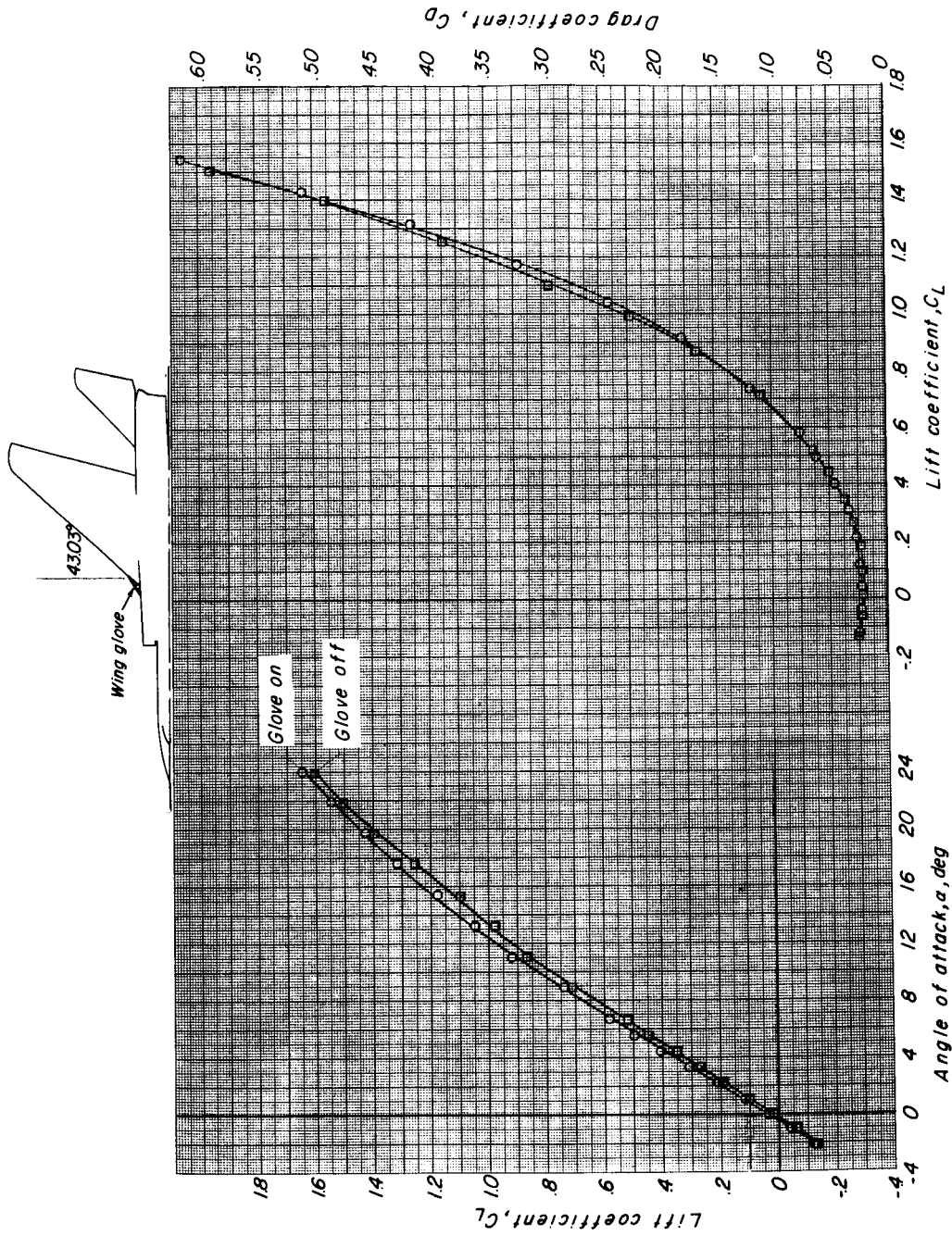
Figure 39.- Effect of addition of wing glove on the longitudinal aerodynamic characteristics of configuration II with canard surface off. $\delta_h = 0°$; $\Gamma_t = 0°$; $\Lambda_{LE} = 43.03°$.
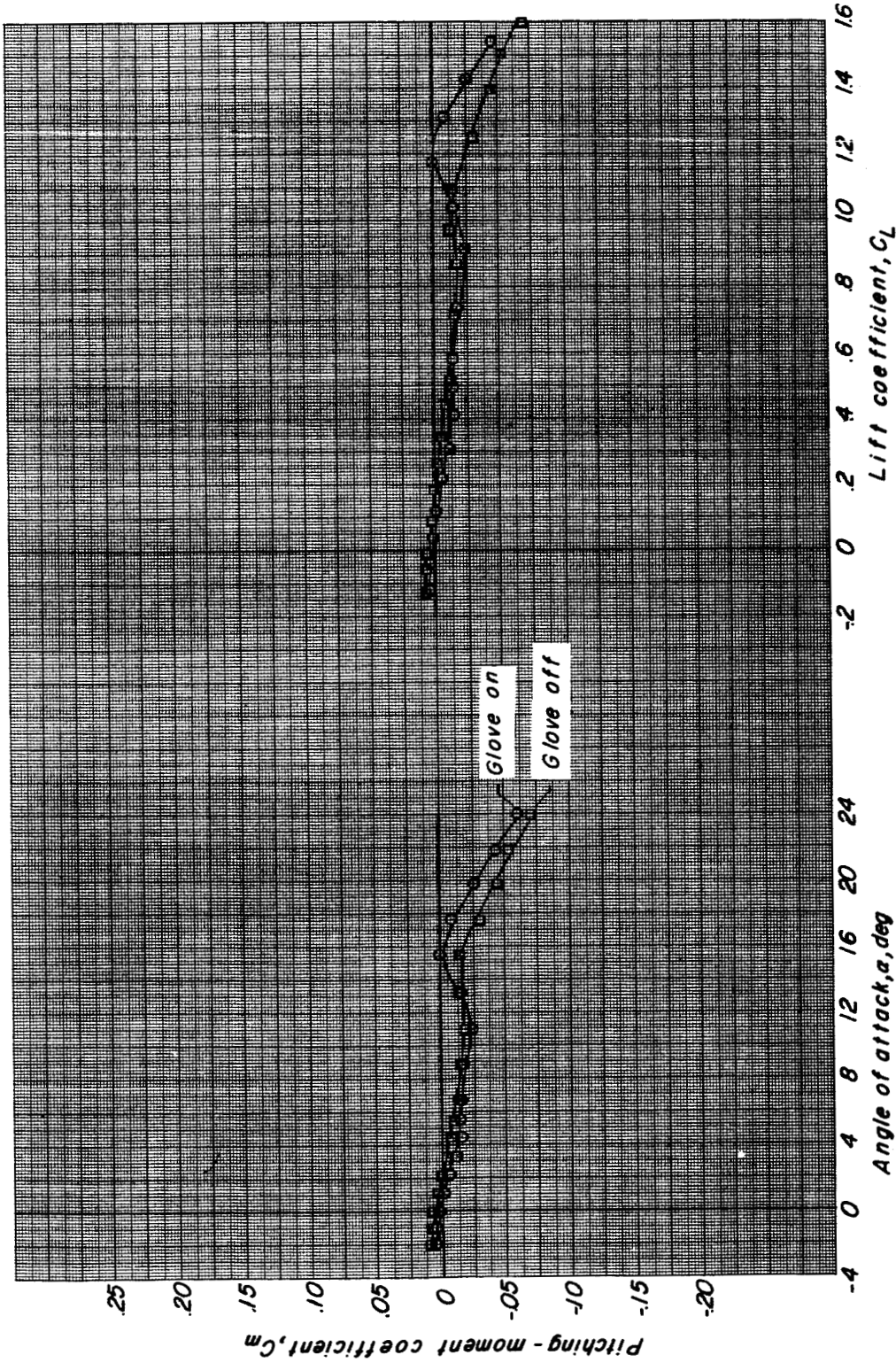
Figure 39.- Concluded.
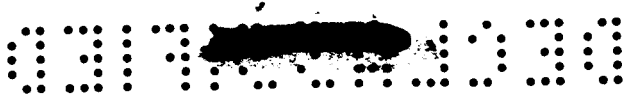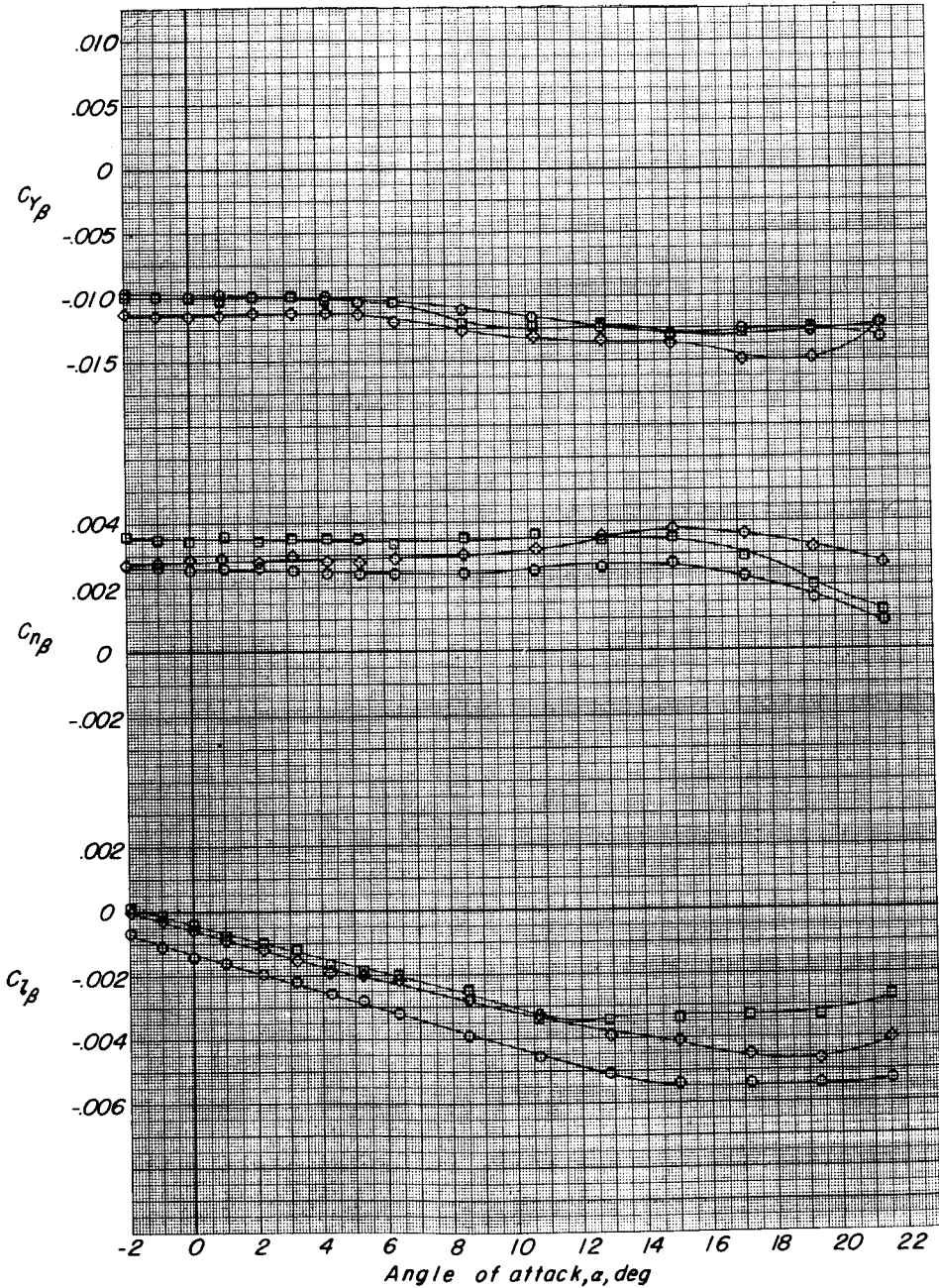
Figure 40.- Variation of sideslip derivatives with angle of attack for configuration II. $\Lambda_{LE} = 70.50°$.
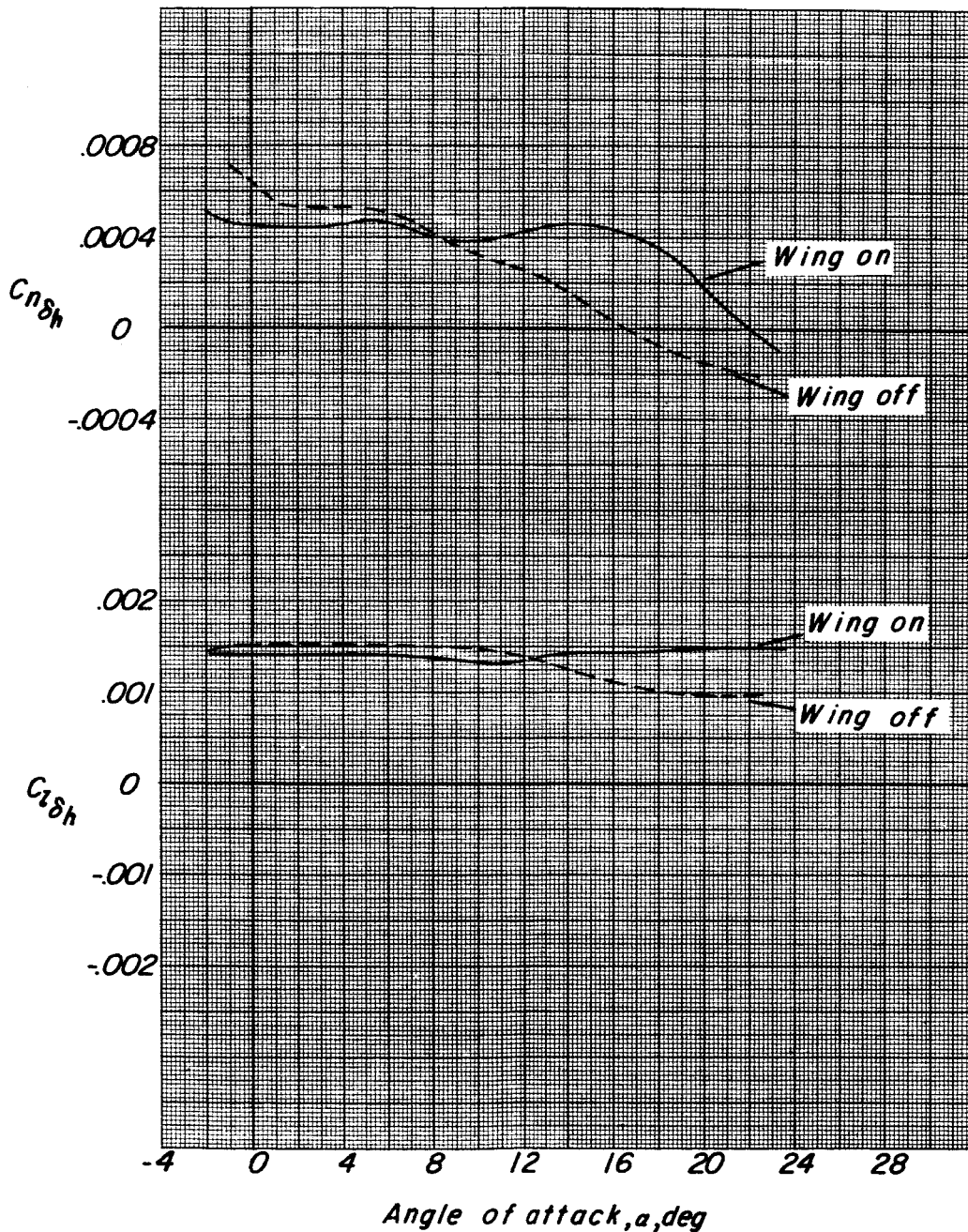
Figure 41.- Lateral control characteristics of configuration II with canard surface off. $\Lambda_{LE} = 70.50°$; $\Gamma_t = 0°$.
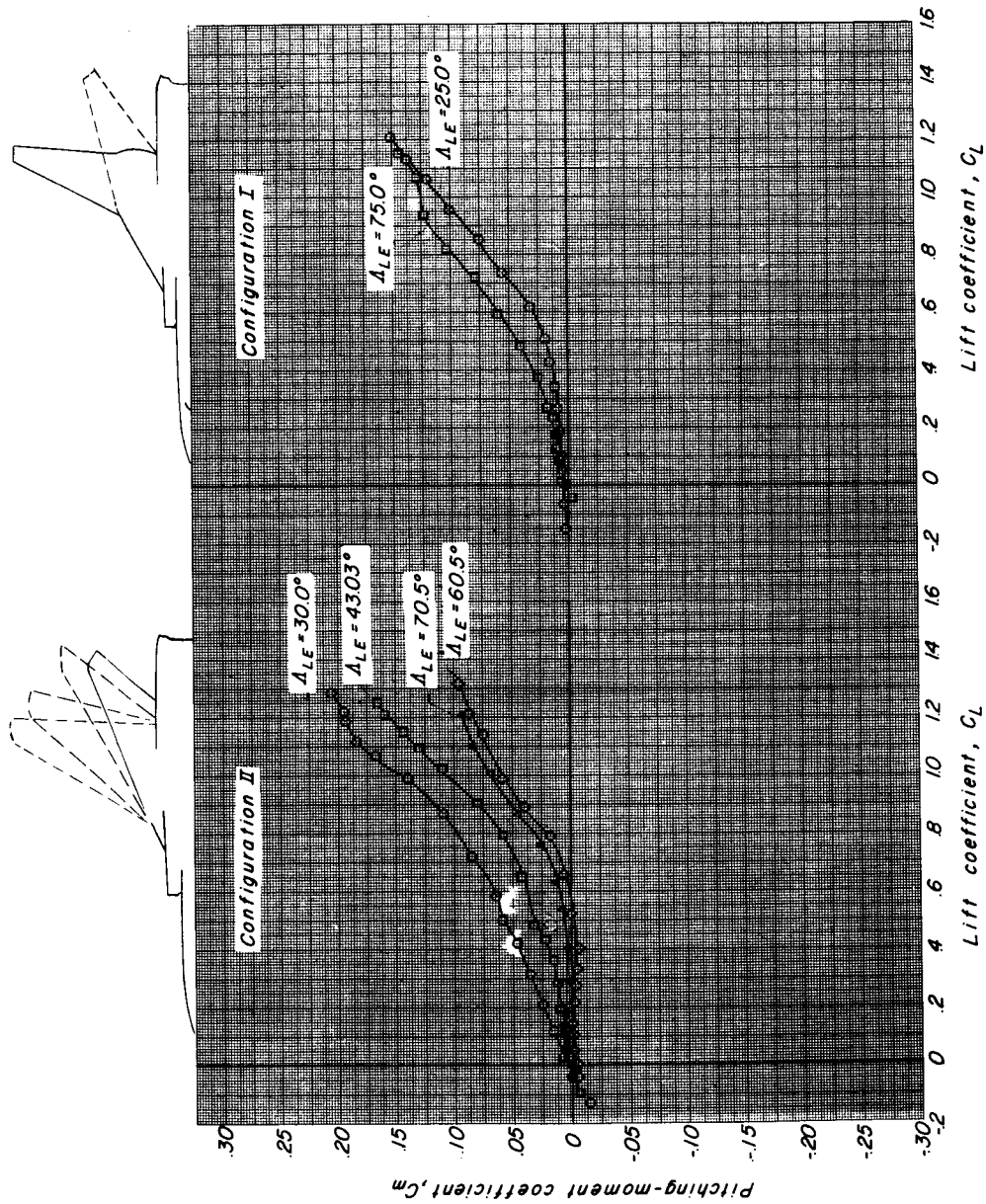
(a) Horizontal tail and canard surface off.

Figure 42.- A comparison of static-margin shift with sweep variation for configurations I and II.
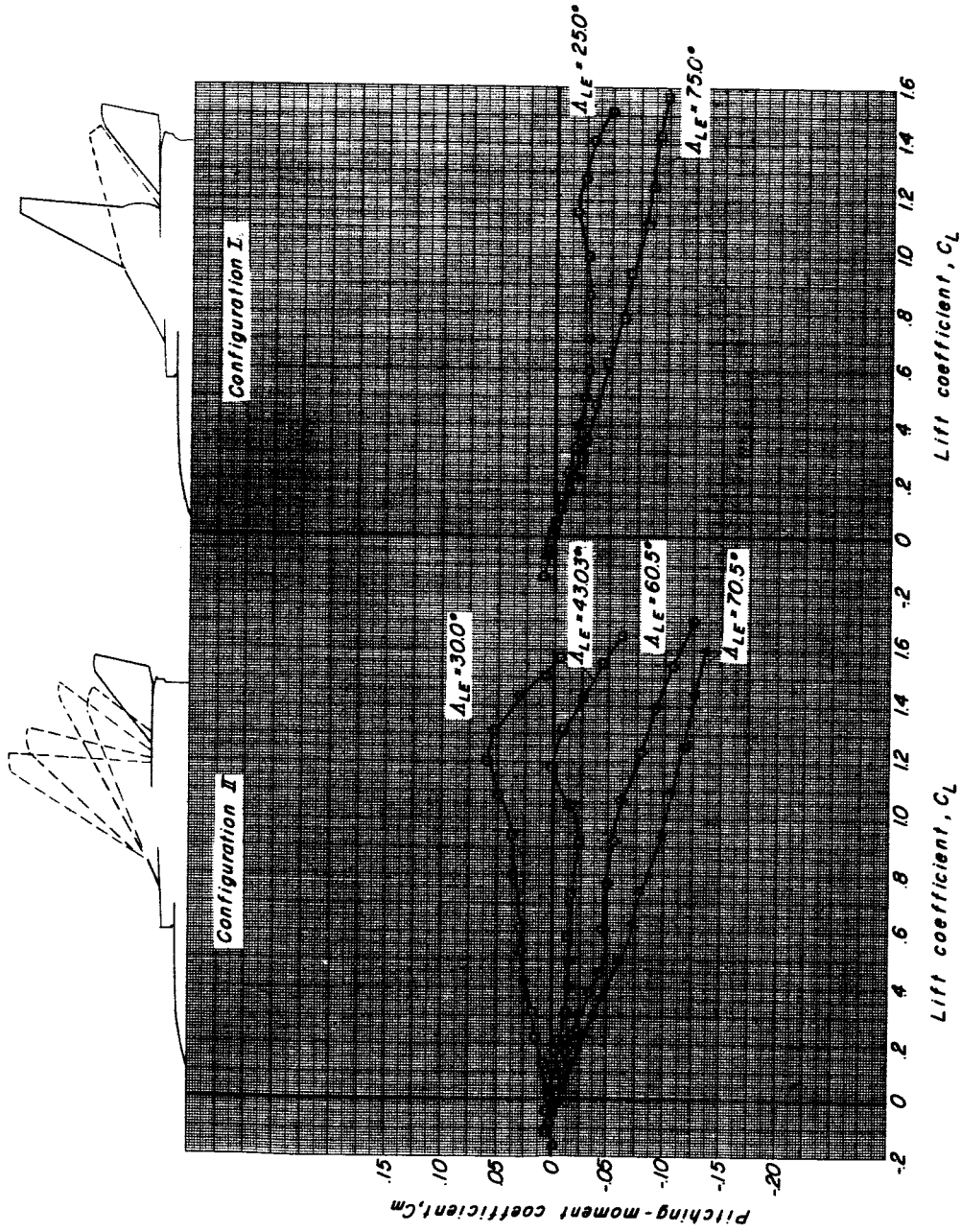
(b) Horizontal tail on and canard surface off. $\Gamma_t = 0°$.

Figure 42.- Concluded.
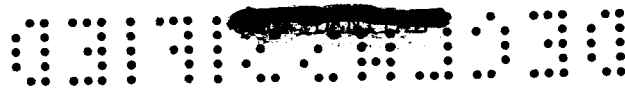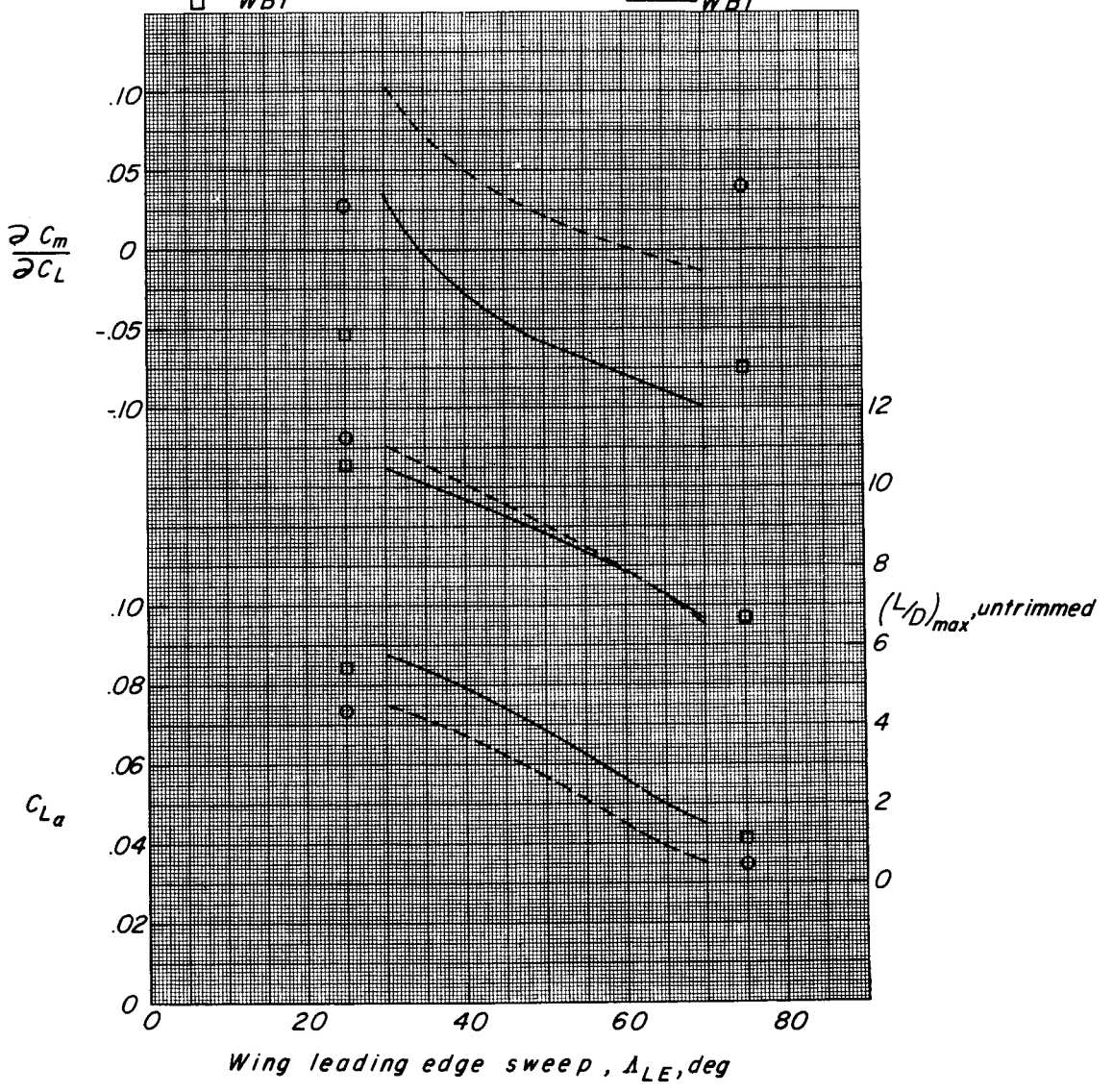
Figure 43.- Variation of static margin, untrimmed $(L/D)_{max}$, and lift-curve slope for the two configurations tested with and without horizontal tail. With tail on, $\delta_h = 0^\circ$; $\Gamma_t = 0^\circ$.

L-1024
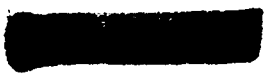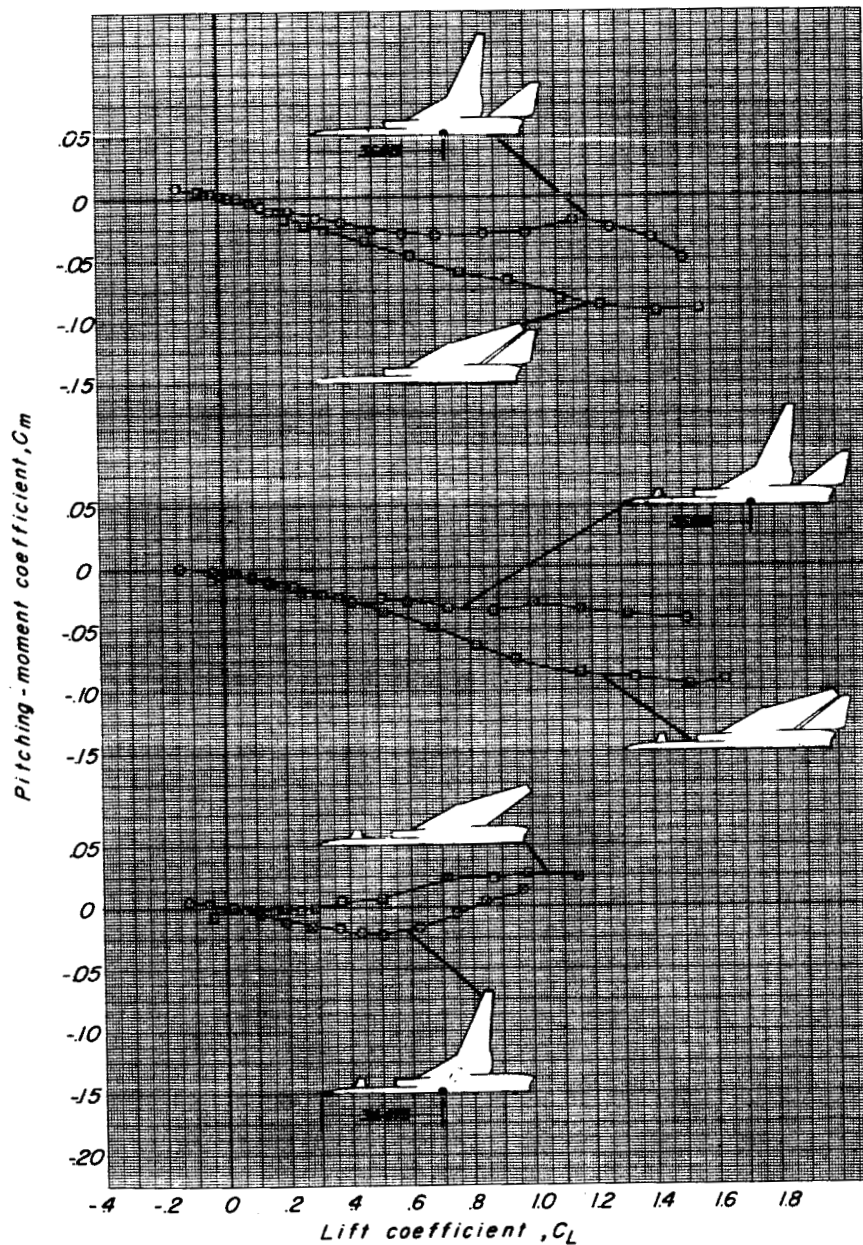
Figure 44.- A comparison of the longitudinal stability characteristics for three arrangements of configuration I having wing leading-edge sweepback angles of 25° and 75°. For comparison purposes, the moment reference location has been adjusted so that all three arrangements have the same static margin in the 25° wing-sweep condition. All control surfaces are at 0° deflection.
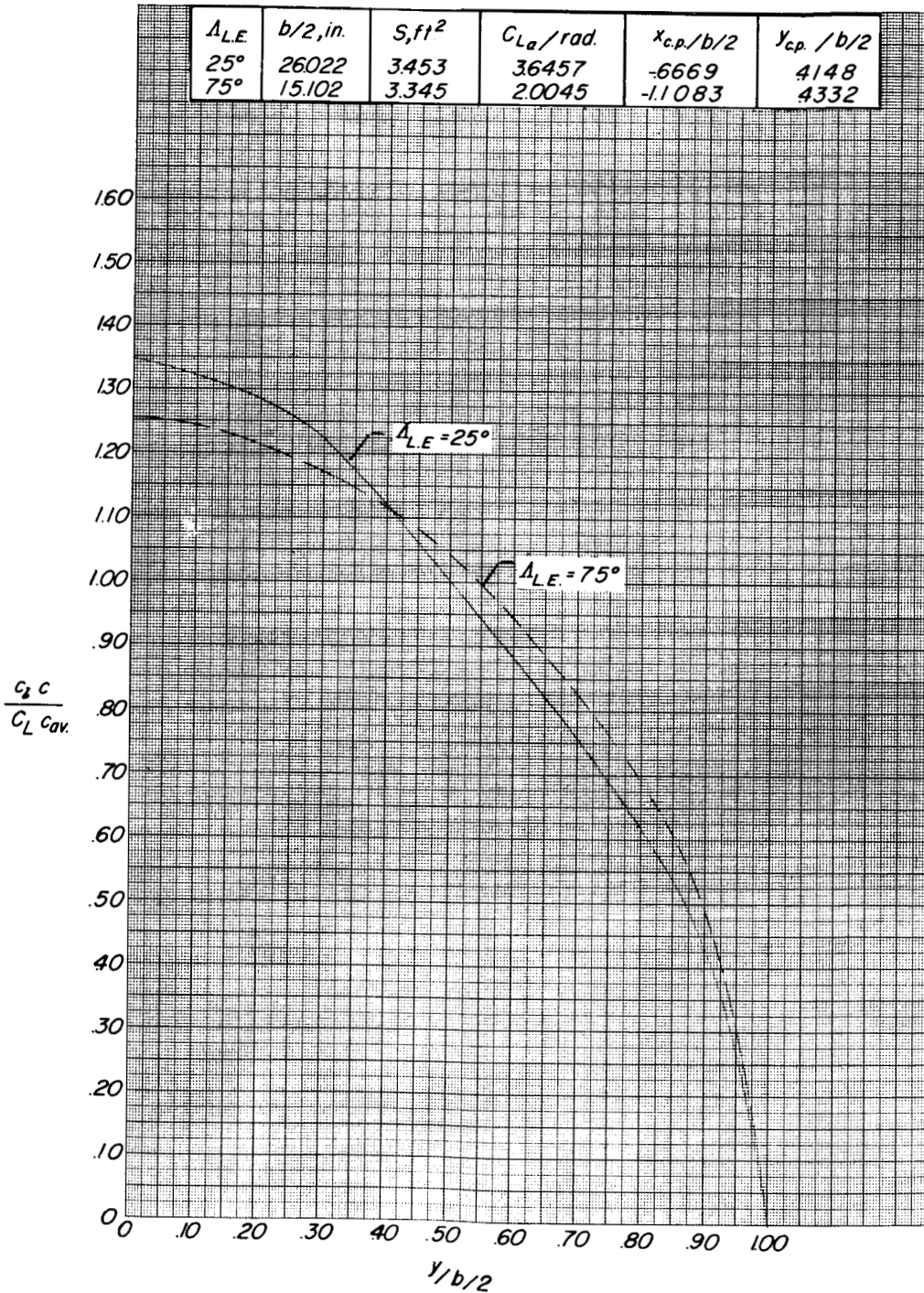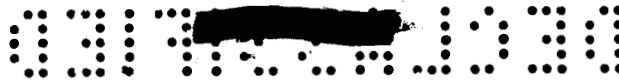
Figure 45.- Span-load distributions for configuration I without horizontal tail and canard surface. $\Lambda_{LE} = 25°$ and $75°$.